INFORMATION TO USERS

This reproduction was made from a copy of a document sent to us for microfilming. While the most advanced technology has been used to photograph and reproduce this document, the quality of the reproduction is heavily dependent upon the quality of the material submitted.

The following explanation of techniques is provided to help clarify markings or notations which may appear on this reproduction.

1. The sign or "target" for pages apparently lacking from the document photographed is "Missing Page(s)". If it was possible to obtain the missing page(s) or section, they are spliced into the film along with adjacent pages. This may have necessitated cutting through an image and duplicating adjacent pages to assure complete continuity.

2. When an image on the film is obliterated with a round black mark, it is an indication of either blurred copy because of movement during exposure, duplicate copy, or copyrighted materials that should not have been filmed. For blurred pages, a good image of the page can be found in the adjacent frame. If copyrighted materials were deleted, a target note will appear listing the pages in the adjacent frame.

3. When a map, drawing or chart, etc., is part of the material being photographed, a definite method of "sectioning" the material has been followed. It is customary to begin filming at the upper left hand corner of a large sheet and to continue from left to right in equal sections with small overlaps. If necessary, sectioning is continued again—beginning below the first row and continuing on until complete.

4. For illustrations that cannot be satisfactorily reproduced by xerographic means, photographic prints can be purchased at additional cost and inserted into your xerographic copy. These prints are available upon request from the Dissertations Customer Services Department.

5. Some pages in any document may have indistinct print. In all cases the best available copy has been filmed.

University Microfilms International
300 N. Zeeb Road
Ann Arbor, MI 48106

Wolfgang, Steven Marc

A STUDY OF THE PHOTOPHYSICAL AND PHOTOREDOX PROPERTIES OF RUTHENIUM(II) COMPLEXES WITH PI-ACCEPTOR LIGANDS

City University of New York PH.D. 1984

A STUDY OF THE PHOTOPHYSICAL AND PHOTOREDOX PROPERTIES OF RUTHENIUM(II) COMPLEXES WITH PI-ACCEPTOR LIGANDS

by

Steven M. Wolfgang

A dissertation submitted to the
Graduate Faculty in Chemistry
in partial fulfillment of the
requirements for the degree
of Doctor of Philosophy, the
City University of New York

October, 1983

This manuscript has been read and accepted for the Graduate Faculty in Chemistry in satisfaction of the dissertation requirement for the degree of Doctor of Philosophy.

Oct 12 1983
date

Harry D. Gafney
Chairman of Examining Committee

12 October 1983
date

David C. Locke
Executive Officer

Klaus R. Fonlach

Arthur D Baker

Harry D. Gafney
Supervisory Committee

The City University of New York

Abstract

A STUDY OF THE PHOTOPHYSICAL AND PHOTOREDOX PROPERTIES OF RUTHENIUM(II) COMPLEXES WITH PI-ACCEPTOR LIGANDS

by

Steven M. Wolfgang

Advisor: Professor Harry D. Gafney

The photophysical and photoredox properties of $Ru(bpy)_3^{2+}$ ionically bound to porous Vycor glass, PVG, are investigated. The complex cation is adsorbed from aqueous solution to the glass. The latter is transparent and therefore, amenable to spectroscopic techniques. Absorption, emission, and resonance Raman spectra of $Ru(bpy)_3^{2+}$ adsorbed to the glass, designated $Ru(bpy)_3^{2+}$ads, resemble spectra of the complex in aqueous or alcoholic solutions.

The quantum yield for the luminescence from the adsorbed complex is 0.12±0.01. When excited at room temperature, 22±1°C, with a low intensity pulse, the luminescence decay of the LMCT state, designated $^*Ru(bpy)_3^{2+}$ads, is exponential and the luminescence lifetime is 740±20 nsec.

Both the intensity and the lifetime of the luminescence from $^*Ru(bpy)_3^{2+}$ads are quenched by N_2O,

SO_2, and O_2, and quenching parallels adsorption of the gases onto PVG. Based upon energetic considerations, SO_2 and N_2O quench via electron transfer, however, a mechanistic distinction among energy transfer and electron transfer quenching by O_2 along these lines is not possible.

$^*Ru(bpy)_3^{2+}$ cannot be completely quenched by any of these three gases, which implies that only a certain fraction of the adsorbed complex is accessible to the coadsorbed quencher. This fraction, designated f_{max}, and the nature of the dominant quenching process, i.e., static or dynamic, parallel the relative adsorption coefficients of the gases $N_2O<O_2<SO_2$. Thus, N_2O, the weakest adsorbed among the 3 gases, quenches entirely via a dynamic mechanism, and exhibits the lowest value for f_{max}, 0.28 ± 0.02. O_2 and SO_2 are more strongly adsorbed than N_2O and therefore, exhibit predominately static quenching and much larger values for f_{max}, 0.74 ± 0.02 and 0.94 ± 0.01, respectively.

The initial slopes of plots of t_o/t vs. the number of moles of adsorbed quencher per gram of PVG, m_{ads}, yield bimolecular quenching rate constants, k_b, of $1.1\pm0.2 \times 10^{11}$, $7.6\pm1.3 \times 10^{11}$, and $5.3\pm1.0 \times 10^9$ gm PVG/mole-sec for dynamic quenching by O_2, SO_2, and N_2O, respectively. Dynamic quenching of the adsorbed complex is attributed to diffusion by coadsorbed quencher molecules along the PVG surface.

Static quenching does not arise from ground state donor-quencher complexation but rather, is ascribed to the presence of adsorbed gas molecules within sufficient proximity of $Ru(bpy)_3^{2+}$ads to quench the latter. Analysis of the static quenching data yields a quenching distance, r, of $11+1 \leq r \leq 17+2$ A^o for O_2. Since SO_2 quenches by an electron transfer mechanism, similar analysis suggests the occurance of long range, 27 ± 2 A^o, electron transfer in PVG.

Laser photolysis at 457.9-nm of $Ru(bpy)_3^{2+}$ads in the presence of a codeposited transparent, conducting SnO_2 film doped with 1% Sb, results in disproportionation of the dication, i.e.,

$$Ru(bpy)_3^{2+}ads \longrightarrow Ru(bpy)_3^{3+} + [Ru(bpy)_2(bpy^-)]^+.$$

The rate of formation of $[Ru(bpy)_2(bpy^-)]^+$ is second order in light intensity, consistent with a previously reported disproportionation in PVG, where the mechanism involves biphotonic ionization of $Ru(bpy)_3^{2+}$ads. The photoionized electron is capable of 50 A^o migration along the PVG surface to another $Ru(bpy)_3^{2+}$ads which gets reduced. Whether or not SnO_2 is present, the maximum quantum efficiency of disproportionation is attained when the amount of $Ru(bpy)_3^{2+}$ is 2.7×10^{-6} moles/gm PVG. This observation suggests that, at higher loading levels, disproportionation is complemented by a thermal back reaction, i.e.,

$$[Ru(bpy)_2(bpy^-)]^+ + Ru(bpy)_3^{3+} \longrightarrow Ru(bpy)_3^{2+}.$$

The presence of a conducting SnO_2 film resulted in an increased quantum yield of disproportionation, although only at $Ru(bpy)_3^{2+}$ads loading levels exceeding ca. 2.5 x 10^{-6} moles/gm PVG. The latter observation is an indication of the enhanced conductivity of the PVG medium due to SnO_2, where the lack of an increase in quantum efficiency at loading levels $\leq$2.5 x 10^{-6} moles/gm PVG may reflect a need for $Ru(bpy)_3^{2+}$ads and the semiconductor to be in direct contact.

Resonance Raman and emission spectra are reported for a series of complexes, $Ru(azpy)_2L^{n+}$ (n = 0-2), where azpy represents 2-(phenylazo)pyridine and L various monodentate or a bidentate ligand. The resonance Raman spectra reveal a relatively localized MLCT excited state with large distortions of the N=N bond in the azpy ligand. Emission maxima for the luminescent complexes are significantly red-shifted relative to other Ru(II) diimine complexes. These data along with previously measured electrochemical data suggest an energy level ordering in which the luminescent LMCT state is an exergonic oxidant and endergonic reductant. Quenching by a series of related oxidative and reductive quenchers is consistent with the calculated energetics of the photoinduced redox process.

ACKNOWLEDGEMENT

I would like to express my appreciation to my research advisor, Dr. Harry D. Gafney, for his assistance in the preparation of this thesis.

I would also like to thank Dr. A. Dave Baker, Dr. Thomas C. Strekas, and Dr. William F. Berkowitz for their helpful suggestions and kind assistance. I am also grateful to Mr. Robert Wurman and Mr. Karl Regnat for aid in assembling instrumentation. Thanks to Dr. Jerome Schulman for advising me to pursue this degree.

Most of all, I would like to thank my parents, Dorothy and Raphael, who were loving and considerate throughout.

TABLE OF CONTENTS

LIST OF TABLES

LIST OF FIGURES

I. Introduction

The excited state chemistry of ruthenium(II) complexes, particularly those containing the pi-acceptor ligands 1,10-phenanthroline (phen) and 2,2'-bipyridine(bpy), has been extensively studied during the last decade.[1] Among the many ruthenium(II) complexes which have been investigated, $Ru(bpy)_3^{2+}$ has received by far the most attention in studies of this nature, and its excited state properties are very well characterized. $Ru(bpy)_3^{2+}$ is one of the most intensely luminescent of all metal complexes, displaying strong emission even in room temperature fluid solution,[2] and with an excited state lifetime ranging from 0.6-0.8 microseconds, depending upon the solvent,[3,4] it is a very effective sensitizer of both energy transfer and electron transfer.[5-9]

A. Photophysics and Photochemistry of $Ru(bpy)_3^{2+}$

(i) Assignment of the Emission

In room temperature, aqueous solution, $Ru(bpy)_3^{2+}$ displays a broad structureless emission band with a maximum at 620-nm.[10,11] At 77°K in an ether-pentane-alcohol(EPA) glass, the emission band consists of a series of 3 vibrational progressions, with maxima appearing at 580 nm, 633 nm, and 692 nm.[12] A considerable amount of controversy persisted for nearly a

decade concerning the assignment of both the spin and orbital nature of this emission.[2,13-17] Dispute over whether the emission was a phosphorescence or a fluorescence was due to the observed excited state lifetime of $Ru(bpy)_3^{2+}$ in fluid solution of nearly a microsecond. This falls well within the range between phosphorescent and fluorescent lifetimes in organic molecules (milliseconds and nanoseconds, respectively). The uncertainty regarding the orbital nature of the emission was essentially a debate over whether it was a metal-centered(d^*-d) or a charge-transfer(π^*-d) transition. It is now firmly established that the luminescence is a spin-forbidden, charge-transfer type, at least at 77°K.[18] The term luminescence is used rather than fluorescence or phosphorescence to indicate that spin states are not as well-defined in this case as they would be for an organic molecule. This lack of clarity arises from extensive spin-orbit coupling of the metal ion[19] which mixes singlets and triplets.

(ii) Characterization of the MLCT Excited State

Ruthenium(II) complexes with pi-acceptor ligands display intense visible absorption bands which are attributed to metal-to-ligand charge transfer(MLCT).[20,21] A transition of this type can be envisioned as a transfer of electronic charge from a ruthenium(II) t_{2g} orbital to a ligand π^* antibonding orbital.[22]

According to an early model proposed by Crosby and coworkers,[23,24] the MLCT excited state of $Ru(bpy)_3^{2+}$ was pictured as a Ru $4d^5$ core with an excited electron delocalized amongst the π^* antibonding orbitals of three coupled bipyridine ligands. Later, convincing evidence was presented for a revision of this model, whereby the excited electron is confined to one of the bipyridine ligands.[25-30] Thus, the MLCT state can be viewed as a Ru $4d^5$ core, two bpy ligands with vacant antibonding orbitals, and one bpy ligand with an unpaired electron in one of its antibonding orbitals, i.e., $*[Ru^{III}(bpy)_2(bpy^-)]^{2+}$. This picture is consistent with the behavior of the MLCT state as a powerful chemical oxidant and reductant (vide supra).

(iii) Photochemical Properties of MLCT Excited State

The vast number of photochemical studies of $Ru(bpy)_3^{2+}$ suggest that the excited state is substitutionally photoinert, and that the excited state chemistry is limited solely to redox reactions. However, more recently it has been found that the complex does undergo photosubstitution, albeit at elevated temperatures.[31-35] This discovery led to the development of the current model of the $Ru(bpy)_3^{2+}$ excited states by Van Houten and Watts.[36] They distinguish between two sets of excited state levels which are separated by some 3600 cm^{-1}, with the lower levels giving rise to the observed luminescence, and the upper levels accounting for substitutional photochemistry.

The luminescent MLCT excited state of $Ru(bpy)_3^{2+}$, hereafter denoted $^*Ru(bpy)_3^{2+}$, lies 2.12 eV[37] greater in energy than the ground state, a quantity that is determined spectroscopically from the 0-0 emission band. $^*Ru(bpy)_3^{2+}$ displays chemical properties that are so radically different from those of the ground state that it can be considered as an entirely new molecule. Meyer and coworkers have shown that the MLCT state can function as either an oxidant or a reductant with very similar driving force, via the calculation of excited state redox potentials.[38] This calculation, which is valid for any molecule provided that all of the excited state energy is available as free energy for redox, can be made for $^*Ru(bpy)_3^{2+}$ by taking the difference between the excited state energy of 2.12 eV and the corresponding ground state redox potentials. The various redox states of $Ru(bpy)_3^{2+}$ along with the energy quantities required to proceed from one state to another can be summarized in an energy level diagram (Figure 1). In this description, endothermic and exothermic processes are represented by arrows pointing in upward and downward directions, respectively. In this scheme, oxidation and reduction of $Ru(bpy)_3^{2+}$ in the ground state are unfavorable by greater than 1.2 V. Clearly, the absorption of a photon with an energy that exceeds 2.12 eV, transforms a molecule with no practical oxidizing or reducing capability into one which is very potent in these respects. Consequently, a

Figure 1

Ground and excited state redox potentials of $Ru(bpy)_3^{2+}$ in aqueous solution at 25°C (see text).

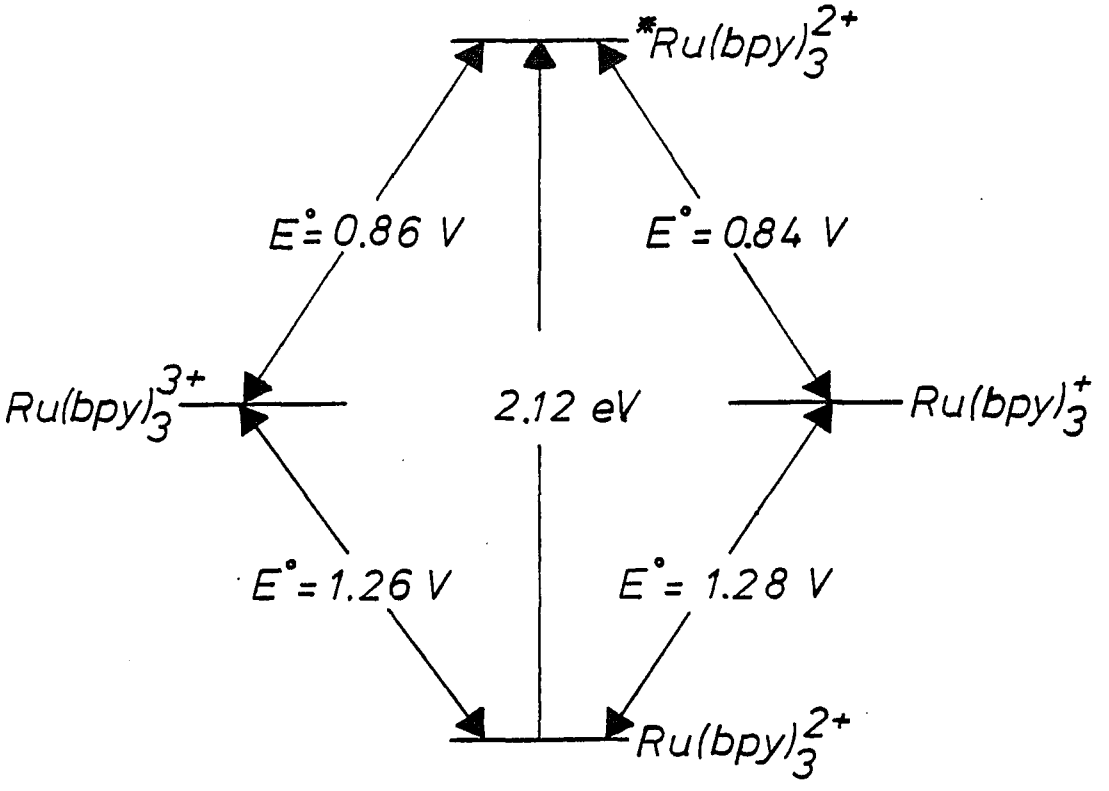
*Ru(bpy)$_3^{2+}$
E° = 0.86 V
E° = 0.84 V
Ru(bpy)$_3^{3+}$
2.12 eV
Ru(bpy)$_3^{+}$
E° = 1.26 V
E° = 1.28 V
Ru(bpy)$_3^{2+}$

Figure 1

vast number of studies of $Ru(bpy)_3^{2+}$ have involved its use as an excited state redox reagent, as either an oxidant or a reductant.

In addition to its rich photoredox chemistry, $^*Ru(bpy)_3^{2+}$ sensitizes the formation of triplet excited states of inorganic and organic molecules via the process of energy transfer. Thus, whenever the excited state is rapidly deactivated in bimolecular reactions with external additives, known as quenchers, one can visualize three principal means:

a) excited state acts as a reductant (oxidative quenching)

$$^*Ru(bpy)_3^{2+} + Q \longrightarrow Ru(bpy)_3^{3+} + Q^- \quad (1)$$

b) excited state acts as an oxidant (reductive quenching)

$$^*Ru(bpy)_3^{2+} + Q \longrightarrow Ru(bpy)_3^{+} + Q^+ \quad (2)$$

c) excited state acts as an energy donor (energy transfer)

$$^*Ru(bpy)_3^{2+} + Q \longrightarrow Ru(bpy)_3^{2+} + {}^*Q \quad (3)$$

The actual quenching mechanism that is operative for a particular quencher can usually be distinguished via thermodynamic considerations. The ability to undergo quenching by energy transfer is directly related to the 0-0 spectroscopic energy levels (spectral overlap) of the donor-acceptor pair, and that of electron transfer quenching to the redox potentials. However, a clear-cut distinction based upon energetics is not always possible and in many of the following examples, a considerable amount of experimental evidence was accumulated prior to resolving the quenching mechanism.

Electron transfer quenching of $^*Ru(bpy)_3^{2+}$ by a variety of inorganic ions and molecules has been investigated. Ions such as Fe^{3+},[39-45] Cu^{2+},[46-48] Eu^{3+},[49,50] Tl^{3+},[41,51] Ag^+,[52,53] Hg^{2+},[54] and $S_2O_8^{2-}$[55,56] quench $^*Ru(bpy)_3^{2+}$ oxidatively to yield $Ru(bpy)_3^{3+}$ as the product (reaction 1). With Eu^{2+},[43] SO_3^{2-},[57] and ascorbate,[58] as well as the cyanide complexes,[59-61] $Fe(CN)_6^{4-}$, $Mo(CN)_8^{4-}$, and $Ru(CN)_6^{3-}$, the excited state is photoreduced (reaction 2). $Ru(bpy)_3^{2+}$ also sensitizes the redox decomposition of metal complexes such as $Co(NH_3)_5Cl^{2+}$[62,63] and $PtCl_4^{2-}$.[5,9,48,64,65]

Among the organic molecules that quench $^*Ru(bpy)_3^{2+}$, nitroaromatics,[38] quinones,[66] and bipyridinium ions (viologens)[38,67-74] quench oxidatively, whereas aromatic amines[67,75] and dithioanions[76] quench reductively.

A number of organic and inorganic molecules quench $^*Ru(bpy)_3^{2+}$ by energy transfer (reaction 3). Sensitization by $^*Ru(bpy)_3^{2+}$ of triplet states of organic molecules,[7,77] e.g. anthracene, stilbene, and aromatic ketones, and of the emission of chromium complexes[59,60,78-81], have been reported. Both energy transfer[82] and electron transfer[83,84] mechanisms have been proposed for the quenching of

$^{*}Ru(bpy)_3^{2+}$ by molecular oxygen. Isolation of $^1O_2$ reaction products when quenching of $^{*}Ru(bpy)_3^{2+}$ by O_2 is carried out in the presence of singlet oxygen traps has been interpreted as evidence for energy transfer quenching. However, an oxidative quenching mechanism has been postulated on the basis of detection of $Ru(bpy)_3^{3+}$ and O_2^- in the flash photolysis of acidic oxygenated $Ru(bpy)_3^{2+}$ solutions:

$$^{*}Ru(bpy)_3^{2+} + O_2 \longrightarrow Ru(bpy)_3^{3+} + O_2^-$$

$$Ru(bpy)_3^{2+} + O_2^- \longrightarrow Ru(bpy)_3^{2+} + {}^1O_2 \quad (4)$$

The initially formed $Ru(bpy)_3^{3+}$ and superoxide ion, O_2^-, react to give $Ru(bpy)_3^{2+}$ and singlet oxygen, $^1O_2$. Thus, the net process appears as the sensitization of ground state triplet molecular oxygen to singlet oxygen, by $^{*}Ru(bpy)_3^{2+}$. An unequivocal distinction between these two mechanisms is not currently available.

To obtain bimolecular rate constants for a quenching reaction a steady state approximation can be made and the well-known Stern-Volmer relationship is obtained,

$$I_o/I = 1 + K_{SV}[Q] \quad (5)$$

where I_o and I refer to the unquenched and quenched steady state emission intensities, respectively. The Stern-Volmer constant, K_{SV}, is $k_q \times t_o$, where t_o is the excited state lifetime in the absence of the quencher, and k_q is the bimolecular quenching rate

constant. Therefore, if the steady state emission intensity is measured as a function of quencher concentration, a plot of I_o/I vs. [Q] has a slope equal to K_{SV}, with a y-intercept of 1.0. In a separate experiment t_o is measured and the bimolecular quenching rate constant is the ratio K_{SV}/t_o, in units $M^{-1}sec^{-1}$.

Bimolecular quenching rates that approach the theoretical diffusion controlled limit, 2×10^9 $M^{-1}sec^{-1}$, are found for many of the photoinduced redox reactions of $Ru(bpy)_3^{2+}$. Although kinetic parameters are a necessary consideration, the thermodynamic constraints imposed upon a particular quenching reaction will determine its feasibility. Thus, an electron transfer quenching mechanism can only be envisioned if the sum of the relevant redox potentials of the donor and the quencher exceeds zero volts.

B. Chemical Modification of Ru(II) Complexes with Pi-acceptor Ligands for Tuning of Photoredox Chemistry

(i) Chemical Modification Strategies

As a means of obtaining metal complexes with desirable photoredox properties one can tune the excited state redox potentials via chemical modification of the ligands.[39] One such method which has been very thoroughly investigated involves the introduction of substituents on the bpy and phen ligands.[85-87]

The spectral and electrochemical properties for a series of substituted bpy and phen complexes of Ru(II) in aqueous solution appear in Table 1. Both the excited state energies and the redox potentials (excited state and ground state) of the substituted complexes are fairly similar to those properties for the unsubstituted bpy and phen complexes. From this data, it is evident that the introduction of ligand substituents on bpy and phen provides a means of chemically "fine-tuning" excited state energies and redox potentials. An undesirable result of chemical modification is that it can yield complexes with significantly shorter excited state lifetimes than the parent unsubstituted complexes. In fact, for several of the substituted complexes appearing on Table 1, no emission is observed in room temperature fluid solution.

An alternative to chemical modification of the bpy and phen ligands involves the preparation of complexes of the type $Ru(bpy)_2L$ or $Ru(phen)_2L$, where L can be virtually any monodentate or bidentate ligand.[18,31,86] However, so few of these complexes are luminescent in room temperature fluid solution that essentially no data on quenching or excited state redox potentials exists.

Ru(II) complexes of a number of bidentate and tridentate nitrogen-donor ligands modeled after bpy and phen have been synthesized, and their photophysical and photoredox properties have been investigated.[85,86,88] Table 2 summarizes the data obtained for several complexes of this

Table 1 - Spectral and Electrochemical Properties of a Series of Substituted Bpy and Phen Complexes of Ru(II) (RuL_3^{2+} Type) in Aqueous Solution

Ligand (L)	Absorption		Emission (298K)		Ground State Redox Potentials (V vs. NHE)		Excited State Redox Potentials (V vs. NHE)		Ref
	λ_{max} (nm)	ϵ(mM)	λ_{max} (nm)	τ(μs)	E(M/M+)	E(M/M-)	E*(M/M+)	E*(M/M-)	
bpy	452	14.6	613,627	0.62	+1.26	-1.28	-0.86	+0.84	85
4,4'-Me_2bpy	460	14.3	628	0.33	+1.10	-1.44	-0.94	+0.69	85
4-NO_2bpy	462	17.0			+1.43	-1.06			86
4,4'-Cl_2bpy	480	20.4			+1.55	-0.55			86
4,4'-t-Bu_2bpy	456	16.8			+1.11				86
phen	447	19.0	605,625	0.92	+1.26	-1.36	-0.87	+0.82	85
5-Mephen	450	19.4	605,625	1.33	+1.23	-1.31	-0.92	+1.00	85
5-Clphen	447	18.4	605,625	0.94	+1.36	-1.15	-0.77		85
5-NO_2phen	449	20.0	606	0.005	+1.46		-0.67		85
5-Brphen	448	18.8	605,625	1.04	+1.37		-0.76		85
4,7-Me_2phen	445	25.3	613,627	1.74	+1.09	-1.47	-0.94	+0.67	85
5,6-Me_2phen	453	20.4	608,625	1.81	+1.20	-1.34	-0.93	+0.80	85
3,4,7,8-Me_4phen	438	24.5	605,625	1.39	+1.02		-1.11		85
3,5,6,8-Me_4phen	440	19.8	605,625	2.22	+1.09		-1.04		85
4,7-Ph_2phen	462	32.8	605,625		+1.22	-1.31			85

Table 2 - Spectral and Electrochemical Properties of Ru(II) Complexes with Pi-acceptor Ligands in Aqueous Solution

Ligand (L)	Absorption		Emission (298K)		Ground State Redox Potentials (V vs. NHE)		Excited State Redox Potentials (V vs. NHE)		Ref.
	λ_{max} (nm)	ϵ(mM)	λ_{max} (nm)	τ(μs)	E(M/M+)	E(M/M-)	E*(M/M+)	E*(M/M-)	
[a]L(I), R=Ph n=2	540	17.1			+1.42	-0.90			86
[a]L(II), R=Me n=2	540	10.6			+1.26	-0.90			86
[a]L(III), R=H n=2	540	9.63			+1.43	-0.76			86
[b]$Ru(bpz)_3^{2+}$	443	15.0	603	1.04		-0.80		+1.30	88
[c]$Ru(terpy)_2^{2+}$	473	16.2	628	0.005	+1.25	-1.36			85
[d]$Ru(TPTZ)_2^{2+}$	501	19.2	505	0.005	+1.49	-0.77			85

a) L = 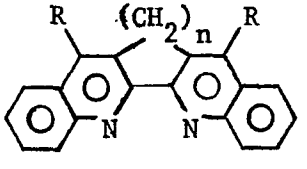

b) bpz = bipyrazyl

c) terpy = terpyridyl

d) TPTZ = 2,4,6-tri-(2-pyridyl)-s-triazine

type. Note that for the tris-bipyrazyl(bpz) and bis-terpyridyl(terpy) complexes the lowest energy absorption maxima and the emission maxima are found in the region of the spectrum associated with the MLCT absorption, and charge-transfer luminescence, respectively, in ruthenium(II) bpy and phen complexes. This is not a surprising consequence, considering the similarity in structure of the bpz and terpy ligands to that of bpy. On the other hand, the 2,4,6-tri-(2-pyridyl)-s-triazine(TPTZ) and the L complexes listed on Table 2 display absorption and luminescence properties rather unlike those exhibited by bpy and phen complexes. For example, none of the L complexes display emission at 298K. The TPTZ complex emits, although with a relatively short lifetime and from an excited state that is of considerably higher energy than the MLCT states of bpy and phen complexes of ruthenium(II). The sharp contrast between the properties of the TPTZ and L complexes and those of Ru(II) complexes of bpy and phen and their substituted analogs implies the potency of synthesis of new pi-acceptor ligands for coupling to Ru(II) as a chemical modification strategy.

The variation in properties of the metal complex with the nature of the ligand suggests that metal-ligand bonding is important in determining properties. If that is the case, then identifying the nature of key metal-ligand interactions and the evaluation of their role in determining properties is a prerequisite for devising a rational

chemical modification strategy. Unfortunately, until now the establishment of clear-cut relationships of this nature has proved elusive. For example, several workers have unsuccessfully attempted to correlate MLCT absorption band energies[89] and ground state redox potentials[90,91] of ruthenium(II) complexes with the degree of metal-ligand pi-bonding. This failure is due, in part, to the inability to develop a reliable method for assessing metal-ligand pi-bonding. Factors other than pi-bonding may be involved in determining properties such as luminescence, excited state energy, and redox potentials of both the ground and excited states.

Therefore, it is worthwhile to synthesize new pi-acceptor ligands to be coupled to Ru(II) as well as to other transition metals, in order to identify the factors responsible for spectral, electrochemical, and photohysical properties in transition metal complexes. Ultimately, the intention is to be able to tune these properties to meet specific requirements. Chemical modification via the synthesis of new pi-acceptor ligands is potentially a very powerful tool if it allows for the tuning of properties over a broader range than that which is accessible through the addition of various substituents on the periphery of the bpy and phen ligands.

Data that is available for a large number of ruthenium(II) complexes with many different pi-acceptor ligands suggest that, for the most part, these complexes are

distinguished by their ability to function either as oxidizing or reducing agents in the excited state. Simply by designing a ligand with the appropriate characteristics, one can, in principle, synthesize a ruthenium(II) complex which behaves as either an excited state oxidant or reductant, but not as both. This can be accomplished by a suitable chemical modification to obtain a complex with the desired excited state redox potentials. The two criteria which determine excited state redox potentials are (1) the ground state redox potentials and (2) the excited state energy.

Ground state reduction of ruthenium(II) complexes can be perceived as the addition of an electron to a ligand-centered π^* orbital. Consequently, the relative stability of the π^* orbital will be a determinant of the reduction potential, and the lower this orbital is in energy, the more easily the complex is reduced. Ground state oxidation of ruthenium(II) complexes involves the removal of an electron from a metal centered t_{2g} orbital. Since the relative stability of this orbital depends upon the ligands that are present, oxidation potentials are more sensitive to the ligand field strength than are the reduction potentials. Metal-ligand bonding will undoubtedly be an important determinant of oxidation potentials, however, the individual sigma and pi-bonding contributions cannot be readily evaluated.[92]

In the excited state, oxidizing and reducing power will be enhanced by, in essence, the excited state energy. Since the lowest lying excited state of a ruthenium(II) complex is the emissive LMCT state, in determining the excited state energy, the difference between the relative energies of the metal t_{2g} and ligand π^* orbitals will be important. In addition, the excited state energy is largely influenced by the degree of distortion from ground state geometry incurred in the emitting state. The latter, referred to as the Stokes shift, is the difference between the Franck-Condon maxima of the two states in absorption and emission,[22] and its magnitude increases with increasing distortion in the excited state. Consequently, decreasing the energy gap between the t_{2g} and π^* orbitals, and/or increasing the magnitude of the Stokes shift, tends to lower the excited state energy, and vice versa.

For a molecule to function in the excited state as either an oxidant or a reductant, but not both, it must be very difficult either to oxidize or reduce such a molecule in the ground state. A second requirement is for the excited state to be sufficiently low-lying such that the additional free energy that is provided for redox via excitation does not convert a poor oxidant or reductant into a powerful one in the excited state.

(ii) Ruthenium(II) Complexes with 2-(Phenylazo)pyridine

(a) Structure of the 2-(Phenylazo)pyridine Ligand

Recently, Krause and Krause reported the synthesis of ruthenium(II) complexes with the ligand 2-(phenylazo)pyridine or azpy, a bidentate nitrogen donor with a conjugated pi system.[93,94] In these respects, azpy can be considered as either a bpy or phen analog although, as shown in Figure 2, there are several structural dissimilarities to distinguish azpy from the latter two. Unlike bpy or phen, azpy possesses an azo (N=N) linkage. In addition, whereas bpy and phen are confined to being completely planar pi systems, azpy is a much less rigid ligand and appears capable of a larger degree of excited state distortion.

(b) Properties of $Ru(azpy)_2L^{n+}$ Complexes

The spectral and electrochemical properties of a series of mixed-ligand ruthenium(II) complexes, $Ru(azpy)_2L^{n+}$ (n=0-2), where L denotes a sequence of monodentate and bidentate coligands, are rather unique. A band appears in the IR spectra of all of the complexes, the frequency of which depends upon the coligand that is present. An apparent correlation of the frequency of this band, assigned to the N=N stretch of the azpy ligand, to the pi-acidity of the coligand suggests that the N=N stretching frequency is a useful probe of Ru(II)-azpy pi-bonding. The sensitivity of the N=N stretch to the nature of the coligand and profound differences between the spectral and electrochemical properties of these new Ru(II) complexes and their bpy and phen analogs are evidence for extensive

Figure 2

Structures of N-bidentate pi-acceptor ligands.

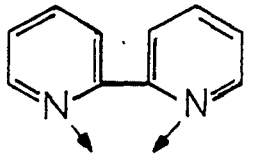

2,2' bipyridine
(bpy)

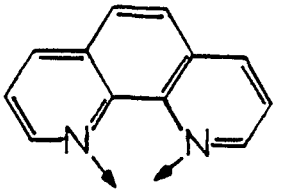

1,10 phenanthroline
(phen)

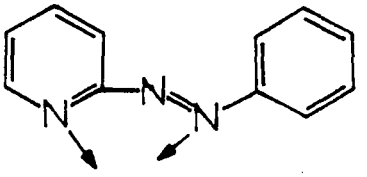

2-(phenylazo)pyridine
(azpy)

Figure 2

Ru(II)-azpy pi-bonding. This can be accounted for if azpy is a better pi-acceptor than both bpy and phen. The spectral and electrochemical properties of the $Ru(azpy)_2L^{n+}$ complexes,[94] listed in Table 3, also suggest a very unique photoinduced redox chemistry. A near-IR emission is displayed by most of the complexes at 298°K in the solid state, while four members of the series emit, albeit weakly, in room temperature fluid solution. The energies of the emission maxima indicate an unusually low-lying luminescent level for ruthenium(II) complexes of ca. 1.5 eV. Furthermore, oxidations of the Ru(II) azpy complexes are extremely unfavorable, while reductions are only mildly unfavorable (Table 3). Comparison of the redox potentials of the Ru(II) tris-complexes of azpy and bpy in aqueous solution at room temperature shows how a significant structural modification on the bpy ligand radically changes redox properties of the respective complexes. The $Ru(azpy)_3^{2+/+}$ potential is -0.30 V vs. NHE whereas that for the 2+/+ couple in the tris-bpy complex is -1.28 V.[49,59] The oxidation potential for the $Ru(bpy)_3^{2+/3+}$ couple is +1.26 V vs. NHE,[95,96] while no oxidation of $Ru(azpy)_3^{2+}$ was observed for applied potentials of up to +1.8 V vs. NHE.

(c) Prediction and Verification of Excited State Redox Properties of $Ru(azpy)_2L^{n+}$ Complexes

From calculation of the excited state redox potentials of $Ru(azpy)_3^{2+}$ an energy level situation where the

Table 3

Spectral and Electrochemical Properties of $Ru(azpy)_2L^{n+}$ Complexes

coligand (L)	E, V vs. SCE[a] III → II	E, V vs. SCE[a] II → I	Visible absorption[a] λ_{max}, nm ($10^{-3}\epsilon$, $M^{-1}cm^{-1}$)
azpy		0.06	498 (13.5)
btz	1.8[b]	-0.43[b]	515
bpy		-0.07	517 (11.6)
en		-0.31[b]	537
$2NO_2^-$		-0.46	538 (9.93)
$acac^-$	1.54	-0.38	565 (12.1)
$2CN^-$		-0.48	577 (16.4)
2tu	1.14[b]	-0.32[b]	585 (6.42)[b]
$2Br^-$	1.19	-0.54	590 (8.41)
$2N_3^-$	0.96	-0.52	615 (7.17)

a) in CH_2Cl_2, unless otherwise indicated.

b) in CH_3CN.

excited state is bracketed by the 3+ and 1+ redox states is predicted. Thus, oxidation of the excited state will be endergonic and $Ru(azpy)_3^{2+}$ should behave only as an excited state oxidant. Since the ground state oxidation potential exceeds +1.8 V, and the excited state energy is nearly 1.5 eV, oxidative quenching of $^*Ru(azpy)_3^{2+}$ demands a quencher with a reduction potential of greater than +0.3 V. On the other hand, reductive quenching of the excited state will be thermodynamically feasible for a quencher whose oxidation potential is less than +1.2 V. Experiments designed to test the calculated energy relationships between the various redox states of $Ru(azpy)_3$ involve investigation of luminescence quenching of the dicationic complex in fluid solution by both members of a series of one-electron reversible redox couples, e.g. the Fe^{2+}/Fe^{3+} couple. The so-called quencher pairs were chosen such that quenching can only occur via an electron transfer mechanism (oxidative or reductive), i.e. the lowest lying excited state of the quencher must lie well in excess of 1.5 eV above the quencher ground state, which is the approximate excited state energy of $^*Ru(azpy)_3^{2+}$, thus precluding an energy transfer quenching mechanism. The quencher couples range in reduction potential from -0.44 V (MV^{2+}/MV^+) to +1.61 V (Ce^{4+}/Ce^{3+}), therefore the data obtained from these quenching experiments provide some indication of the excited state redox potentials of $^*Ru(azpy)_3^{2+}$.

(d) Chemiluminescent Redox Reactions

$Ru(bpy)_3^{2+}$ in its oxidized and reduced forms undergoes thermally activated electron transfer reactions in solution, with subsequent light emission from the LMCT state, a phenomenon known as chemiluminescence.[97-108] Chemiluminescent reductions of $Ru(bpy)_3^{3+}$ by N_2H_4, $NaBH_4$, OH^-, and EDTA, to name a few, have been reported. Similar observations have been made for the action of oxidants upon $Ru(bpy)_3^{+}$. In chemiluminescent reactions of $Ru(bpy)_3^{3+}$ and $Ru(bpy)_3^{+}$, a significant thermodynamic barrier has to be overcome in order to generate the LMCT state through which the emission is observed. Another requirement to observe chemiluminesce is that the redox reaction be very rapid such that a significant population of excited states is achieved within the lifetime thereof. If $Ru(azpy)_3^{3+}$ is indeed unstable with respect to the $Ru(azpy)_3^{2+}$ LMCT excited state, the thermodynamic criterion for chemiluminescence is satisfied by even the weakest of reducing agents. The only remaining requirement for the chemiluminescent reduction of $Ru(azpy)_3^{3+}$ is favorable kinetics. Reductive chemiluminescence of $Ru(azpy)_3^{3+}$ can be investigated by generating the oxidized complex and reducing it in situ.

(e) Resonance Raman Spectra of $Ru(azpy)_2L^{n+}$ Complexes

Resonance Raman spectroscopy is very useful in the structural characterization of molecular excited states.

The resonance effect provides intensity enhancement of Raman bands assignable to the molecular coordinates which undergo the most distortion in an electronic transition associated with a visible absorption band that is "pumped" via laser excitation.[109] Ru(II) complexes with bpy and phen and their analogs typically exhibit very intense visible absorption bands assigned to MLCT transitions from the Ru(II) t_{2g} orbital to the ligand π^* orbital. Therefore, the resonance Raman spectra obtained on excitation into the visible absorption band in these complexes reveal that electron density is transferred from the metal to the ligand in the MLCT excited state and is distributed throughout the periphery of the pyridyl rings.[110] The resonance Raman spectra of the $Ru(azpy)_2L^{n+}$ complexes not only draw a picture of the excited state, but also aid in assigning the nature of the transition which gives rise to the intense, visible absorptions. On the basis of their high extinction coefficients and comparison to spectra of Ru(II) complexes with bpy and phen, these are presumably MLCT transitions, Ru(II) $t_{2g} \rightarrow$ azpy π^*, although the distribution of electron density in the excited states of the azpy complexes is found to be somewhat different from that in the bpy and phen complexes.

C. $Ru(bpy)_3^{2+}$ as a Photosensitizer in Solar Energy Conversion of H_2O into H_2 and O_2

(i) Water Cleavage with Visible Light

The extensive photoinduced redox chemistry exhibited by $Ru(bpy)_3^{2+}$ has prompted a number of investigations concerning the utilization of this complex as a photosensitizer in the conversion and storage of visible light energy.[111] The bulk of the studies of this nature involve the photodissociation of H_2O into H_2 and O_2. This decomposition process can be divided into two half-cell reactions:

$$2e^- + H_2O \longrightarrow 2OH^- + H_2 \qquad (6)$$

$$2H_2O \longrightarrow 4H^+ + O_2 + 4e^- \qquad (7)$$

As indicated in reactions 6 and 7, the generation of a molecule of hydrogen or oxygen involves multielectron transfers ($2e^-$ per H_2 and $4e^-$ per O_2) and the redox potentials for the above processes are -0.41 V and -0.82 V vs. NHE, respectively, at pH 7. From the thermodynamic standpoint, cleavage of H_2O should be possible with light of $\leq$1000 nm, using 4 photons to oxidize H_2O to one molecule of O_2.[111] Since H_2O is transparent to visible and near-UV light, a suitable system which utilizes solar energy to carry out H_2O decomposition requires the presence of a dye sensitizer to capture light energy and transfer it to the aqueous medium.

(ii) Types of Light Harvesting Units

(a) Sensitizer-Relay System

Three suitable light-harvesting units which employ a photosensitizer have been investigated and are depicted in

Figures 3 and 4. Figure 3 shows a two-component system consisting of a sensitizer (S) and an electron relay (R). Absorption of a photon by S with subsequent electron transfer to R results in the formation of 2 very energetic radical ions, S^+ and R^-. Thus, light functions as a pump which operates against a chemical potential gradient. Alternatively, the excited state of the sensitizer can oxidize a relay to produce S^- and R^+. If the driving force exceeds +0.3 V, the photoinduced redox reaction between S and the relay is expected to nearly diffusion controlled. On the other hand, the thermal back electron transfer reactions,

$$S^+ + R^- \longrightarrow S + R \qquad (8)$$

or

$$S^- + R^+ \longrightarrow S + R \qquad (9)$$

which are extremely exergonic, are almost always diffusion controlled. This tendency to back-react to regenerate the original S-R pair imposes severe limitations upon solar energy conversion in that the lifetimes of the radical ion intermediates are at most several milliseconds under solar irradiation. Thus, only the net conversion of solar energy into heat is accomplished. Methods which aim to retard undesirable thermal electron transfer reactions can involve well-conceived heterogeneous systems.

(b) Colloidal Semiconductor System

A typical heterogeneous light harvesting unit suitable for H_2O cleavage is depicted in Figure 4. In this

Figure 3

Sensitizer-relay system for water cleavage with visible light.

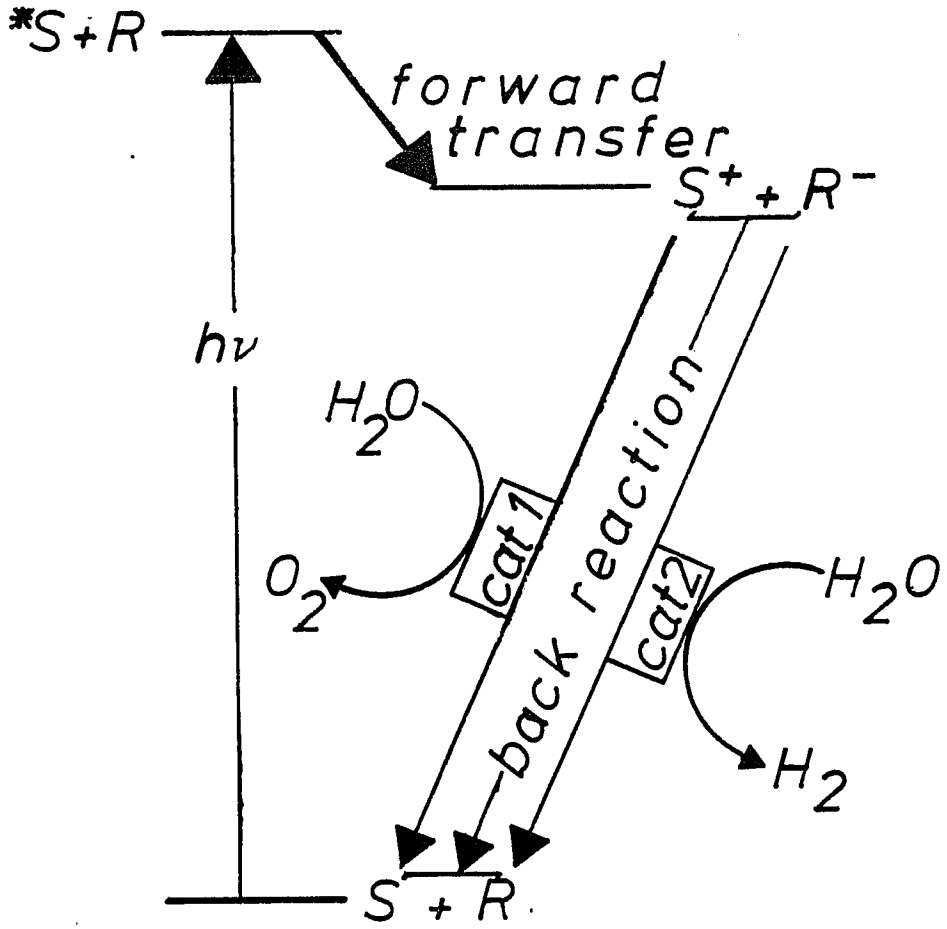
*S+R
forward
transfer
S+ + R-
hν
H2O
cat1
O2
back reaction
cat2
H2O
H2
S + R

Figure 3

system, the sensitizer is adsorbed directly onto a colloidal semiconductor particle, and no electron relay is necessary. A wide bandgap semiconductor is desirable in order to suit the thermodynamic requirements for water cleavage (vide infra). Since such a material is normally tranparent to visible and near-UV light, a dye sensitizer is needed to absorb solar energy and transfer it to the semiconductor particle. The excited state of the sensitizer injects an electron into the conduction band (CB) of the semiconductor where it is channeled to a catalytic site for H_2 generation. At a separate site on the semiconductor particle, a second catalyst mediates the formation of oxygen from the oxidized sensitizer, whereby the original sensitizer is regenerated.

(c) Dye-Sensitized Electrode System

An alternative to the use of dye sensitized colloidal semiconductors to carry out water photolysis, involves the adsorption of dye molecules onto an electrode surface. A thin surface coating of the dye improves the response of a wide-bandgap semiconductor (≥ 3 eV) electrode to visible light. The individual electron transfer processes in this system are analogous to those of the colloidal system, where a semiconductor electrode replaces the semiconductor particle in Figure 4.

(iii) Energetic Constraints upon Selection of Sensitizer and Electron Relay or Semiconductor

Figure 4

Sensitizer-colloidal semiconductor system for water cleavage with visible light.

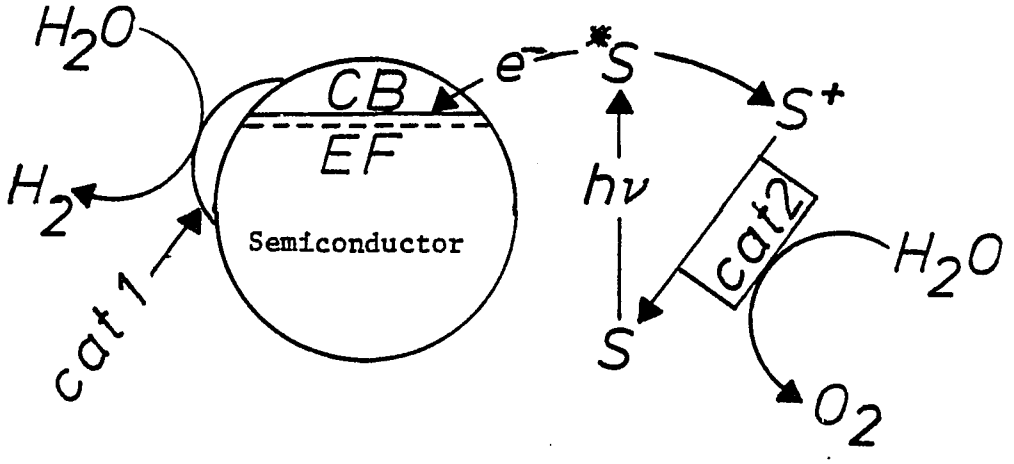

Figure 4

For any of the situations outlined above the choice of sensitizer and acceptor (relay or semiconductor) is subject to certain thermodynamic requirements. In a sensitizer/relay system, the redox properties of the sensitizer and the relay must be suitable for each of the fuel producing transformation steps. At pH 7, the redox potentials for the H_2 and O_2 half-reactions are -0.41 V and -0.82 V vs. NHE, respectively. If the reduced relay is to function as H_2O reductant, E^o (R^-/R) must be >+0.41 V. Similarly, for the oxidized sensitizer to oxidize H_2O, E^o (S^+/S) must be >+0.82 V. In addition, the excited state oxidation potential of the sensitizer must be compatible with the reduction potential of the relay for oxidative quenching to be realized. In systems which utilize a semiconductor particle or electrode, the sensitizer excited state must lie energetically above the conduction band of the semiconductor for electron injection to occur. Furthermore, the oxidized sensitizer must satisfy the identical criteria for redox potentials as in the sensitizer/relay system, and the conduction band of the semconductor must lie at a potential more negative than the redox potential of the ($2H^+/H_2$) couple for the simultaneous oxidation and reduction of H_2O to be thermodynamically feasible.

In addition to meeting the thermodynamic requirements outlined above, $Ru(bpy)_3^{2+}$ features other properties which make it an ideal sensitizer of visible light energy.

The complex displays a broad, intense absorption in the visible spectrum, and can thus capture a large portion of the incident radiant energy. The LMCT state is formed with nearly unit efficiency[18,29] and is sufficiently long-lived in room-temperature aqueous solution (t = 620-ns) for quenching by electron transfer reagents to occur readily.

(iv) Review of Previous Studies of $Ru(bpy)_3^{2+}$ in Water Photolysis

(a) Sensitizer-Relay Systems

A number of electron relay molecules can be employed with $Ru(bpy)_3^{2+}$ as the sensitizer. Since $Ru(bpy)_3^{3+}$ and $Ru(bpy)_3^{+}$ can oxidize and reduce H_2O, respectively, sensitizer/relay systems based upon either oxidative or reductive quenching of $^*Ru(bpy)_3^{2+}$ can be envisioned. Among the $Ru(bpy)_3^{2+}$/relay systems investigated, the relay compounds include most notably, the viologens,[112-114] Eu^{3+} and V^{3+}, and their respective salicylate complexes,[115] $Ru(bpy)_3^{3+}$,[116,117] and cobalt complexes.[118]

In a typical sensitizer/relay system, $Ru(bpy)_3^{2+}$ is excited by visible light and subsequently reduces methylviologen (MV^{2+}):

$$Ru(bpy)_3^{2+} + MV^{2+} \xrightarrow[k_{th}]{h\nu} Ru(bpy)_3^{3+} + MV^{+} \qquad (10)$$

In the presence of a colloidal Pt catalyst water reduction occurs:

$$MV^{+} + H_2O \xrightarrow{Pt} MV^{2+} + OH^{-} + 0.5H_2 \qquad (11)$$

An excess of an electron donor, e.g. ethylenediaminetetraacetate (EDTA), is needed not only to regenerate $Ru(bpy)_3^{2+}$, but also to prevent the diffusion controlled thermal back reaction between photoproduced $Ru(bpy)_3^{3+}$ and MV^+ (reaction 10). EDTA is, therefore, a sacrificial reagent, acting as the ultimate electron source for photoreduction of H_2O, thereby being irreversibly consumed. Despite their sacrificial character, these systems provided useful information concerning the optimization of the water reduction catalyst. Catalytic activity was found to increase as the dimensions of the Pt particle decrease, and this knowledge was important for obtaining ultrafine Pt particles[119] which are excellent catalysts in the colloidal semiconductor water photolysis systems.[120]

(b) Colloidal Systems

The greatest advantage of the sensitizer/colloidal semiconductor system over the S/R system is in the ability to assemble the reagents and catalysts within a highly ordered and confined reaction volume. In such an environment, the goal of light-induced charge separation can be achieved without the need for diffusion of redox relays into and out of a solvent cage. Thus, undesirable thermal electron transfer reactions can be avoided by spatially arranging the reactants and catalysts to form reaction sites where H_2O cleavage can take place very efficiently. The employment of very active, highly selective catalysts

enhances the rates of desirable reactions, which then dominate over undesirable ones.

With regard to the semiconductors which can be used in colloidal systems, TiO_2 and $SrTiO_3$ powders show the most promise.[121,122] For efficient water photolysis with visible light in such a system, a sensitizer which is strongly adsorbed to the particle surface is required. Gratzel, et al, have reported cyclic water cleavage with visible light using a bifunctional redox catalyst, Pt and RuO_2, loaded onto the surface of a colloidal TiO_2 particle which contains an adsorbed $Ru(bpy)_3^{2+}$ surfactant derivative as a sensitizer.[123-125]

(c) Photoelectrochemical Cells

Spectral sensitization by $Ru(bpy)_3^{2+}$ and its surfactant derivatives of n-SnO_2,[126,127] n-TiO_2,[128] and n-$SrTiO_3$[129] electrodes has been verified by the observation of an anodic photocurrent whose action spectrum matches the absorption spectrum of the dye. These reports generated interest in the utilization of surface-modified electrodes in photoelectrochemical cells (PEC) that convert visible light energy into storeable chemical fuels. Cyclic water cleavage in a photoelectrochemical cell is ideal for the spatial separation of the two product gases, H_2 and O_2, in that the water oxidation and reduction half-cell reactions can take place in individual compartments. The failure to observe water cleavage in a PEC employing a dye-sensitized

electrode with no electron relay and in the absence of an externally applied potential is attributed to a poor match between the energy of the electrode conduction band and both the sensitizer excited state energy and the potential of the ($2H^+/H_2$) redox couple. The dye/semiconductor systems are ideal in that an electron relay is unnecessary since electrons are transferred between the dye molecule and the semiconductor in only one direction, and thus, thermal back transfer of electrons cannot occur.

D. $Ru(bpy)_3^{2+}$ in Heterogeneous Media

(i) Controlling Thermal Reversibility of Photoredox Reactions

In an attempt to control the thermal reversibility of photoinduced redox reactions of $Ru(bpy)_3^{2+}$, there has been a movement towards examining the photophysical properties of the complex in heterogeneous media, where the underlying strategy involves the physical separation of $Ru(bpy)_3^{2+}$ and quencher molecules. In addition to the studies involving semiconductor powders and electrode surfaces outlined above, there have been a number of investigations of $Ru(bpy)_3^{2+}$ in a wide diversity of heterogeneous media, including cation exchange resins,[130] Zeolites,[131,132] micelles,[133,134] clays,[135,136] and membranes.[137] The photophysical properties and luminescence quenching behavior in several of these media is observed to be quite different from fluid solution. Although it remains to be seen whether or not

heterogeneous media are the solution to the dilemma of control of reaction reversibility, it is worthwhile to consider $Ru(bpy)_3^{2+}$ in new environments.

(ii) Nature of the Porous Vycor Support

An ideal medium in which to study the photophysics and photochemistry of a supported metal complex, e.g. $Ru(bpy)_3^{2+}$, is one that is transparent to visible light. The support should permit easy access of reagents to $Ru(bpy)_3^{2+}$ so that photochemical properties, e.g. luminescence quenching, can be readily investigated. Preferably, the support should be inert such that, on adsorption to the support, the primary coordination sphere of the metal complex remains intact.

Porous Vycor glass (PVG) satisfies all of the above criteria, and is best described as a surface hydroxylated, transparent ($\lambda \geq 290$ nm), support material containing a myriad of 70 ± 20 A° cavities or pores interconnected throughout the glass in a random three-dimensional array.[138,139] Although they are manufactured by different processes, PVG and silica gel are alike in many respects. Both materials possess similar pore sizes and surface silanol groups, although the number of silanol groups per unit area (silanol number) depends upon hydration and prior heating.[140] The silanol groups of PVG are slightly acidic[141] and cation exchange with ions in fluid solution occurs readily.[142,143] While the intent of this comparison is not to suggest that the two materials

are equivalent, there are many structural similarities between porous Vycor and silica gel so that, in a general sense, porous Vycor can be viewed as a transparent form of silica gel.

(iii) Photophysical Properties of $Ru(bpy)_3^{2+}$ Bound to PVG

Earlier studies in this laboratory established that $Ru(bpy)_3^{2+}$ cation exchanges onto PVG by binding to anionic silanol sites.[144] UV-VIS absorption, luminescence, and resonance Raman spectra of the adsorbed complex are quite similar to spectra of the complex in either aqueous or alcoholic solutions. These observations are consistent with the presence of silanol sites from PVG in the secondary coordination sphere of the adsorbed complex and furthermore, establish that the structural integrity of the complex remains intact upon adsorption onto PVG.

Despite the apparent similarities in properties of $Ru(bpy)_3^{2+}$ in PVG to those in fluid solution, the adsorbed complex does exhibit several unique characteristics which are directly attributable to the nature of the PVG environment. On excitation in vacuo with a low intensity pulse of visible light, the luminescence of the adsorbed complex decays exponentially with a lifetime of 740±20 ns, which is well within the range of lifetimes found for $^*Ru(bpy)_3^{2+}$ in deaerated fluid solution.[38,63] However, if excited via a high intensity source, the observed emission spectrum of $Ru(bpy)_3^{2+}$ is quite different from that in fluid solution, displaying what

appear to be two bands instead of one.[145] Furthermore, under high intensity irradiation the luminescence decay of the LMCT state in PVG is non-exponential.

(iv) Photoinduced Disproportionation of $Ru(bpy)_3^{2+}$ in PVG

The photoinduced disproportionation of $Ru(bpy)_3^{2+}$ in PVG[146] proceeds via a mechanism that involves a biphotonic ionization of $Ru(bpy)_3^{2+}$ with subsequent reduction of another molecule of $Ru(bpy)_3^{2+}$ by $e^-(aq)$:

$$\text{(a)}\quad Ru(bpy)_3^{2+} \xrightarrow{2h\nu} Ru(bpy)_3^{3+} + e^-(aq)$$

$$\text{(b)}\quad e^-(aq) + Ru(bpy)_3^{2+} \longrightarrow Ru(bpy)_3^{+}$$

$$2Ru(bpy)_3^{2+} \xrightarrow{2h\nu} Ru(bpy)_3^{+} + Ru(bpy)_3^{3+} \qquad (12)$$

A biphotonic ionization of $Ru(bpy)_3^{2+}$ has already been observed in flash photolysis and pulse radiolysis of aqueous solutions of the complex, although most of the effective photolyzing light was found to be in the range 300-340 nm.[96] Alternative mechanisms have been postulated for the disproportionation of the dication in other heterogeneous media. For instance, the fast component of a non-exponential decay for $^*Ru(bpy)_3^{2+}$ in cellulose[147] is attributed to triplet-triplet annihilation, which is followed by electron transfer leading to disproportionation of the dication:

$$\text{(a)}\quad 2Ru(bpy)_3^{2+} \xrightarrow{2h\nu} 2\,^*Ru(bpy)_3^{2+}$$

$$\text{(b)}\quad 2\,^*Ru(bpy)_3^{2+} \longrightarrow Ru(bpy)_3^{+} + Ru(bpy)_3^{3+}$$

$$2Ru(bpy)_3^{2+} \xrightarrow{2h\nu} Ru(bpy)_3^{+} + Ru(bpy)_3^{3+} \qquad (13)$$

Rabani et al proposed triplet-triplet annihilation in anionic SDS micelles,[148] occuring this time by energy transfer. This was later confirmed by the observation of a very similar non-exponential decay exhibited by $^{*}Ru(bpy)_3^{2+}$ in this medium.[149] Apparently, the high local concentrations of reactants that are required for annihilation can be achieved in cellulose and in micelles. In contrast to the latter media, once adsorbed to PVG, $Ru(bpy)_3^{2+}$ exhibits no evidence of macroscopic diffusion and thus, spatial separation of reactants via anchoring to the support probably accounts for the absence of a triplet-triplet annihilation mechanism for the disproportion in PVG.

The limitations imposed by the glass environment upon diffusion is evidenced by the unusual stabilities of the photoproducts of the disproportionation. Thus, the spectrally quantitated lifetime of $Ru(bpy)_3^{+}$ in PVG is >36 hours in vacuo,[146] which is considerably longer than its lifetime of milliseconds in fluid solution.[96] Since $Ru(bpy)_3^{3+}$ absorbs only very weakly, $\varepsilon_{675nm} = 436\ M^{-1}cm^{-1}$,[150] a spectral determinantion of its lifetime is difficult. With diffusion virtually nonexistent, species which tend to react at diffusion controlled rates in fluid environments display unusually long lifetimes in PVG. Consequently, PVG can function as a room temperature isolation matrix.

The quantum yield for the formation of $Ru(bpy)_3^+$, which is determined spectrally, depends critically upon the amount of adsorbed $Ru(bpy)_3^{2+}$, attaining a maximum at a concentration where the mean separation between the $Ru(bpy)_3^{2+}$ molecules in PVG is ca. 50 A^o.[146] If the reacting centers are situated in closer proximity, the thermal back electron transfer between the products of the disproportionation reaction to regenerate the 2 $Ru(bpy)_3^{2+}$ molecules (reaction 12) becomes significant, and the quantum yield of $Ru(bpy)_3^+$ declines. On the other hand if the reacting centers are further apart than 50 A^o, the available driving force is insufficient to promote electron migration from the donor to the acceptor. Since the adsorbed photoproducts are cationic, they are probably unable to diffuse due to electrostatic interaction with silanol sites. Thus, a means is established whereby, in PVG, the rate of a thermally activated reaction can be retarded by physically separating the reactants by an appropriate distance. Ideally, one may be able to construct a reactive site within the cavities of PVG which meets desired specifications for spatial arrangement of the reactants. A situation can be envisioned in which a reaction center which mimics the lamellae of plants carries out the photosynthesis of energy rich molecules.[111] Since $Ru(bpy)_3^{3+}$ and $Ru(bpy)_3^+$ are powerful oxidant and reductant, respectively, which, when bound within the PVG environment

at a suitable distance apart, are stable for many hours, it is worthwhile to investigate this system for its enormous potential in the conversion of solar energy.

A method to further enhance the photoinduced electron transfer, and at the same time retard the back reaction is to combine the strategies of the dye-sensitizer/semiconductor electrode system with that of the diffusion free environment of PVG. As mentioned above, $Ru(bpy)_3^{2+}$ photosensitizes wide bandgap semiconductor electrodes, e.g. n-SnO_2, via electron injection into the conduction band of the latter.[126,127] Since the electron transfer occurs only in the light-driven direction, i.e. there is no reverse electron transfer from the semiconductor to the dye, a semiconductor is an ideal mediator of photoredox reactions. The thermal back reaction can be avoided by separating the donor and acceptor by a suitable distance. This effect has already been domonstrated in the photoinduced disproportionation of $Ru(bpy)_3^{2+}$, where the quantum yield of $Ru(bpy)_3^{+}$ is very sensitive to the spacing of the reacting molecules.[146] This quantum yield as a function of the distance between $Ru(bpy)_3^{2+}$ centers in PVG has been determined in the presence of n-SnO_2 conducting thin films which were deposited on the PVG surface via a spray pyrolysis technique.[151,152] Since the redox reaction between the two excited states presumably involves electron migration it was anticipated that the amount of

adsorbed complex giving the maximal quantum yield of $Ru(bpy)_3^+$ would remain essentially the same. However, at lower impregnation levels where the mean separation between adsorbed $Ru(bpy)_3^{2+}$ molecules exceeds 50 A^o, the quantum yield was expected to be increased due to the enhanced conductivity of the PVG surface, in tandem with the decreased facility of the thermal back reaction at larger reactant separation distance.

(v) Quenching of $^*Ru(bpy)_3^{2+}$ Luminescence in Heterogeneous Media

(a) Diffusional (Dynamic) vs. Non-diffusional (Static) Quenching

Luminescence quenching of $Ru(bpy)_3^{2+}$ by various redox reagents has been investigated in a number of heterogeneous media.[130,131,134,135,137] The quenchers which have been studied include primarily the more familiar quenchers of the complex in fluid solution, i.e. viologens, metal cations, and molecular oxygen.

In heterogeneous media, two types of quenching mechanisms can be envisioned.[153a,154] If the relative positions of the donor and acceptor are fixed at the instant quenching occurs, the mechanism is said to be static. Since static quenching occurs without diffusion, it exhibits no time dependence, i.e. there is no change in the excited state lifetime. Diffusional type quenching requires a collisional encounter between the donor and acceptor, and the mechanism is referred to as dynamic. For dynamic quenching to occur, the quencher and donor must meet within

the lifetime of the excited state, and therefore the lifetime of the donor emission is curtailed. Both static and dynamic quenching reduce the steady state emission intensity, since both decrease the number of molecules in the excited state. Thus, it is possible to distinguish between the two quenching mechanisms by measuring both the emission intensity and the emission lifetime for a given amount of quencher. Although the nature of heterogeneous media is such that adsorbed molecules can be fixed to the support, there are also diffusional processes taking place. If the supported species is in equilibrium with another phase (liquid or gas), there is constant diffusion of molecules to and from the solid phase from the surrounding medium.[155a] As a result, both static and dynamic quenching can be envisioned for a quencher in equilibrium between an adsorbed and a non-adsorbed state. Molecules which are adsorbed can diffuse within the support if the binding interaction is weak. Indeed, two independent groups of investigators have observed dynamic quenching of $Ru(bpy)_3^{2+}$ luminescence in cation exchange resins by co-adsorbed ions, which quite possibly suggests the mobility of the ions in the resin phase.[130,156] Quenching of $^*Ru(bpy)_3^{2+}$ by metal ions in colloidal clays proceeds via a purely dynamic mechanism.[157] It is surprising, particularly in cation-exchange resin, where electrostatic attraction to the support should severely restrict diffusion of adsorbed metal cations, that no component attributable to static quenching was found.

(b) Kinetics of Quenching in Heterogeneous Media

The kinetics of quenching of $^{*}Ru(bpy)_3^{2+}$ are sensitive to the nature of the surrounding medium. In both membranes and micelles, non-homogeneous quenching behavior occurs as the rate of quenching approaches the diffusion controlled limit, and deviations from Stern-Volmer behavior are observed.[137,158-160] These results suggest that the presence of a phase boundary separating donor and acceptor molecules leads to unusual types of quenching behavior, reflecting the constraints imposed upon accessibility of quencher molecules to excited molecules.

It is worthwhile to investigate quenching of $^{*}Ru(bpy)_3^{2+}$ in different media. Being strongly luminescent in virtually all of the media in which it has been investigated, $Ru(bpy)_3^{2+}$ can serve as a useful probe of excited state quenching phenomena in heterogeneous systems.

(c) Quenching by Gases

The quenching of $^{*}Ru(bpy)_3^{2+}$ in a support medium by gaseous molecules is one type of investigation which one might like to undertake. Quenching of an excited molecule by gases in fluid solution is limited not only by diffusion, but more importantly by the solubility of the gas. Furthermore, solvolysis can radically change the properties of the gas molecule. Since gases are readily adsorbed to porous solids, reactions which are difficult to effect in solution can be more efficiently carried out in a porous support medium.

Quenching of the MLCT state of $Ru(bpy)_3^{2+}$ adsorbed to porous Vycor by the gases O_2, SO_2, and N_2O have been examined, in the hopes of observing a reactive quenching encounter. Molecular oxygen is a well-studied efficient quencher of the MLCT state in fluid solution.[64,82,84,161-163] Investigation of quenching by N_2O is worthwhile since it is a rather unreactive gas[164] which can function as an electron scavenger.[165,166] SO_2 is an air-pollutant which originates primarily from the combustion of sulfur-containing fossil fuels.[167] Quenching by SO_2 via electron transfer suggests a possible route towards the photoconversion of this undesirable air pollutant to the more useful sulfuric acid.

In order to establish the nature of the quenching process for each gas, intensity and lifetime quenching measurements have been made. The data from adsorption measurements for the complex and the gases provide valuable information concerning the distribution of the reagents on the glass, and in conjunction with the quenching data, are helpful in distinguishing features of the quenching process in PVG.

II. Experimental

A. Studies in Porous Vycor Glass

(i) Materials

$[Ru(bpy)_3]Cl_2 \cdot 3H_2O$ was prepared according to the procedure of Palmer and Piper,[19] and the UV-VIS absorption spectra of the twice recrystallized complex agreed with published spectra.[18]

All gases were obtained from the Linde Corporation and with the exception of argon, were used without further purification since the purity levels of each exceeded 99%. Argon was dried by passage through a 6" x 1" column of either $CaSO_4$ or $Mg(ClO_4)_2$. O_2 was removed from argon by scrubbing the gas with a solution of Cr^{2+}.

95% aqueous ethanol (reagent grade) required no further purification. Reagent grade isopropanol and methanol were dried by reflux over Linde 4A molecular sieves and were subsequently distilled, immediately prior to use. H_2O was distilled in a Corning distillation apparatus and stored in polyethylene containers. All remaining chemicals were reagent grade and were used as received from commercial suppliers.

Porous Vycor glass, code no. 7930, was received from the Corning Glass Company in the form of 30-cm x 30-cm x 4-mm sheets. Samples of the glass for impregnation with reagents were obtained and pretreated in the following manner. The glass sheet was immersed in water to saturate

the pore volume, and then cut into 25-mm x 25-mm sections with a water/oil-cooled tungsten carbide saw. The cutting oil was rinsed from the cut glass by Soxhlet extraction for 6 hours with hot distilled water, after which the glass was heated to 40°C under reduced presssure to remove bulk adsorbed water. When the glass became completely transparent, an indication that bulk water is no longer present, it was placed in a muffle furnace. The furnace temperature was increased from 25° to 550°C at a rate of ca. 100°C/hour. Moderately increasing the temperature prevents cracking of the glass induced by rapid release of adsorbed H_2O molecules. As the glass is heated, it begins to char, eventually becoming transparent, indicative of the burning of carbonaceous impurities which are adsorbed to the glass. The glass was maintained at 550°C until immediately prior to its impregnation with reagents.

(ii) Impregnation of PVG

(a) General Procedure for Adsorption from Solution

Impregnation of porous Vycor with compounds that are low vapor pressure solids at room temperature involves adsorption from a solution of the compound. One to three clean PVG samples were weighed and mounted upright in an Eastman Kodak Chromagram Developing Jar (catalogue no. 3256) containing 50 or 100 ml of the adsorbate solution. After several hours, equilibration of the glass with the solution was attained,[168] and the samples were removed

from the solution and rinsed with the solvent to prevent a layering of the adsorbate on the glass surface. The solvent was then removed from the glass by pumping under vacuum.

To obtain the number of moles adsorbed per gram of PVG the absorbance of the adsorbate solution was recorded at a convenient wavelength before and after impregnation, correcting the absorbance for the change in solution volume owing to pore penetration by the solvent. The number of moles adsorbed, n_{ads}, is given by

$$(OD_i - OD_f/OD_i) \times n_i \qquad (14)$$

where OD_i and OD_f are the volume corrected optical densities at the monitoring wavelength, before and after impregnation, respectively, and n_i is the number of moles of adsorbate in the solution prior to impregnation. Dividing n_{ads} by the total weight of clean glass placed in the developing jar gives the number of moles adsorbed per gram of PVG. The PVG samples used weighed 4-6 grams, and loading levels ranged typically from 10^{-7} to 10^{-5} moles of adsorbate/gram PVG. The amount of adsorbate was purposely limited to allow measurement of absorption spectra of the impregnated glasses.

Glasses containing only $Ru(bpy)_3^{2+}$ were prepared according to the above procedure. The following sections describe the preparation of samples which contained, in addition to $Ru(bpy)_3^{2+}$, other reagents.

(b) Preparation of PVG Samples Containing SnO_2/1%Sb and $Ru(bpy)_3^{2+}$

A spray pyrolysis technique, similar to those previously described,[151,152] was employed to deposit transparent, conducting, thin films of SnO_2 doped with 1%Sb on one 25-mm x 25-mm face of 1-mm thick PVG samples. An acidic methanol solution of Sn^{+4} and the dopant was prepared by dissolving one part $SbCl_3$ and 199 parts anhydrous $SnCl_4$, by weight, in methanol. The Sn^{4+} concentration in these solutions was typically ca. 1M. The solution was placed in a glass bottle equipped with a screw top consisting of a pump handle and a fine nozzle. Squeezing the handle produces a fine mist of the Sn^{4+}/Sb^{3+} solution which was directed at a clean PVG sample situated face up in a beaker within a furnace at 600°C. This method yielded optically transparent ($\lambda \geq 350$-nm), conducting, thin films of SnO_2 doped with Sb. After deposition of the semiconductor film, these samples were impregnated with $Ru(bpy)_3^{2+}$ in the manner described above, to obtain samples containing 5.0×10^{-7} to 9.8×10^{-6} moles of the adsorbed complex/gm PVG.

(c) Preparation of PVG Samples Containing TiO_2 and Pt

Porous Vycor was impregnated with TiO_2 by equilibration of the glass with an acidic $Ti(i\text{-}OC_3H_7)_4$ solution prepared by dissolving anhydrous $TiCl_4$ in isopropanol.[169] The number of moles of Ti adsorbed was calculated via the spectroscopic method described above. The solvent was removed under reduced pressure, after which the glass was heated in air to

600° in a 3 zone Lindbergh Heavy-Duty furnace (Model 9744), raising the temperature of all 3 zones simultaneously at a rate of ca. 100°C/hour. The UV-VIS absorption spectra of the impregnated glasses were recorded before and after heating. This procedure yielded transparent glass samples ($\lambda \geq 350$-nm) containing from 10^{-7} to 10^{-5} moles of TiO_2/gm PVG.

Samples containing TiO_2 were impregnated with Pt by adsorption from aqueous 10^{-3}M solution of H_2PtCl_6, and the number of moles adsorbed were calculated as described above. The glass was then heated in air to 200°C in a 3 zone furnace. The addition of an external reducing agent, necessary for the formation of a Pt sol,[124,125] was not required for the deposition of Pt in PVG. Absorption spectra recorded at intervals during heating showed a gradual increase in optical density throughout the entire visible spectrum. When no spectral change was detected over a period of 1 hour, the blackened, platinized glass was removed from the furnace. Glass samples for spectral sensitization studies were then impregnated with $Ru(bpy)_3^{2+}$ in the manner described above.

(iii) Mounting of Impregnated Samples in Cells

An impregnated PVG sample was rigidly mounted in an upright position with a Teflon holder in a 3-cm x 4-cm x 1-cm pyrex cell such that the 25-mm x 25-mm face of the sample was parallel to the 3-cm x 4-cm windows of the cell.

For UV spectra and UV photolyses, a quartz cell of similar dimensions was used. Both quartz and pyrex cells are equipped with a 2" diameter O-ring joint for mating to an upper section which has a hi-vacuum stopcock and a 10/30 joint. The latter joint was used to attach the cells to a vacuum line for evacuation and introduction of gases. The lower and upper sections of the cell were fastened by 2" diameter aluminum rings held together with 3 screws and nuts.

(iv) Instrumentation and Physical Measurements

(a) Electronic Absorption Spectra

Electronic absorption spectra were recorded on a Cary 14 spectrophotometer. To obtain spectra of impregnated PVG samples, the glass was mounted in a pyrex or quartz cell and the latter placed into a rectangular cell holder within the sample compartment such that the 25-mm x 25-mm face of the sample was perpendicular to the path of the spectrophotometer source beam. A clean piece of PVG was rigidly mounted in the reference compartment to compensate for absorption and scattering by the glass itself. Prior to impregnation, the absorption spectrum of the PVG sample was monitored versus the reference piece in order to obtain a baseline. Following impregnation and evaporation of the solvent, the absorption spectrum of the impregnated sample was taken, and the difference between this spectrum and the baseline spectrum gave the absorption spectrum of the adsorbate.

(b) Steady State Emission Intensities and Emission Spectra

Room temperature emission intensities and emission spectra of $Ru(bpy)_3^{2+}$ were recorded on a Perkin-Elmer Hitachi MPF-2A emission spectrophotometer equipped with a red-sensitive photomultiplier tube. To measure the emission from $Ru(bpy)_3^{2+}$ on the glass, the cell holder was adapted to rigidly hold the rectangular cell and the PVG sample within at an angle of 50° relative to the exciting light. The emission was monitored from the glass surface at an angle of 90° to the excitation.

(c) Emission Decay Measurements

Luminescence decays of adsorbed $Ru(bpy)_3^{2+}$ were monitored using the apparatus illustrated in Figure 5. The cell containing the glass sample was mounted in a rectangular holder within a sample compartment made of aluminum. The sample was excited perpendicular to the 25-mm x 25-mm face by a 2-ns FWHM light pulse from an Ortec Model 9352 nanosecond light pulser operated at 20 kHz with a continuous flow of prepurified N_2 gas. The pulses consist predominately of 337 and 358-nm light, the most intense lines in the N_2 emission spectrum. An Ortec Model 9290 high-voltage power supply charged the hot electrode to 8 kV. The emitted light at 90° relative to the excitation (from the 25-mm x 4-mm face of the glass) was passed through a Bausch and Lomb Model 33-86-76 grating monochromator set at 610 nm and was detected by an RCA Model C31034A photomultiplier tube. The latter was charged to

Figure 5

Block diagram of apparatus for measurement of room temperature luminescence lifetimes.

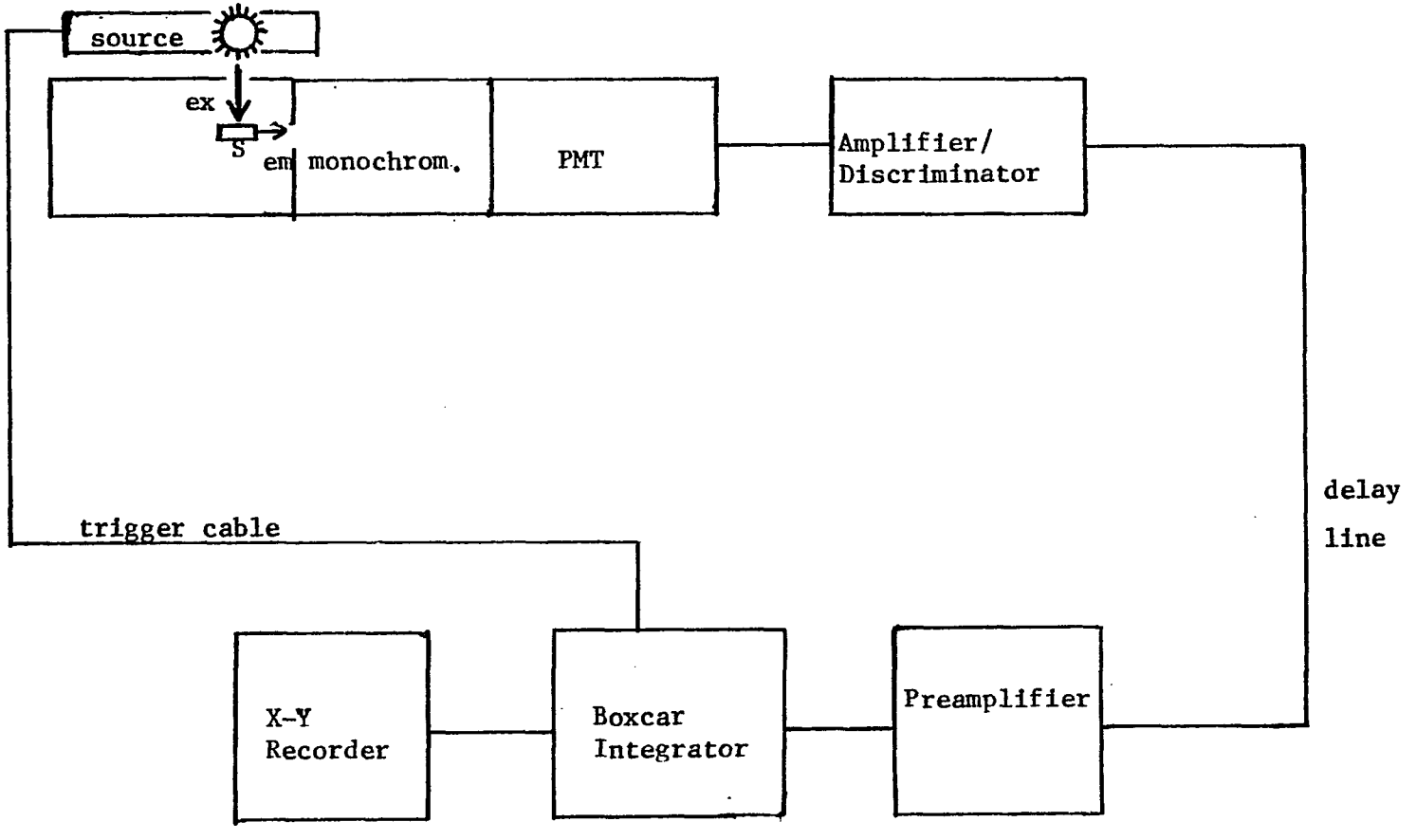
source
ex
S
em monochrom.
PMT
Amplifier/
Discriminator
delay
line
trigger cable
X-Y
Recorder
Boxcar
Integrator
Preamplifier

Figure 5

-1800 V by a Tennelec Model TC941 negative high-voltage power supply. The photomultiplier was mounted in a Pacific Precision Instruments Model 3470 AD/6 thermoelectrically cooled housing where its output was fed directly into a 100-fold amplifier/discriminator. The latter was set at a triggering threshold of 350 mv to maximize signal/noise triggering ratio. The 25-mV discriminator output pulses were fed into a PAR Model 115 wideband preamplifier to provide 10-fold amplification prior to being fed into a PAR Model 164 gated integrator module/Model 162 boxcar averager. The time resolved emission intensity was generated by triggering the boxcar averager scan across a 2 μsec time base via the negative output of the light pulser. Scanning is accomplished by sweeping a 50-nsec conducting aperture across the time base by means of a voltage ramp. The latter increases the delay between the trigger and the opening of the aperture on successive triggers. This process was repeated until the aperture had moved completely across the time base. Since the first aperture opening can occur no sooner than 75 nsec after the first trigger, the signal input to the gated integrator was delayed in order to monitor the rise of the emission. Sixty feet of RG 58/AU 50-ohm coaxial cable originating at the discriminator output and terminating at the preamplifier input served as a signal delay line.

Narrowing the aperture of the boxcar averager increases the signal/noise improvement ratio[170] however, the

amount of scan time that is necessary to resolve the input waveform is inversely proportional to the aperture width. Thus, for aperture durations of 50 nsec a 20-40 minute scan was required. At this scan rate, and a trigger repitition rate of 20 kHz, the number of aperture openings per scan is on the order of 10^7, and the signal/noise improvement ratio is ca. 200.[170]

The time resolved emission intensity was displayed on a Hewlett Packard Model 7044B X-Y recorder at the scanning rate by feeding the voltage output of the boxcar averager to the Y-input of the recorder and utilizing the 0-1 VDC scan ramp of the boxcar to generate the time (x) axis.

(v) Studies of Impregnated PVG Samples

(a) Distribution of $Ru(bpy)_3^{2+}$ on PVG

The cross-sectional distribution of $Ru(bpy)_3^{2+}$ adsorbed to porous Vycor was determined spectrophotometrically for glass samples containing from 10^{-7} to 10^{-5} moles of complex/gm PVG, by mapping the absorbance of the adsorbed complex at 500 nm as a function of relative sample thickness. Variable thicknesses of the samples were obtained by grinding the glass surface using 220 grit carborundum paper. The sample thickness was measured at various stages of grinding with a vernier caliper, after which the absorbance of the remaining adsorbed $Ru(bpy)_3^{2+}$ was recorded at 500 nm. Since grinding the PVG surface results in an immediate loss of transparency to visible light due to scattering, prior to

each spectral measurement the glass was immersed in chlorobenzene, whose refractive index, 1.532[171a], is very similar to that of the glass, 1.5.[172] When the ground glass is saturated with chlorobenzene it is completely transparent to visible light. Once grinding produced no further change in absorbance, the glass was turned over and the procedure was repeated for the opposite side. The absorbance was plotted as a function of relative sample thickness which is the ratio of the sample thickness at the time of the spectral measurement to the sample thickness prior to any grinding. For absorbance readings made after the glass was turned over, the thickness after grinding was corrected for the portion of the glass which was found not to contain any adsorbed complex, prior to calculating the relative thickness.

(b) Quenching of Luminescence of $Ru(bpy)_3^{2+}$ in PVG by Gases

To obtain data for quenching of the steady state luminescence intensity and the luminescence lifetime of $Ru(bpy)_3^{2+}$ in PVG, samples impregnated with $1.0\pm0.2 \times 10^{-6}$ moles of complex/gm of glass were rigidly mounted in a pyrex cell and equilibrated with various pressures of the gaseous quencher. The adsorption isotherm of each gas onto both clean PVG and impregnated samples was obtained at room temperature, $22\pm1^{\circ}C$, by a manometric method involving differential pressure measurements, detailed by Ross and Olivier.[155b] This procedure was repeated for each sample to obtain the adsorption isotherms concurrent

with the quenching data. To correct for adsorption onto surfaces other than the glass sample, which occurs principally with SO_2, adsorption measurements were made both in the presence and absence of the samples.

To obtain the quenched emission intensities, the impregnated samples, under various pressures of the gaseous quenchers, were excited at 420 nm and the emitted light was monitored at 620 nm, the emission maximum of adsorbed $Ru(bpy)_3^{2+}$.

Quenched emission lifetimes were obtained by monitoring the luminescence decays of impregnated samples in the presence of various pressures of quencher, using the apparatus described above (Figure 5).

(c) Luminescence Quantum Yield of $Ru(bpy)_3^{2+}$ on PVG

To calculate the quantum yield of emission for $Ru(bpy)_3^{2+}$ on the glass, a series of samples containing from 10^{-7} to 10^{-5} moles of the adsorbed complex per gram of PVG were prepared. For each sample, the absorbance at 450 nm of $Ru(bpy)_3^{2+}$ was recorded. The emission was then monitored at 620 nm, exciting the sample with 450-nm light. For glass samples where the absorbance at 450 nm was ≥ 4, it was assumed that all of the exciting light gets absorbed on the surface of the glass nearest to the source. Thus, to calculate the quantum yield on the glass, a $Ru(bpy)_3^{2+}$ solution of high optical density (absorbance = 4) was used as a standard. This was to insure that all of the exciting light was absorbed in a

very narrow path of the solution, such that light absorption in the solution nearly mimics light absorption on the outermost surface of the glass. To make certain that the exciting light was absorbed and the emitted light collected in a similar fashion, the glass samples and solution standards were placed in the spectrophotometer sample compartment in the following manner. A 1-mm cell containing a $Ru(bpy)_3^{2+}$ solution was degassed and mounted upright with a Teflon holder such that the front face of the cell was situated at the same distance from the excitation source as were the degassed PVG samples mounted in the pyrex cell. The solution standard or glass sample was situated at an angle of 50° relative to the exciting light, and the emitted light at 90° to the excitation was monitored off of its front face.

The emitted intensities from glass samples ranging in absorbance from 0.42 to 50, λ = 450 nm, were recorded and compared to those from $Ru(bpy)_3^{2+}$ aqueous solutions spanning a similar range in absorbance at 450 nm.

(d) Quantum Yield of Formation of $Ru(bpy)_3^{+}$ on PVG in the Presence of a Transparent, Conducting SnO_2 Thin Film

The apparatus for measuring the quantum yield of $Ru(bpy)_3^{+}$ appears in Figure 6. A series of PVG samples onto which a transparent, conducting SnO_2/Sb thin film had been deposited, were impregnated with from 5.0×10^{-7} to 9.8×10^{-6} moles of $Ru(bpy)_3^{2+}$/gm PVG. These samples were degassed, mounted in a rectangular

Figure 6

Block diagram of apparatus for simultaneous continuous laser photolysis and monitoring of spectral changes. Mono. = monochromator; Rec. = chart recorder; M = mirror.

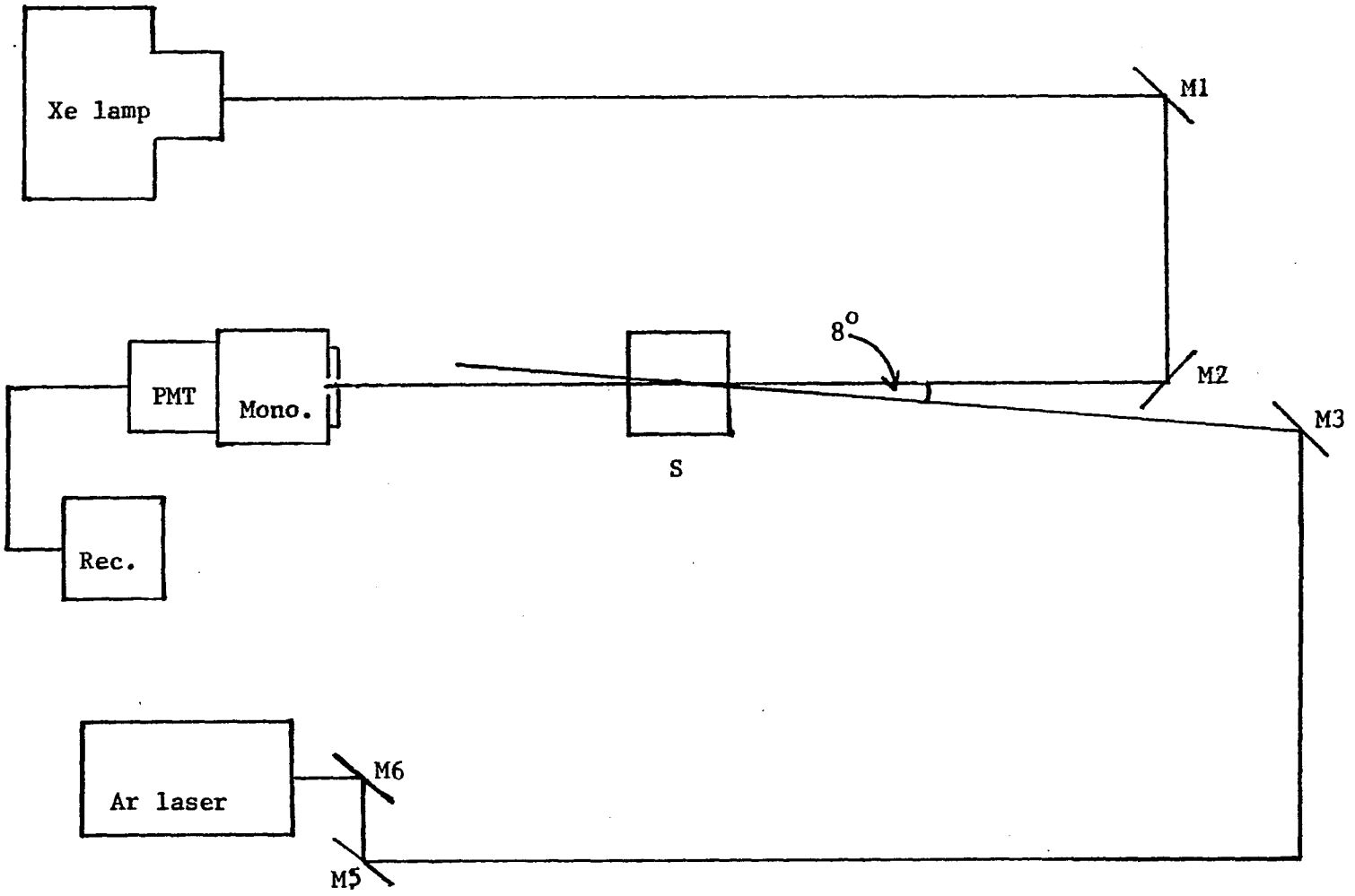

Figure 6

cell holder, and then irradiated with the 457.9-nm line from a Spectra Physics Model 1164-08 CW Ar ion laser. The white light output from a 100 W high-pressure Xe lamp serving as a single beam CW spectrophotometer source was directed at an angle of 8^{o} relative to the incident laser beam and perpendicular to the sample. The transmitted light was passed through a Bausch and Lomb Model 33-86-76 grating monochromator, and the exiting 510-nm light was detected by a Hammamatsu Model 928 red-sensitive photomultiplier tube, charged to 1 kV by a Pacific Precision Instruments Model 203 high-voltage DC power supply. The photomultiplier output as a function of photolysis time was displayed on a Honeywell Electronik 19 strip chart recorder. The rate of appearance of $[Ru(bpy)_2(bpy^-)]^+$ was monitored via the increase in absorbance at 510-nm, the absorption maximum of the latter, using the equation,

$$Abs = \log(1/T) \qquad (15)$$

where T is the ratio of the amount of light transmitted by the photolyzed sample to that by the unphotolyzed sample.

(e) Water Photolysis

Several different light sources were employed for studies of photocatalytic water reduction involving both visible light (sensitizing) and UV light (non-sensitizing) conditions. Glasses impregnated with TiO_2, Pt and $Ru(bpy)_3^{2+}$, where the latter is a sensitizer, were irradiated with visible light from an Illumination Industries 450-W high-pressure Xe lamp using a Melles-Griot

KG3 near-IR filter and a 0.5" thick sheet of plexiglass as a near-UV filter. The filtered light was focused with a pyrex lens onto the sample which was mounted upright with a Teflon holder in a pyrex cell. Glasses impregnated with TiO_2 and Pt, but without the sensitizer, were mounted in a similar fashion in a quartz cell and irradiated with UV light in a Southern New England Ultraviolet Rayonet Reactor employing either 350, 310, or 254-nm sources. Glass samples impregnated with reagents and catalysts were photolyzed under several torr of either H_2O vapor or a mixture of H_2O and CO vapors. H_2O was degassed via 3 freeze-pump-thaw cycles prior to exposure of the impregnated samples to H_2O vapor. After a period of photolysis the vapor phase was isolated via 3 Toepler pump cycles and swept with argon carrier gas into a Gow-Mac Model 69-100 gas chromatograph equipped with a 3' x 1/4" column packed with 5 A^o molecular sieves, and a thermal conductivity detector. The column temperature was maintained at 100°C and the retention times and integrated peak areas of the components of the gaseous effluent were compared to those of pure samples of H_2, O_2, N_2, CO, and CO_2, measured under the same conditions.

B. Photophysical and Photoredox Properties of Ru(II) Complexes with 2-(phenylazo)pyridine

(i) Materials

$Ru(azpy)_2L^{n+}$ complexes (n = 0-2), where L denotes 2-(phenylazo)pyridine (azpy), 4,4'-bithiazole (btz), 2,2'-bipyridine (bpy), ethylenediamine (en), acetylacetonate ($acac^-$), thiourea (tu), $(CN^-)_2$, $(NO_2^-)_2$, $(Cl^-)_2$, and $(Br^-)_2$, were prepared according to the published procedure of Krause and Krause,[93,94] and were isolated either as neutral complexes or as perchlorate or hexafluorophosphate salts. Ceric ammonium sulfate was standardized with As_2O_3 according to the procedure of Skoog and West.[173] All remaining chemicals were reagent grade and solutions were prepared with spectral grade solvents or with water distilled in a Corning distillation apparatus. Solutions were deaerated by bubbling with prepurified N_2 (Linde).

(ii) Physical Measurements

(a) Absorption and Emission Spectra

UV-visible absorption spectra were recorded on either a Cary 11 or Cary 14 spectrophotometer. At room temperature, these complexes are weak emitters and the spectral sensitivity of a Perkin-Elmer Hitachi MPF-2A emission spectrophotometer, although equipped with a red-sensitive photomultiplier, was not sufficient to reliably detect the emission.

A block diagram of the apparatus used to obtain the emission spectra appears in Figure 7. Solid samples or 10^{-5} to 10^{-4}M solutions of the complexes were placed in 1-mm i.d. quartz capillary tubes and excited at an

Figure 7

Block diagram of Raman spectrophotometer. This apparatus was also used to obtain emission spectra and emission intensity quenching of $Ru(azpy)_2L^{n+}$ complexes.

M = mirror; L = lens; A/D = amplifier/discriminator;

PC = photon counter; Rec. = chart recorder.

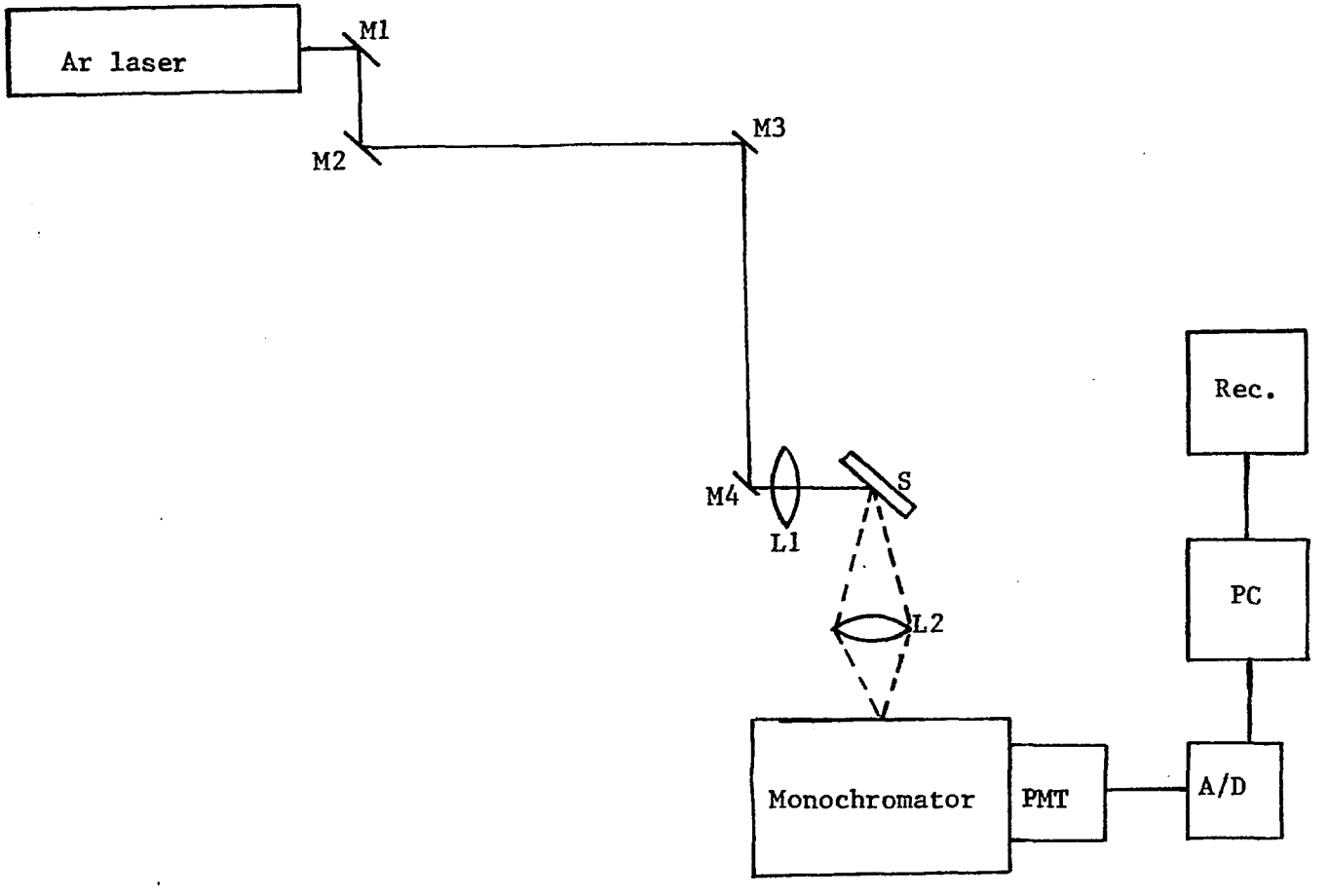

Figure 7

incident power of 30 mW with the 514.5-nm line from a Spectra Physics Model 1164-08 CW Ar ion laser. CAUTION: Solid samples of $[Ru(azpy)_2btz](ClO_4)_2$ spontaneously detonated when exposed to a focused, 30-mW, 514.5-nm laser beam. The emitted light at 90° to the excitation beam was focused onto the entrance slit of a Spex Model 14018 double grating monochromator. Since the emission from these complexes is very weak, even with laser excitation, the entrance and exit slits of the monochromator were opened to 1 mm, thereby sacrificing spectral resolution for a detectable quantity of emitted light. An RCA C31034A red-sensitive photomultiplier charged with -1800 V and mounted in a Pacific Photometric Instruments Model 3470 thermoelectrically cooled housing detected the emitted light. The photomultiplier output was fed into a Pacific Photometric Instruments AD6 amplifier discriminator providing 100-fold amplification of photomultiplier output pulses and rejection of amplified pulses less than 300 mV in amplitude. When triggered, the discriminator puts out 25 mV pulses which were than fed into a Pacific Precision Instruments Model 126 photon counter. The monochromator was scanned at a rate of 10 cm^{-1}/sec from 550 nm to 833 nm, the latter being the near-IR sensitivity limit of the photomultiplier. The output of the photon counter was displayed on a Beckman chart recorder as the emission spectrum. For each sample, the emission intensity was monitored at the wavelength maximum for 30 minutes to establish whether or not any photoreaction was occuring.

(b) Emission Intensity Quenching

2-3 x 10^{-5}M stock solutions of $Ru(azpy)_3^{2+}$ were prepared by dissolving $[Ru(azpy)_3](PF_6)_2$ in water or 1N aqueous acid. 10^{-3} to 10^{-2}M stock solutions of each quencher were prepared immediately prior to use. Solutions of Fe^{2+}, Fe^{3+}, Ce^{3+}, and Ce^{4+} were 1N in acid to prevent precipitation of hydroxide complexes.[174] Otherwise aqueous solutions of the quencher were used. Aliquots of the $Ru(azpy)_3^{2+}$ and quencher stock solutions were mixed and the resulting solutions were placed in 1-mm i.d. quartz capillary tubes for monitoring of the $Ru(azpy)_3^{2+}$ emission intensity at 830 nm. Solutions containing Fe^{2+} were deaerated and remained so until placement into the capillary tubes. The apparatus used to obtain the quenched emission intensities appears in Figure 7, and was described in the preceding section. The emission intensities were monitored for 30 minutes to ensure that there were no net photoreactions between $Ru(azpy)_3^{2+}$ and the quenchers. In addition, the emission intensity from a standard sample of $Ru(azpy)_3^{2+}$ was rechecked periodically to make certain that the alignment of the sample stage remained constant throughout the course of a series of measurements with each quencher.

(c) Emission Lifetimes

The apparatus used to obtain the room temperature luminescence lifetime of $Ru(azpy)_3^{2+}$ in aqueous

solution was described above and is schematically illustrated in Figure 5. The lower energy and lesser intensity of the emission in the remaining complexes did not allow for a reliable measurement of luminescence lifetimes, even with extensive signal averaging.

(d) Resonance Raman Spectra

Resonance Raman spectra of chloroform or water solutions of the complexes were recorded with the apparatus appearing in Figure 7. Typically, a 10^{-3}M solution was placed in a 1-mm i.d. quartz capillary tube and excited with an Ar ion laser line which was tuned to the frequency nearest to the visible absorption maximum, and the Raman scattered light was monitored at 90^{o} to the transverse excitation beam with the components described above.

III. Results

A. Studies in Porous Vycor Glass

(i) Characterization of $Ru(bpy)_3^{2+}$ Adsorbed to Porous Vycor

When pulverized and dispersed in distilled H_2O, porous Vycor glass deveops a zeta potential of -26±2 mV, indicative of an anionic surface and a decrease in the pH of the aqueous phase.[175] Adsorption of various colorimetric acid-base indicators onto PVG yields a surface pH of 4 to 5.[176] The results suggest proton dissociation from the silanol group, i.e.,

$$SiOH \longrightarrow SiO^- + H^+ \qquad (16)$$

and PVG is capable of cation exchange. Adsorption of $Ru(bpy)_3^{2+}$ onto the glass confirms the cation exchange character of PVG. Placing the glass into an aqueous solution of $[Ru(bpy)_3]Cl_2$ results in adsorption of the dicationic metal complex without a concurrent adsorption of the Cl^- counterion.[175] Furthermore, adsorption occurs without any apparent disruption of the primary coordination sphere of the complex. Figure 8 provides a comparison of the absorption and emission spectra of $Ru(bpy)_3^{2+}$ adsorbed to PVG, hereafter designated $Ru(bpy)_3^{2+}$ads, to spectra of aqueous solutions of the complex. The visible absorption spectrum of $Ru(bpy)_3^{2+}$ads is dominated by an intense MLCT band with a maximum at 452 nm and a half-width of 70±2

Figure 8

Cross-sectional absorbance, ϵ', vs. wavelength for $Ru(bpy)_3^{2+}$ adsorbed to PVG (●), and $Ru(bpy)_3^{2+}$ in H_2O solution (▲). Inside ordinate scale is molar extinction coefficient of $Ru(bpy)_3^{2+}$ in aqueous solution. Molar extinction coefficient in PVG is calculated from $\epsilon' = A/\text{moles-cm}^{-2}\ Ru(bpy)_3^{2+}\text{ads}$, where A is the absorbance. Moles-cm^{-2} calculated assuming optical path length is 2 x 0.2 cm, the latter being the penetration depth of the complex (see text). Emission spectra of $Ru(bpy)_3^{2+}$ adsorbed to PVG (---), and in H_2O solution (——). Relative emission intensities in the two media are normalized to facilitate comparison of emission maxima.

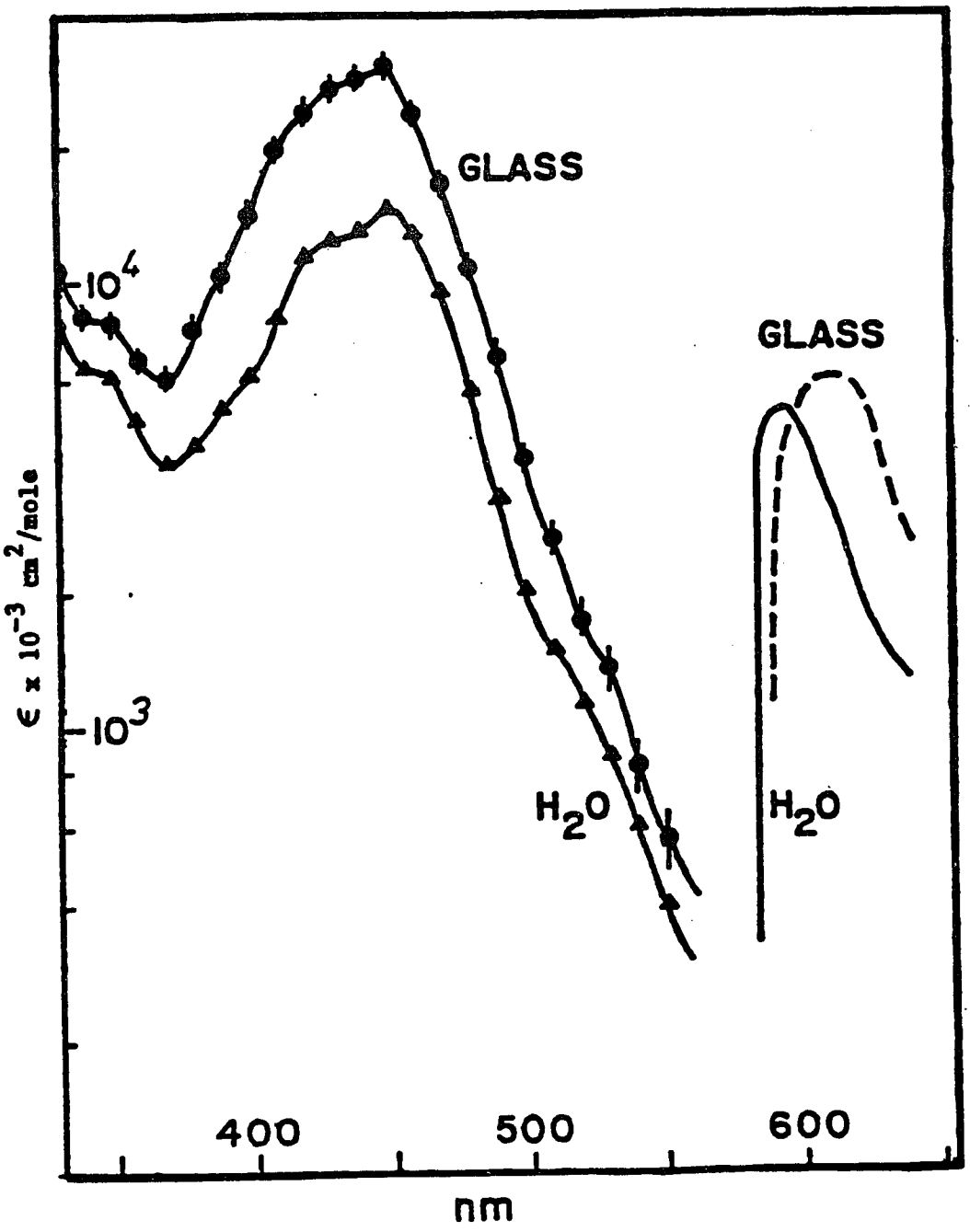
GLASS
GLASS
10^4
10^3
$\epsilon \times 10^{-3}$ cm^2/mole
H_2O
H_2O
400
500
600
nm

Figure 8

nm, similar to the MLCT band maximum, 452 nm, and band width, 68 nm, of an aqueous solution spectrum of the complex. The emission spectrum of $Ru(bpy)_3^{2+}$ads shows a maximum at 620 nm which, although red-shifted from the maximum in aqueous solution, 600 nm,[18] is similar to the band maxima reported for alcoholic solutions of the complex.[36] As shown in Figure 9, the resonance Raman spectrum of $Ru(bpy)_3^{2+}$ads consists of seven bipyridine vibrations differing by $\leq 1 cm^{-1}$ from those found for the complex in aqueous solution.[110] The luminescent lifetime of $^*Ru(bpu)_3^{2+}$ads, 740±20 nsec, falls well within the range of 600±20 nsec, measured in deaerated aqueous solution[63], to 862±10 nsec, measured in deaeated acetonitrile.[38] The similarity of the spectral and photophysical properties of $Ru(bpy)_3^{2+}$ads to those found in fluid solution establishes the integrity of the adsorbed complex and suggests an environment similar to that of an aqueous or alcoholic medium.

(ii) Distribution of $Ru(bpy)_3^{2+}$ads

Absorption and emission spectra recorded at various points on the 25-mm x 25-mm face of a PVG sample impregnated with $Ru(bpy)_3^{2+}$ are within experimental error, suggesting a relatively uniform distribution of the adsorbed complex across the glass surface. The cross-sectional distribution profile for 10^{-6} moles of $Ru(bpy)_3^{2+}$ads/gm PVG appearing in Figure 10 is

Figure 9

Resonance Raman spectra of $Ru(bpy)_3^{2+}$ in aqueous solution and adsorbed to PVG. Excited with 457.9-nm line from argon ion laser.

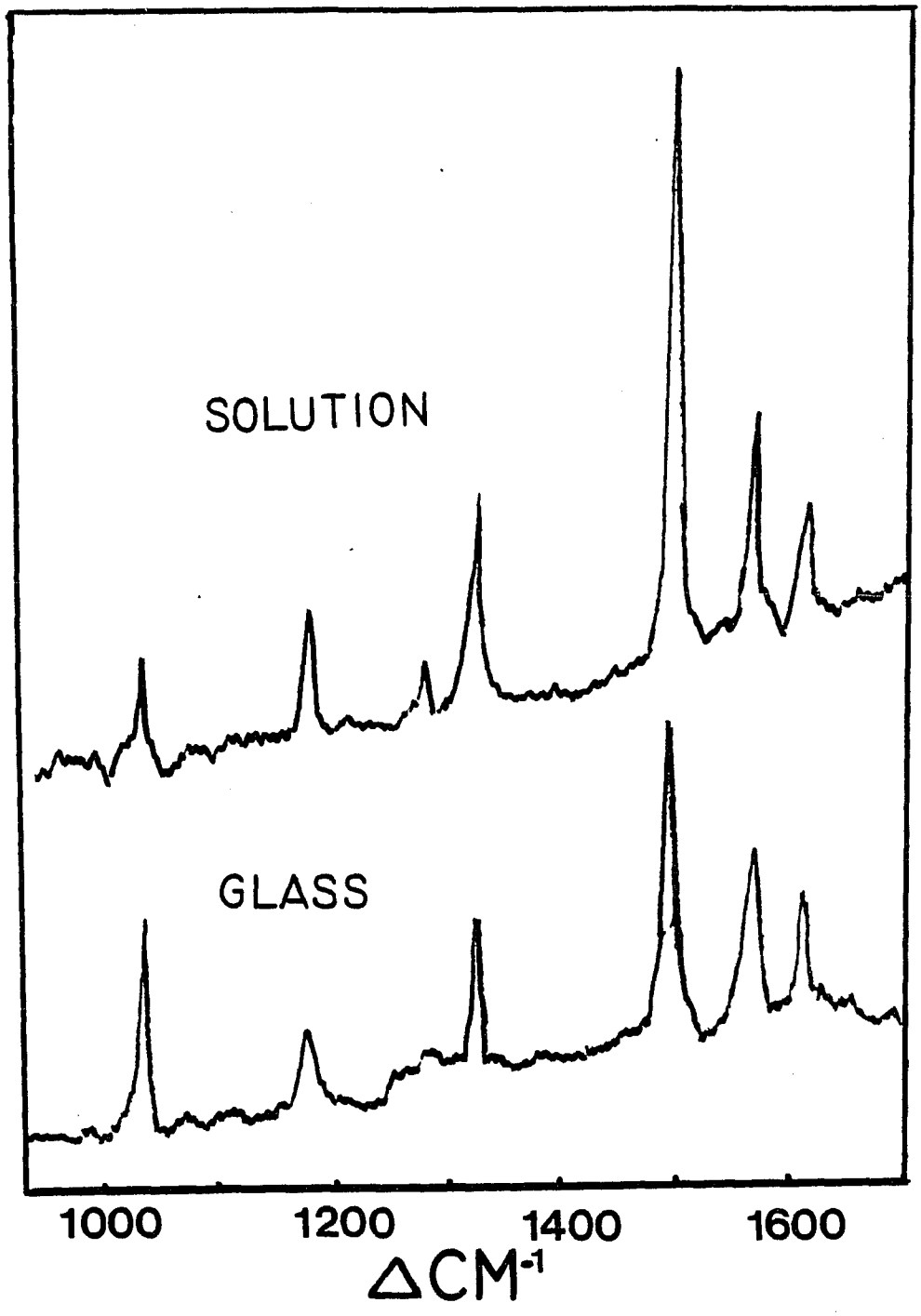

Figure 9

Figure 10

Absorbance at 500 nm as a function of the relative thickness of the glass. Initial dimensions of the glass sample: 25-mm x 25-mm x 4.04-mm.

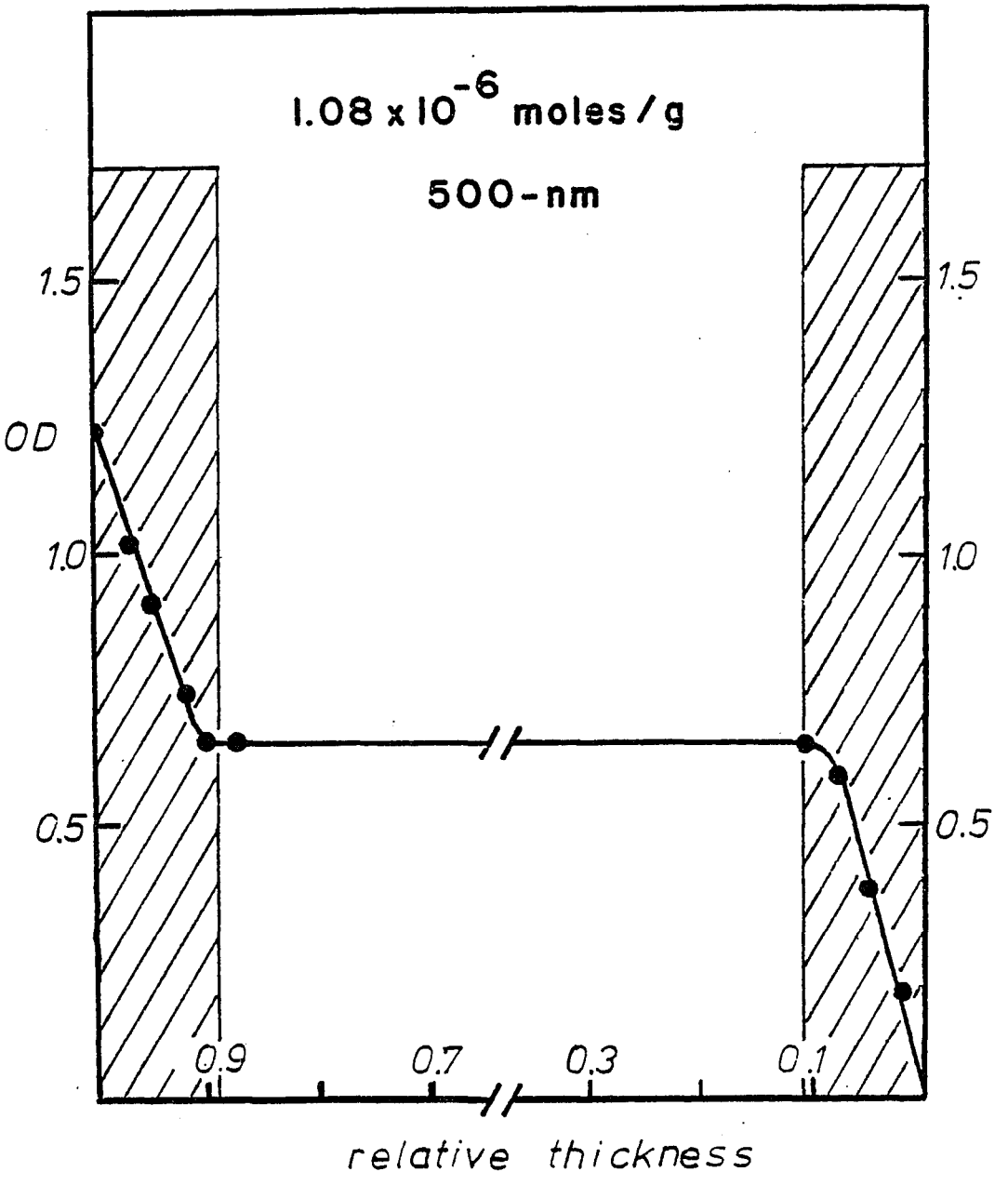
1.08 x 10^-6 moles / g
500-nm
1.5
OD
1.0
0.5
1.5
1.0
0.5
0.9
0.7
0.3
0.1
relative thickness

Figure 10

representative of the data for all levels of impregnation. As the sample thickness is reduced by grinding the glass surface, there is a linear decrease in optical density until ca. 0.2 mm of the initially 4-mm thick sample have been ground from either 25-mm x 25-mm face, indicating a uniform depthwise distribution of $Ru(bpy)_3^{2+}$ads on the outermost region of the glass. Although PVG contains a random distribution of silanol groups located throughout the entire matrix, there is apparently no penetration of the adsorbed complex into the interior of the glass. The symmetry and linearity of the cross-sectional distribution profile and the similarity of spectra recorded at various points along the glass surface suggests that impregnation by adsorption from aqueous solutions of $Ru(bpy)_3^{2+}$ yields a uniform distribution of the adsorbed complex that is limited to the pore volume of PVG adjacent to the outermost surfaces.

(iii) Adsorption of Gaseous Quenchers

Taking 7.4 A° as the radius of $Ru(bpy)_3^{2+}$ads and 130 m^2/gm and 1.38 gm/cc as the PVG surface area and density, respectively, impregnation of the outer pore volume of PVG with 10^{-6} moles of complex per gram of PVG corresponds to a surface coverage of $\leq$1%. Consistent with the low surface coverage of the metal complex, at pressures of $\leq$1atm of gas, the adsorption of N_2O, SO_2, and O_2 is unbiased by the presence of 10^{-6} moles of $Ru(bpy)_3^{2+}$/gm PVG. This observation, and the absence

of any measureable changes in the absorption and emission spectra of $Ru(bpy)_3^{2+}$ads in the presence of these gases, suggests that the gases adsorb randomly to vacant sites on PVG.

For SO_2 there was a noticeable amount of adsorption onto surfaces other than PVG which was not found for N_2O nor for O_2. When SO_2 gas was introduced into the cell containing the impregnated PVG sample, an initial pressure drop which revealed some adsorption had occurred, was followed by a much slower decline in pressure over a period of ca. 30 minutes. When SO_2 was introduced into the cell in the absence of the impregnated sample, the initial pressure change was not observed, whereas the slower decline, which paralleled that in the presence of the sample did occur. Consequently, the slow decline is attributed to adsorption onto cell surfaces, and the initial rapid decline to adsorption onto PVG. Hence, the initial pressure change was used to calculate the number of moles of SO_2 adsorbed to the impregnated PVG sample.

Representative isotherms for the adsorption of O_2, SO_2, and N_2O onto PVG at $22\pm1^{\circ}C$ are shown in Figure 11. Langmuir-type isotherms[177] were obtained for O_2 and SO_2, and the calculated adsorption parameters are listed in Table 4. Two possible surface coverages were assumed for the calculation of site areas for O_2 and SO_2, designated σ° in Table 4. The upper limit corresponds to monolayer coverage of the surface area

Figure 11

Adsorption isotherms for (a) N_2O onto 5.86-gm (▲) and 6.25-gm (■) samples of PVG; (b) SO_2 onto a 4.47-gm sample of PVG; and (c) O_2 onto a 5.38-gm sample of PVG. All isotherms are measured at room temperature, $22\pm1^{\circ}C$, and each PVG sample contains $1.5\pm0.5 \times 10^{-6}$ moles of $Ru(bpy)_3^{2+}$/gm PVG.

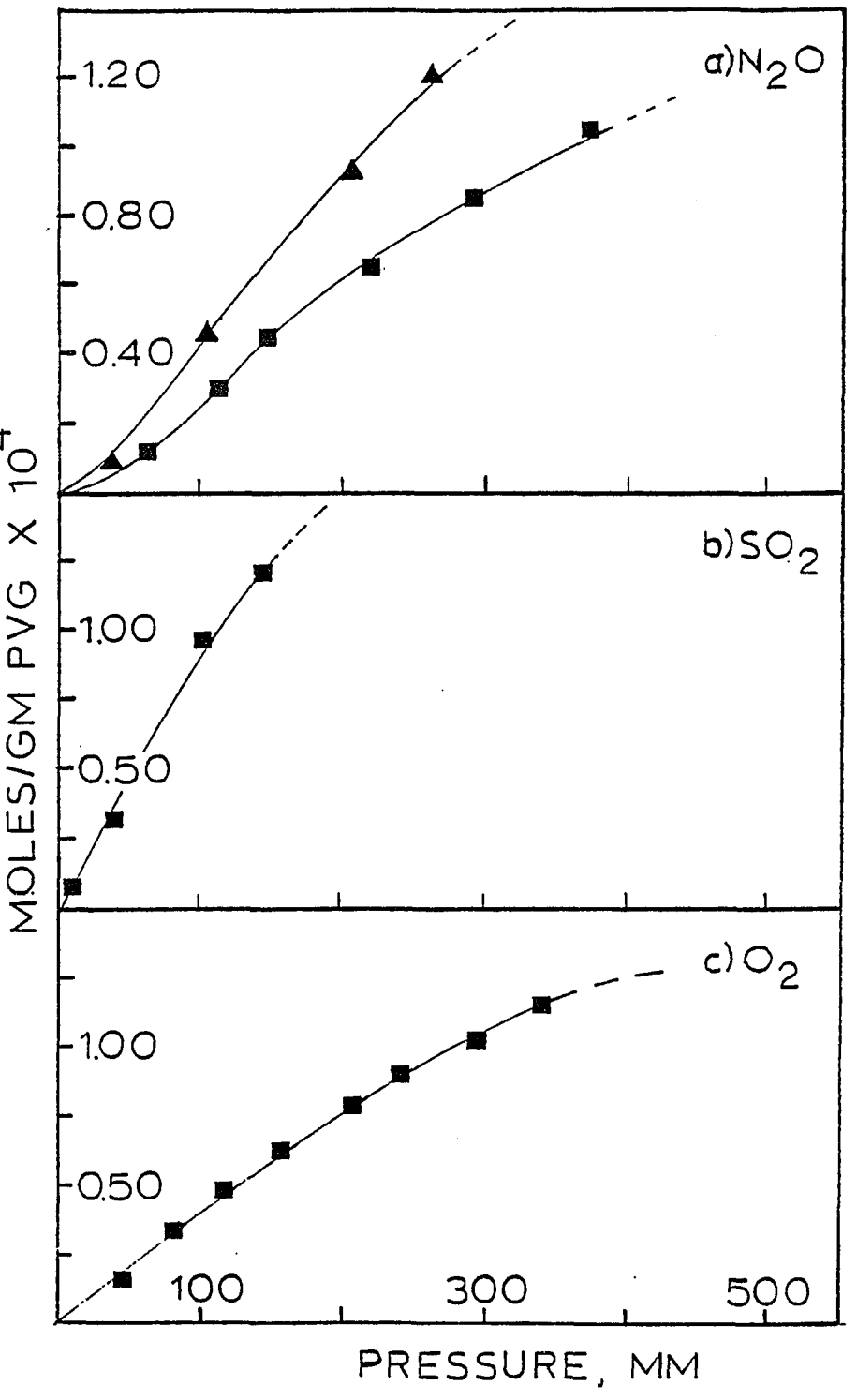
a)N_2O
1.20
0.80
0.40
b)SO_2
1.00
0.50
c)O_2
1.00
0.50
100
300
500
PRESSURE, MM
MOLES/GM PVG X 10^4

Figure 11

Table 4

Parameters for Adsorption[a] onto PVG and Quenching by Adsorbed O_2, SO_2, and N_2O

Quencher	Adsorption, Coefficient, b, $mm^{-1} \times 10^4$	m_{max}, moles adsorbed$_4$gPVG^{-1} x10[b]	Site Area $\sigma°$, $A°^2$[c]	f^d_{max}	$K^{e,g}_{SV}$, gPVG $mole^{-1}$ x10^{-4}	k_q[f,g] gPVG $mole^{-1}s^{-1}$ x 10^{-11}
O_2	7.72 ± 1.65	5.63 ± 1.00	11.5 - 38.4	0.78 ± 0.02	8.5 ± 1.3	1.1 ± 0.2
SO_2	32.4 ± 6.9	4.18 ± 0.73	15.5 - 51.7	0.94 ± 0.01	56 ± 8	7.6 ± 1.3
N_2O	-	-	-	0.28 ± 0.02	0.39 ± 0.06	0.053 ± 0.010

a) Adamson, A.W., "Physical Chemistry of Surfaces," Third Ed., Wiley-Interscience, New York, 1976, p. 553.

b) at monolayer coverage.

c) upper limit calculated by assuming adsorption throughout the entire pore surface area, $\Sigma = 130\ m^2/gm$, whereas lower limit assumes adsorption only onto region of glass impregnated with $Ru(bpy)_3^{2+}$ads (see text).

d) see text.

e) from initial slope of τ_o/τ va. m_{ads}.

f) lifetime of $Ru(bpy)_3^{2+}$ads, $\tau_o = 740 \pm 20$ ns.

g) units of $conc^{-1}$, gPVG $mole^{-1}$, are convenient for expressing K_{SV} and kq in this work. As such, the magnitude of the above values cannot readily be compared to the analogous values in fluid solution.

available throughout the entire pore volume of PVG, while the lower limit refers to adsorption only in those regions of PVG impregnated with $Ru(bpy)_3^{2+}$ads.

For O_2 and SO_2, the adsorption isotherms measured for different samples of impregnated PVG differ by $\leq$15%, but the moles of N_2O adsorbed/gm PVG differ by as much as 65% when different samples of impregnated PVG are exposed to identical pressures of N_2O. Although the absolute amount of N_2O adsorbed/gm differs, as illustrated in Figure 11a, the shape of the isotherms are similar. The sigmoidal character of the N_2O adsorption isotherms is typical of porous adsorbents and is indicative of capillary condensation[162b] by N_2O. Thus, the different adsorption isotherms obtained for N_2O onto various PVG samples may be due to variations in pore volume among the latter. The variation in the amount of N_2O adsorbed/gm prevents calculation of a realistic adsorption coefficient, but the relative rates of adsorption and desorption indicate that N_2O is only weakly adsorbed. For example, adsorption by impregnated PVG of O_2 and SO_2 is complete in <1 minute, whereas N_2O requires *ca*. 30 minutes to equilibrate. After exposure of an impregnated PVG sample to 1 atm of SO_2, 12-15 hours of continuous pumping, $p \leq 5 \times 10^{-4}$ torr, is necessary to desorb the gas and regenerate a $Ru(bpy)_3^{2+}$ads emission intensity equivalent to that recorded prior to exposure to the gas. Under the same conditions, however,

O_2 desorbs in 10 minutes and N_2O in <1 minute. These rates suggest that the relative magnitudes of the adsorption coefficients are $SO_2 > O_2 > N_2O$.

(iv) Quenching of Luminescence of $Ru(bpy)_3^{2+}$ads by Gases

When samples of PVG impregnated with $Ru(bpy)_3^{2+}$ are exposed to O_2, SO_2 , and N_2O, lifetime and intensity quenching occur. The relative extent of each type of quenching depends upon the specific gas. The relative emission intensity, I_o/I, where I_o is the emission intensity in vacuo and I is the intensity in the presence of the gas, is initially a function of P_q, but becomes independent of P_q at higher pressures. The point at which quenching becomes independent of P_q corresponds to quencher surface coverage of significantly less than a monolayer. In terms of both shape and uncertainty, plots of I_o/I vs. P_q resemble the adsorption isotherms for the gases. With O_2 and SO_2, the fractional quenching at a given pressure differs by $\leq$18% from one sample to the next. For N_2O, however, the variation is as much as 70%, similar to the variation in the moles of N_2O adsorbed/gm, m_{ads}, by the various samples. As indicated in Figure 12a, the plots of quenching by N_2O are reproducible functions of m_{ads} which establishes that the variation in the amount of quenching by N_2O is a consequence of different amounts of N_2O adsorbed/gm by the various impregnated PVG samples. Reproducibility with respect to m_{ads}

Figure 12

Lifetime and intensity quenching of $1.5\pm0.5 \times 10^{-6}$ moles of $Ru(bpy)_3^{2+}$/gm PVG by (a) N_2O, 5.86-gm sample t_o/t (●) and I_o/I (○), 6.25-gm sample t_o/t (■) and I_o/I (□); (b) SO_2, 4.47-gm sample t_o/t (●) and I_o/I (■); and (c) O_2, 5.38-gm sample t_o/t (●) and I_o/I (■). All measurements are at room temperature, $22\pm1^{\circ}C$.

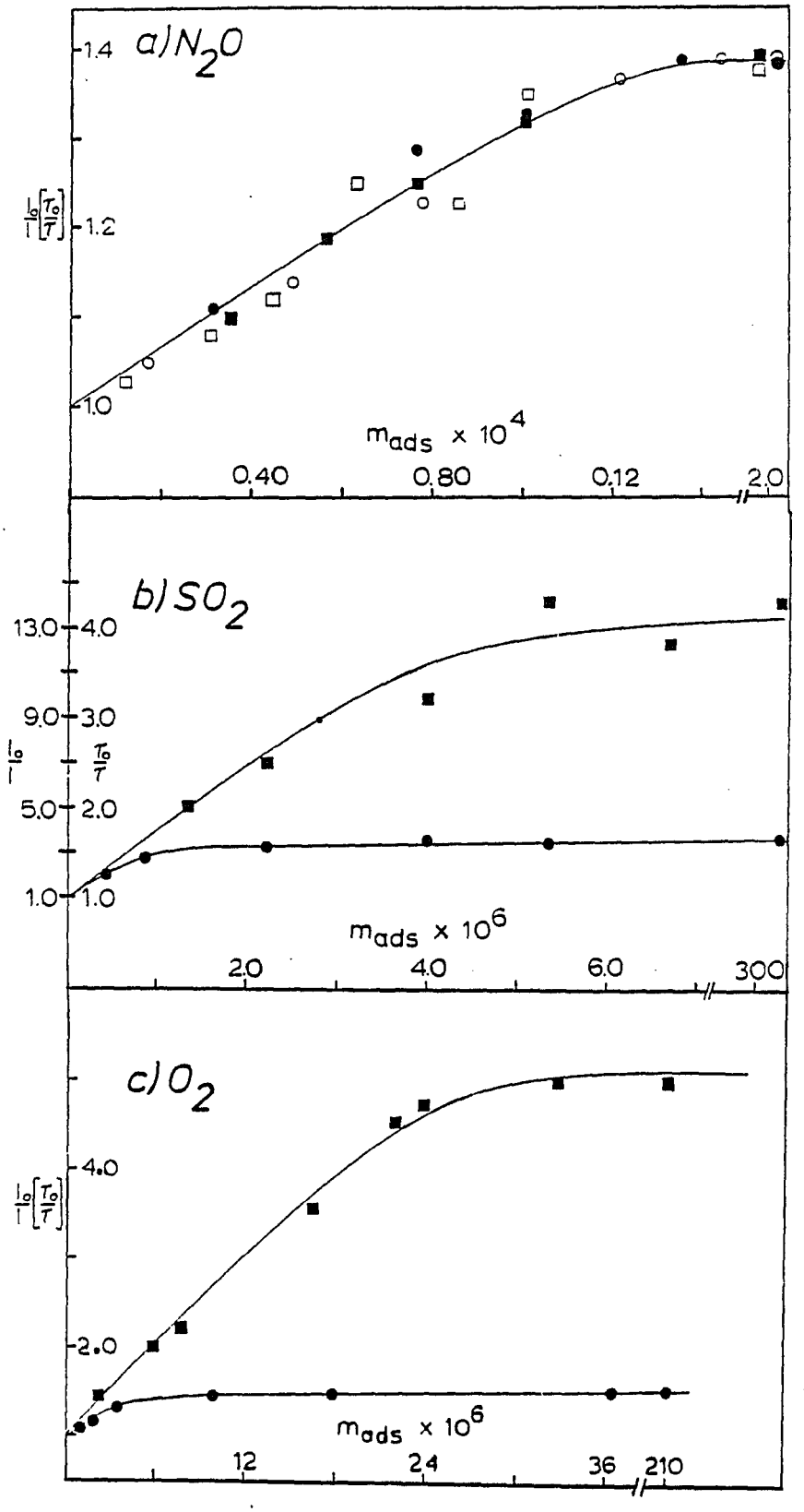
a) N_2O
1.4
1.2
1.0
$\frac{I_0}{I}\left[\frac{T_0}{T}\right]$
$m_{ads} \times 10^4$
0.40
0.80
0.12
2.0
b) SO_2
13.0
9.0
5.0
1.0
4.0
3.0
2.0
1.0
$\frac{I_0}{I}$
$\frac{T_0}{T}$
$m_{ads} \times 10^6$
2.0
4.0
6.0
300
c) O_2
4.0
2.0
$\frac{I_0}{I}\left[\frac{T_0}{T}\right]$
$m_{ads} \times 10^6$
12
24
36
210

Figure 12

rather than P_q suggests that quenching of $Ru(bpy)_3^{2+}$ads, at least by N_2O, is limited to adsorbed gas molecules. For SO_2 and O_2, the dependence of intensity quenching upon the moles of gas adsorbed per gram is not unequivocal, since quenching by these gases is dependent upon m_{ads} at low surface coverage of gas where m_{ads} is essentially a linear function of pressure. However, values for the maximum fraction quenched, designated f_{max} in Table 4, and taken as $1 - (I_o/I)$ where I is independent of P_q, parallel the adsorption coefficients of the gases, suggesting the dependence of f_{max} upon the strength of adsorption of the gas.

Quenching which demands the prior adsorption of a quencher molecule can be distinguished from that involving a collision between a gas phase quencher molecule and $Ru(bpy)_3^{2+}$ads through a comparison of intensity and lifetime quenching data.[154] The luminescent decay of $^*Ru(bpy)_3^{2+}$ads in vacuo, $p \leq 10^{-4}$ torr, at room temperature, $22 \pm 1^\circ C$, is exponential with a rate constant of $1.35 \pm 0.05 \times 10^6$ sec^{-1}, corresponding to a luminescence lifetime of 740 ± 20 nsec. Under various pressures of these gases, the decays remain exponential, although the lifetimes, t, are shorter. As shown in Figure 12a, lifetime quenching, t_o/t, by N_2O is within experimental error of the intensity quenching. The equivalence establishes a dynamic quenching process and is

interpreted within the Stern-Volmer model, $t_o/t = 1 + K_{SV}m_{ads}$, where K_{SV} is the Stern-Volmer constant and m_{ads} is the moles of N_2O adsorbed/gm PVG from the adsorption isotherm. Least squares analysis of the initial dependence on m_{ads} yields $K_{SV} = 3.9\pm0.6 \times 10^3$ gm PVG/mole, and dividing the latter by t_o, 740±20 nsec, yields a bimolecular quenching rate constant for N_2O of $5.3\pm0.1 \times 10^9$ gm PVG/mole-sec.

Figures 12b and 12c show quite different results for SO_2 and O_2. At 1 atm of each gas, the difference in lifetime and intensity quenching indicates that 89±1% of the quenching by SO_2 and 70±1% of the quenching by O_2 occur by a static process. The occurence of static quenching by O_2 and SO_2 confirms that, to a large extent, quenching involves adsorbed quencher molecules and thus, the quenching data are plotted as a function of m_{ads} rather than P_q in Figures 12b and 12c. Both gases exhibit dynamic quenching which, at low pressures, is dependent upon m_{ads} and, in turn, the equilibrium pressure of each gas. However, at pressures corresponding to much less than monolayer coverage, dynamic quenching becomes independent of m_{ads} and P_q. Least squares analyses of the initial dependencies yield Stern-Volmer constants of $8.5\pm1.3 \times 10^4$ gm PVG/mole and $5.6\pm0.8 \times 10^5$ gm PVG/mole for O_2 and SO_2, respectively. Dividing these values by t_o, 740±20 nsec, yield bimolecular quenching rate constants of $1.1\pm0.2 \times 10^{11}$

gm PVG/mole-sec for O_2 and $7.6 \pm 1.3 \times 10^{11}$ gm PVG/mole-sec for SO_2.

In part, the purpose of these experiments was to explore the possibility of initiating a redox reaction within these gases, particularly SO_2, by a photoinduced electron transfer. However, absorption spectra recorded before and after these quenching experiments give no indication of a net formation of either $Ru(bpy)_3^{3+}$[150] or $[Ru(bpy)_2(bpy^-)]^+$.[178]

(v) Water Cleavage

(a) Deposition of TiO_2 onto PVG

The water photolysis catalysts were characterized and their loading levels determined spectrophotometrically. A UV-VIS absorption spectrum of a PVG sample after impregnation from an acidic isopropanol solution of $Ti(OCH\text{-}(CH_3)_2)_4$ followed by evaporation of the solvent appears in Figure 13. The impregnated sample exhibits no absorbance in the visible spectrum, although there is a slight decrease in the amount of transmitted light approaching shorter wavelelengths due to scattering. A very sharp increase in absorbance, however, is observed at $\lambda \leq 350$ nm, the onset of which depends upon the level of impregnation. This sharp spectral cutoff is characteristic of a semiconductor[179] and in this case, the spectrum is reminiscent of spectra of colloidal dispersions of TiO_2 in H_2O/isopropanol.[169] However, TiO_2ads, even at the highest impregnation levels achieved in the glass,

Figure 13

Absorption spectrum of a 4.0-gm PVG sample impregnated with 2.6×10^{-6} moles TiO_2/gm PVG.

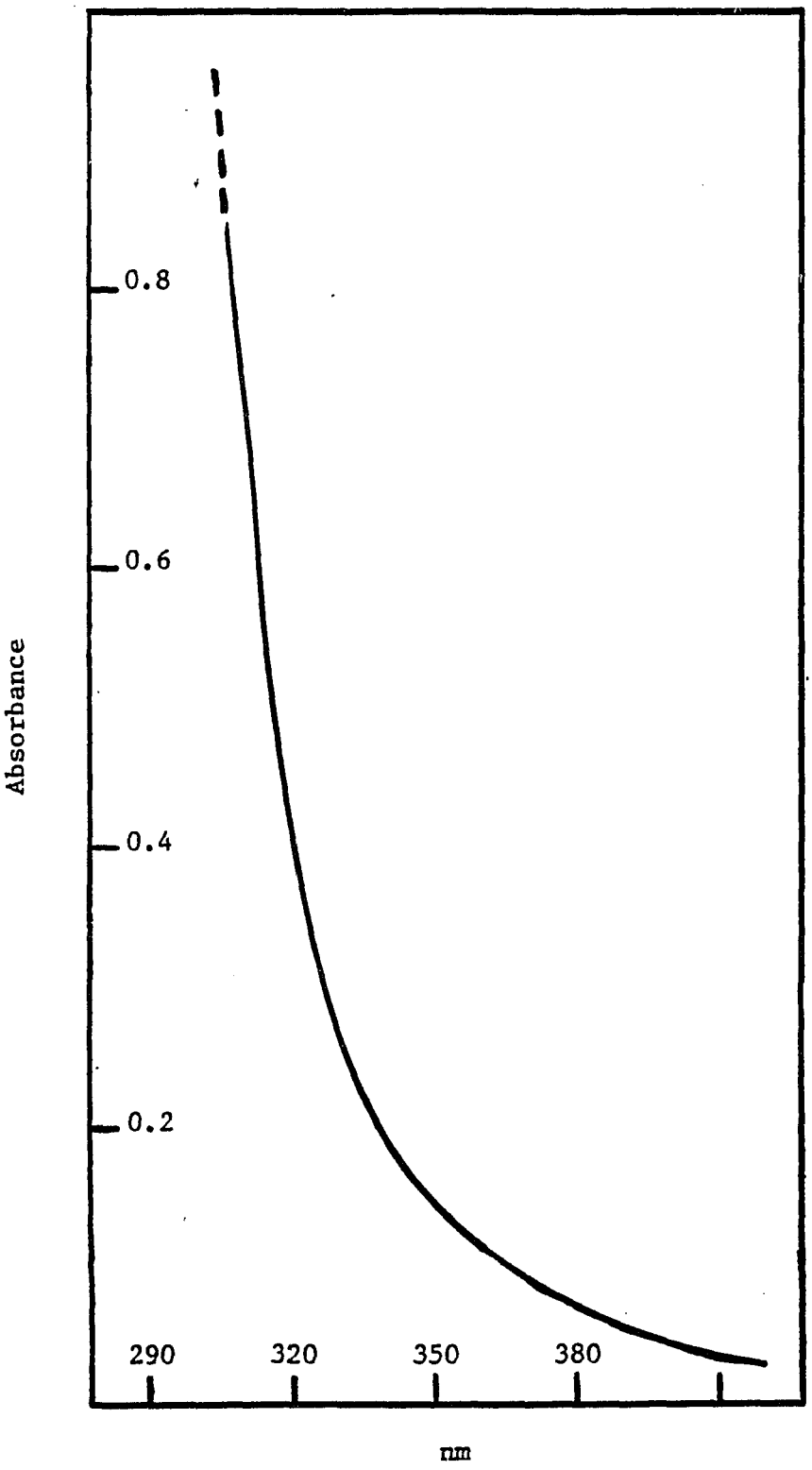

Figure 13

10^{-5} moles/gm, exhibits much less scattering than the colloidal TiO_2 particle suspensions. This is probably an indication that TiO_2 is dispersed on PVG, rather than deposited as an aggregate of colloidal dimensions and therefore, does not scatter as much light as a colloidal particle. A nearly identical absorption spectrum to that in Figure 15 is obtained even if the impregnated glass is heated to 550°C following evaporation of the solvent, indicating that hydrolysis of $Ti(OCH-(CH_3)_2)_4$ is complete within the time it takes for impregnation of the glass and evaporation of the solvent. The optical absorption coefficient near the band edge, α, obeys the equation,[180]

$$\alpha = A(h\nu - E_g)^{n/2}/h\nu \qquad (17)$$

where $n = 4$ for TiO_2,[181] A is a constant, ν is the light frequency, and E_g is the bandgap of the semiconductor. When $h\nu = E_g$, α is zero, and thus, the bandgap obtained for TiO_2ads is ca. 3.5 eV. This energy is somewhat larger than the 3.2-eV and 3.0-eV bandgaps of anatase[169] and rutile[179] TiO_2, respectively.

(b) Photolyses of Glass Impregnated with Water Photolysis Catalysts

Continuous irradiation for up to 6 hours of PVG impregnated with 5.4×10^{-6} moles of TiO_2/gm PVG and 2.3×10^{-6} moles of Pt/gm PVG at 254 nm, 310 nm, and 350 nm, under 20-torr of H_2O vapor did not produce

quantities of H_2 gas detectable by gas chromatography. Assuming a minimum detectable quantity of 10^{-8} moles of H_2, and an ability to sample 100% of the gas evolved, yields a H_2 quantum efficiency for 6 hours of photolysis of $<10^{-5}$. No H_2 was found for similar photolyses in the presence of a mixture of 20 torr of H_2 and 10 torr of CO.

Continuous irradiation for up to 6 hours with visible light of PVG impregnated with 6.0×10^{-7} moles of $Ru(bpy)_3^{2+}$/gm PVG, 3.0×10^{-7} moles of TiO_2/gm PVG, and 1.4×10^{-6} moles of Pt/gm PVG under 20 torr of H_2O vapor, and a combination of 20 torr of H_2O and 10 torr of CO did not yield any measureable quantities of H_2 gas either.

(vi) Disproportionation of $Ru(bpy)_3^{2+}$ads in Presence of SnO_2

In a previous study it was shown that continuous irradiation of $Ru(bpy)_3^{2+}$ads with a 457.9-nm Ar ion laser beam results in disproportionation of the dication.[146,168] The mechanism (see reaction 12) involves a biphotonic ionization of $Ru(bpy)_3^{2+}$ads followed by migration of the photoejected electron along the glass surface to another $Ru(bpy)_3^{2+}$ which is then reduced. Via this earlier study, it had been established that, once ionized, the electron is capable of migrating ca. 50 A^o in PVG. In an attempt to enhance the conductivity of the medium, and thus, increase the distance which an electron can migrate on the glass surface, a thin film of

SnO_2 doped with 1%Sb was deposited onto the PVG surface by a spray pyrolysis technique.[151,152] A UV-VIS absorption spectrum of a PVG sample coated with such a film appears in Figure 14, and reveals that the doped SnO_2 film is optically transparent ($\lambda \geq 350$ nm). The extinction coefficient near the band edge obeys equation 17, where n = 4 for SnO_2[181], and the bandgap energy, E_g = 3.5 eV, in good agreement with E_g for a SnO_2 electrode in a pH 1 aqueous electrolyte.[182] Figure 15 shows the resistance, obtained with a digital ohmmeter, of the surface of a SnO_2-coated PVG sample as a function of the distance between the points of contact by the meter electrodes. In the absence of the SnO_2 film, similar measurements show that the resistance of PVG is infinite between any two points chosen on the glass surface. The measurement of a finite resistance ($\sim$10 M Ω) between points along the glass surface situated >2 cm apart establishes that the doped SnO_2 film is indeed conductive.

An absorption spectrum of the SnO_2-coated glass after impregnation with $Ru(bpy)_3^{2+}$ appears in Figure 16. No new absorption bands attributable to an interaction between $Ru(bpy)_3^{2+}$ads and SnO_2 appear in the spectrum, although the MLCT absorption band maximum of the adsorbed complex which normally appears at 452 nm, is slightly blue-shifted by virtue of a long-wavelength tail, presumably due to scattering by the adsorbed semiconductor (see Figure 14). Consequently, the spectrum in Figure 16

Figure 14

Absorption spectrum of a conducting SnO_2/1%Sb film deposited onto a 1.9-gm PVG sample.

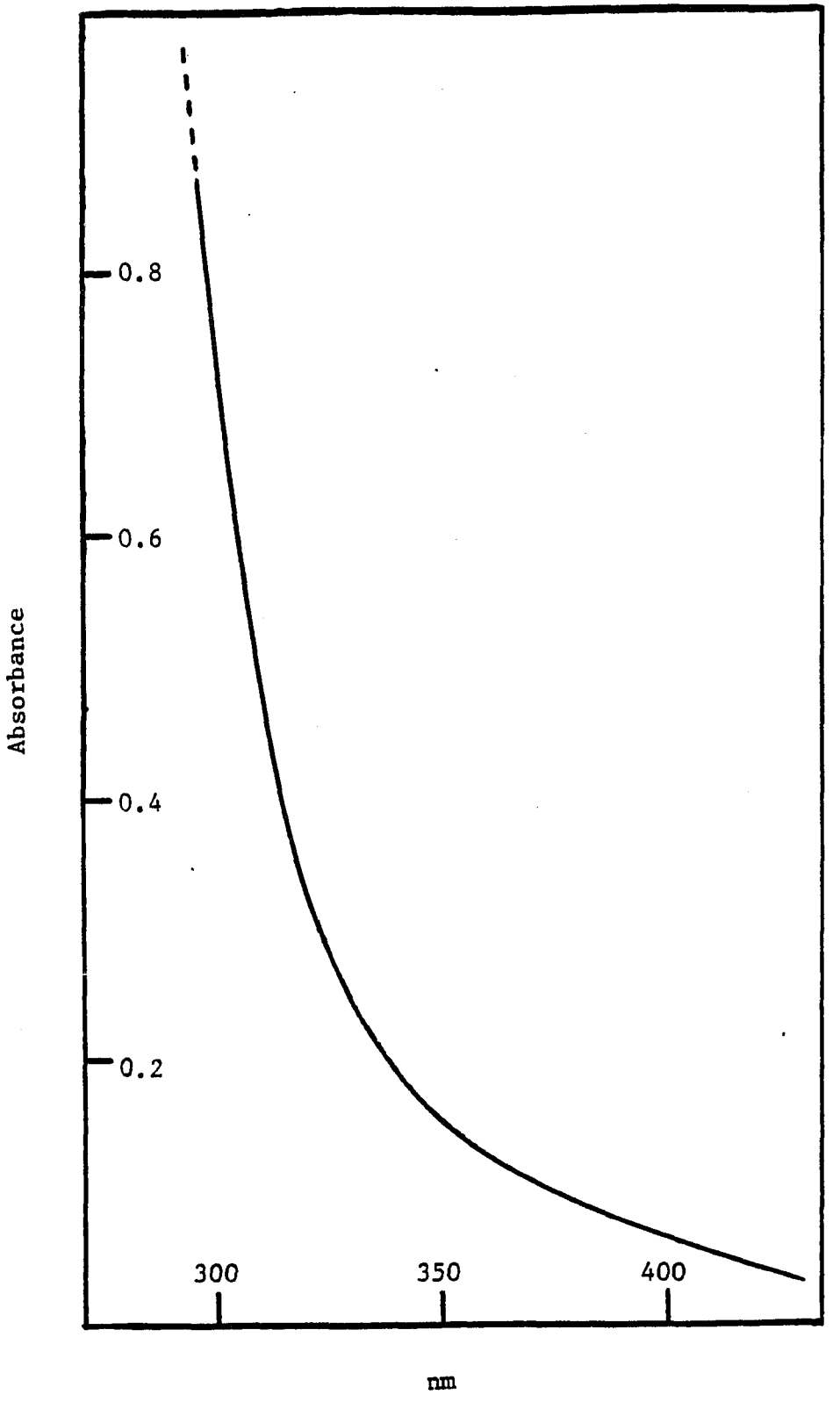

Figure 14

Figure 15

Resistance of a SnO_2/1%Sb film deposited onto a 2.0-gm PVG sample *vs.* the distance between the contact points of the ohmmeter electrodes.

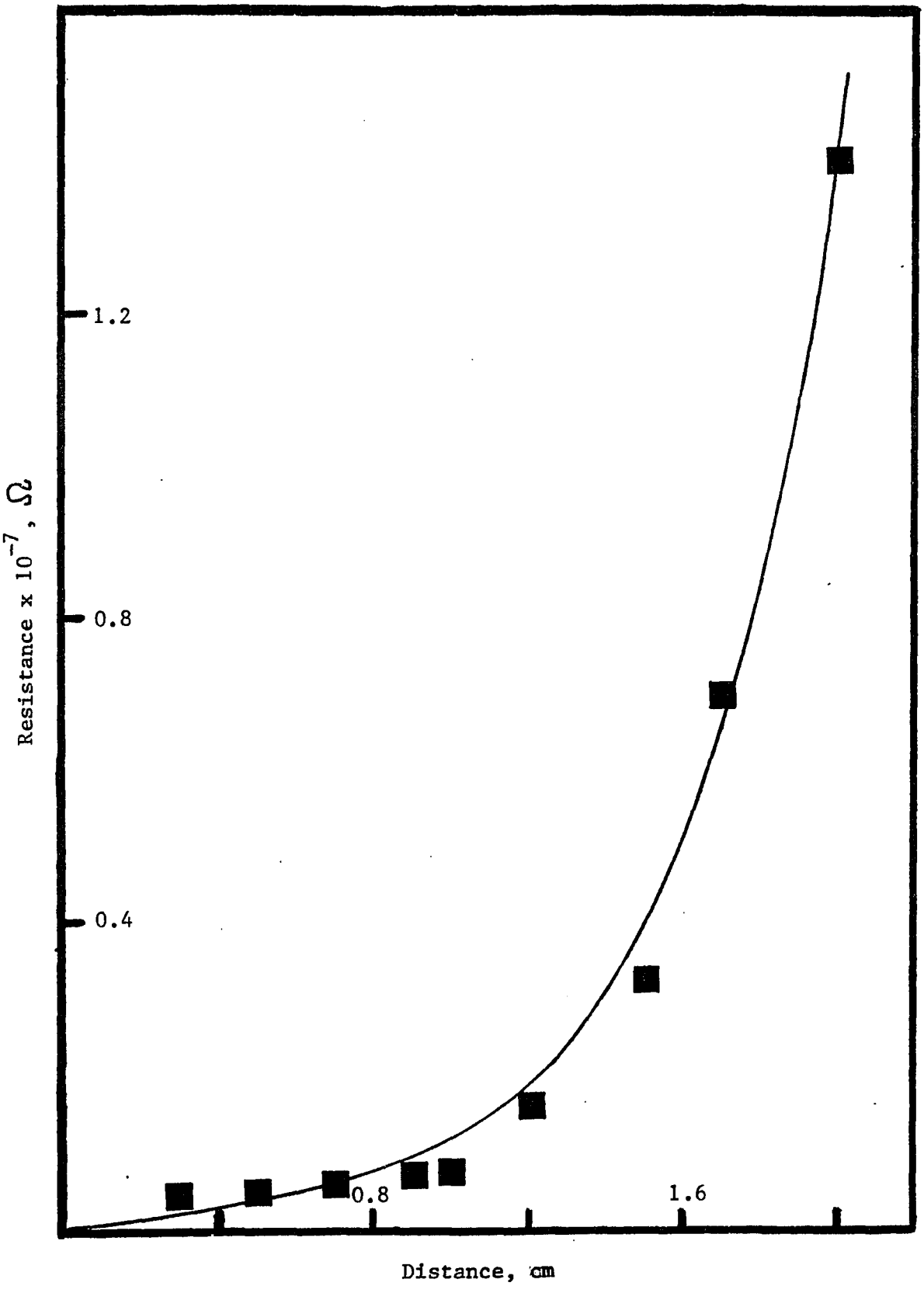

Figure 15

Figure 16

Absorption spectrum of a 1.9-gm PVG sample impregnated with 3.9×10^{-8} moles $Ru(bpy)_3^{2+}$/gm PVG and containing a codeposited SnO_2/1%Sb film.

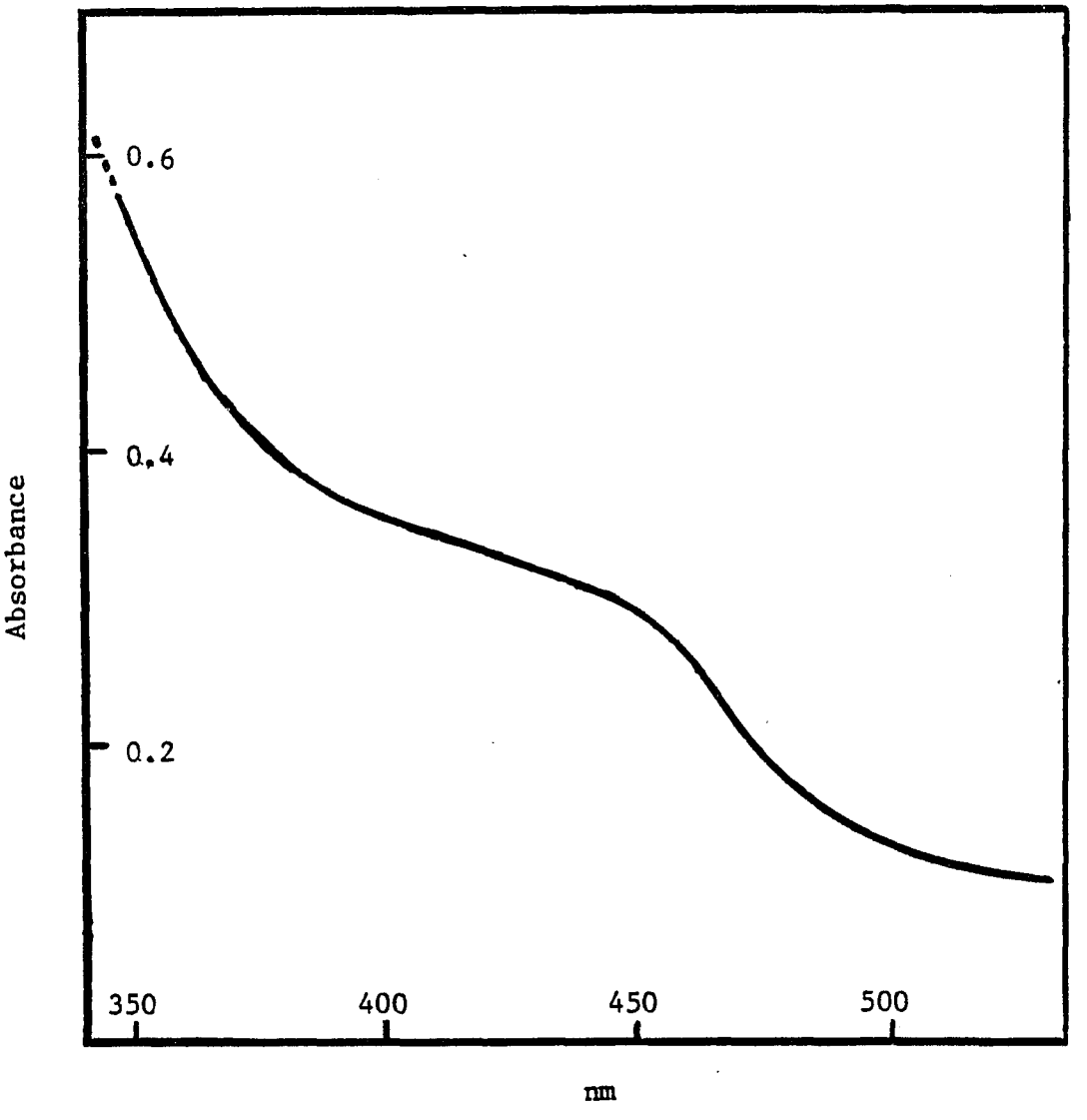

Figure 16

is a composite of the individual $Ru(bpy)_3^{2+}$ads and SnO_2 absorption spectra, where the former is the dominant visible-light absorbing species. The emission spectrum of $Ru(bpy)_3^{2+}$ads is also unaltered by the presence of SnO_2, suggesting that the excited state energy is likewise, unchanged. In the presence of a codeposited, doped SnO_2 film, 457.9-nm laser irradiation of PVG impregnated with $Ru(bpy)_3^{2+}$ results in an increase in the absorbance at 510 nm, attributable to the formation of $[Ru(bpy)_2(bpy^-)]^+$ (Figures 17 and 18).[168,178] At this wavelength, the extinction coefficient of $Ru(bpy)_3^{2+}$ in aqueous solution, 1.1×10^3 $M^{-1}cm^{-1}$, is <10% of 1.2×10^4 $M^{-1}cm^{-1}$, the extinction coefficient of $[Ru(bpy)_2(bpy^-)]^+$ in H_2O.[178] Assuming the relative extinction coefficients in the glass parallel those in H_2O, the light-induced change in absorbance at 510 nm is directly related to the appearance of a Ru(I) species. Thus, the rate of formation of $[Ru(bpy)_2(bpy^-)]^+$ is obtained from the initial slopes of plots of absorbance at 510 nm vs. time. As seen in Figures 17 and 18, the rate of formation of $[Ru(bpy)_2(bpy^-)]^+$ depends upon the number of moles of $Ru(bpy)_3^{2+}$/gm PVG.

Increasing the laser intensity accelerates the rate of growth of absorbance at 510 nm. Since both the intensity dependence and the quantum yield of $[Ru(bpy)_2(bpy^-)]^+$ are given by,[168]

Figure 17

Absorbance at 510 nm *vs.* photolysis time. PVG samples contain 3.5×10^{-7} moles $Ru(bpy)_3^{2+}$/gm PVG (▲); 4.7×10^{-7} moles $Ru(bpy)_3^{2+}$/gm PVG (■); and 2.0×10^{-6} moles $Ru(bpy)_3^{2+}$/gm PVG, (●), as well as a codeposited SnO_2/1%Sb film. All samples are photolyzed at 457.9 nm with a 170-mW argon ion laser beam.

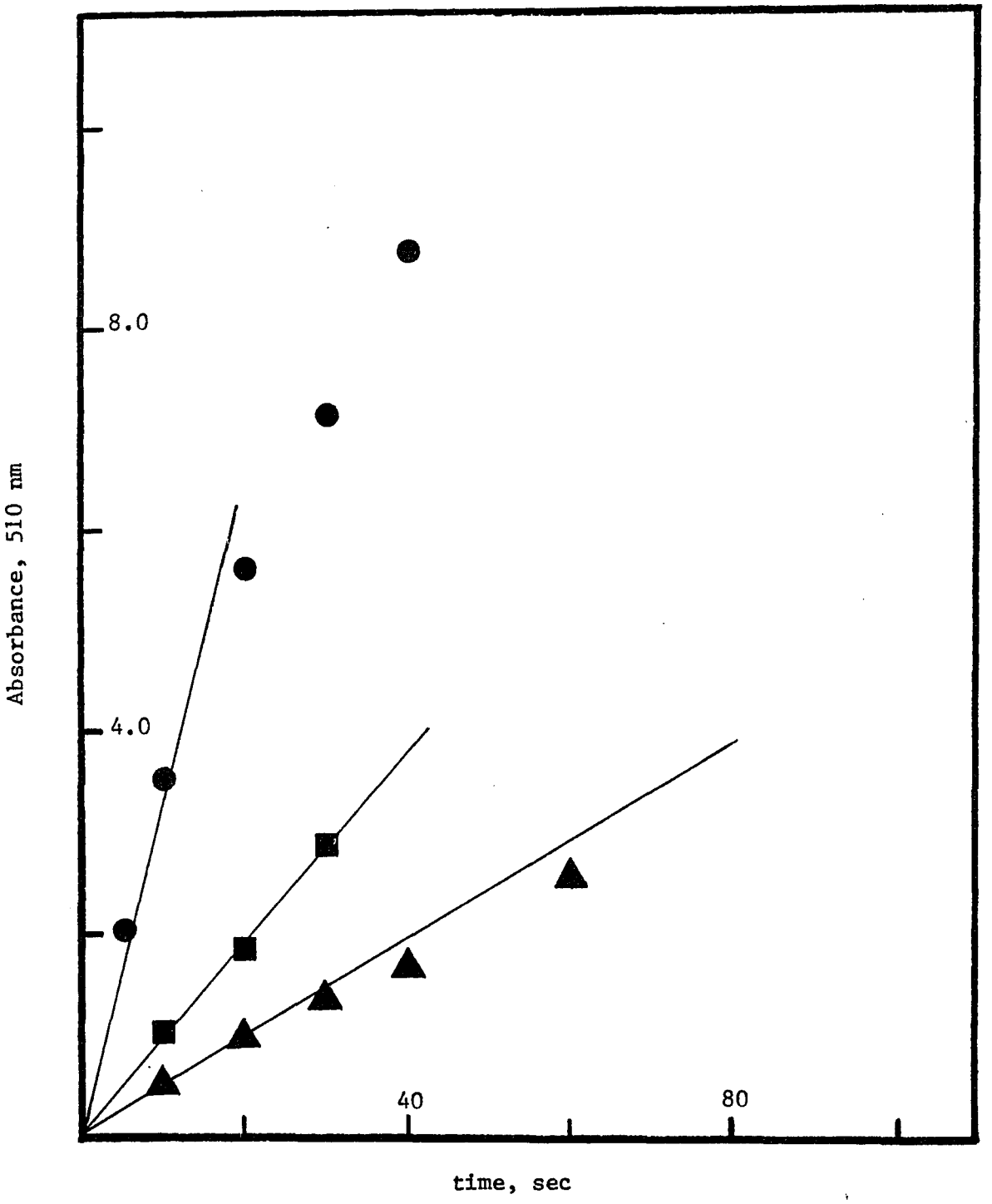

Figure 17

Figure 18

Absorbance at 510 nm *vs.* photolysis time. PVG samples contain 4.2×10^{-6} moles $Ru(bpy)_3^{2+}$/gm PVG (■); and 9.8×10^{-6} moles $Ru(bpy)_3^{2+}$/gm PVG (●), as well as a codeposited SnO_2/1%Sb film. Both samples are photolyzed at 457.9 nm with a 140-mW argon ion laser beam.

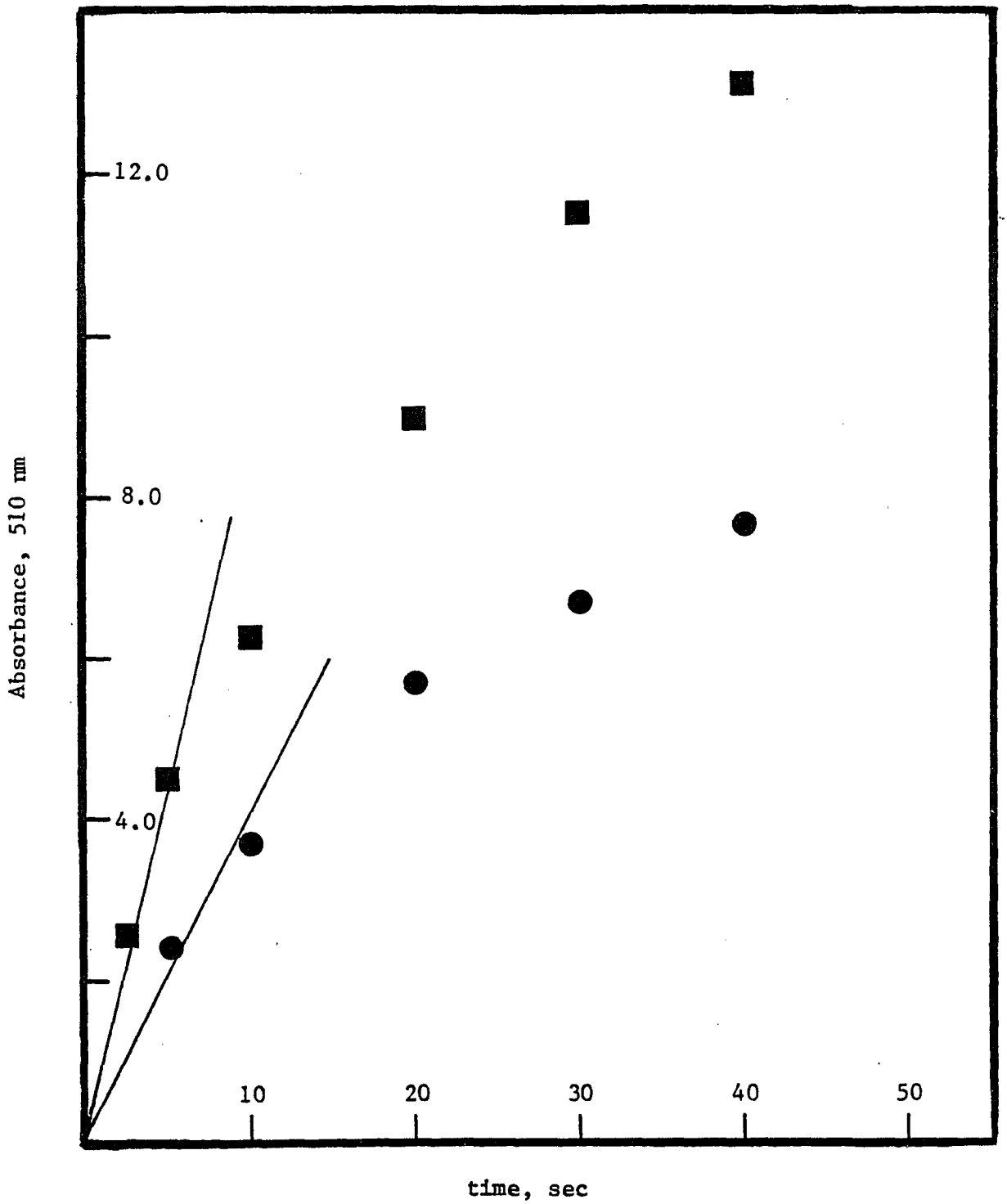

Figure 18

$$\log R = \log \phi + n \log I \qquad (18)$$

where R is the initial rate of formation of $[Ru(bpy)_2(bpy^-)]^+$, ϕ is the corresponding quantum yield, I is the power of the photolyzing beam in mW, and n is the order of the reaction in light intensity, the quantum yield of $[Ru(bpy)_2(bpy^-)]^+$ and the intensity dependence are extracted from plots of -log R vs. -log I for various impregnation levels.

A second order intensity dependence has already been obtained for the formation of $[Ru(bpy)_2(bpy^-)]^+$ via the photoinduced disproportionation of $Ru(bpy)_3^{2+}$ in PVG.[146,168] Likewise, plots of -log R vs. -log I (Figure 19) for the formation of $[Ru(bpy)_2(bpy^-)]^+$ in samples containing from 5.0×10^{-7} up to 9.8×10^{-6} moles of $Ru(bpy)_3^{2+}$/gm PVG, in the presence of doped SnO_2, display slopes of 2.0 ± 0.5, indicating that the photoreaction is second order in light intensity.

Listed in Table 5 are the relative quantum yields for the formation of $[Ru(bpy)_2(bpy^-)]^+$ at various levels of impregnation of PVG with the dicationic complex. For comparison, relative quantum yields are listed for samples both with and without codeposited doped SnO_2 films. As shown in Figure 20, whether or not SnO_2 is present, the quantum yield of $[Ru(bpy)_2(bpy^-)]^+$ increases in a similar fashion as the amount of adsorbed metal complex is increased from 5.0×10^{-7} to 2.7×10^{-6} moles/gm. As the number of moles of complex per

Figure 19

Plot of -log R vs. -log I for PVG samples containing 1.1×10^{-6} moles $Ru(bpy)_3^{2+}$/gm PVG (●); and 2.0×10^{-6} moles $Ru(bpy)_3^{2+}$/gm PVG (■), in addition to a codeposited SnO_2/1%Sb film, where R is the relative rate of formation of $[Ru(bpy)_2(bpy^-)]^+$, and I is the laser intensity in mW. Samples are photolyzed at 457.9-nm.

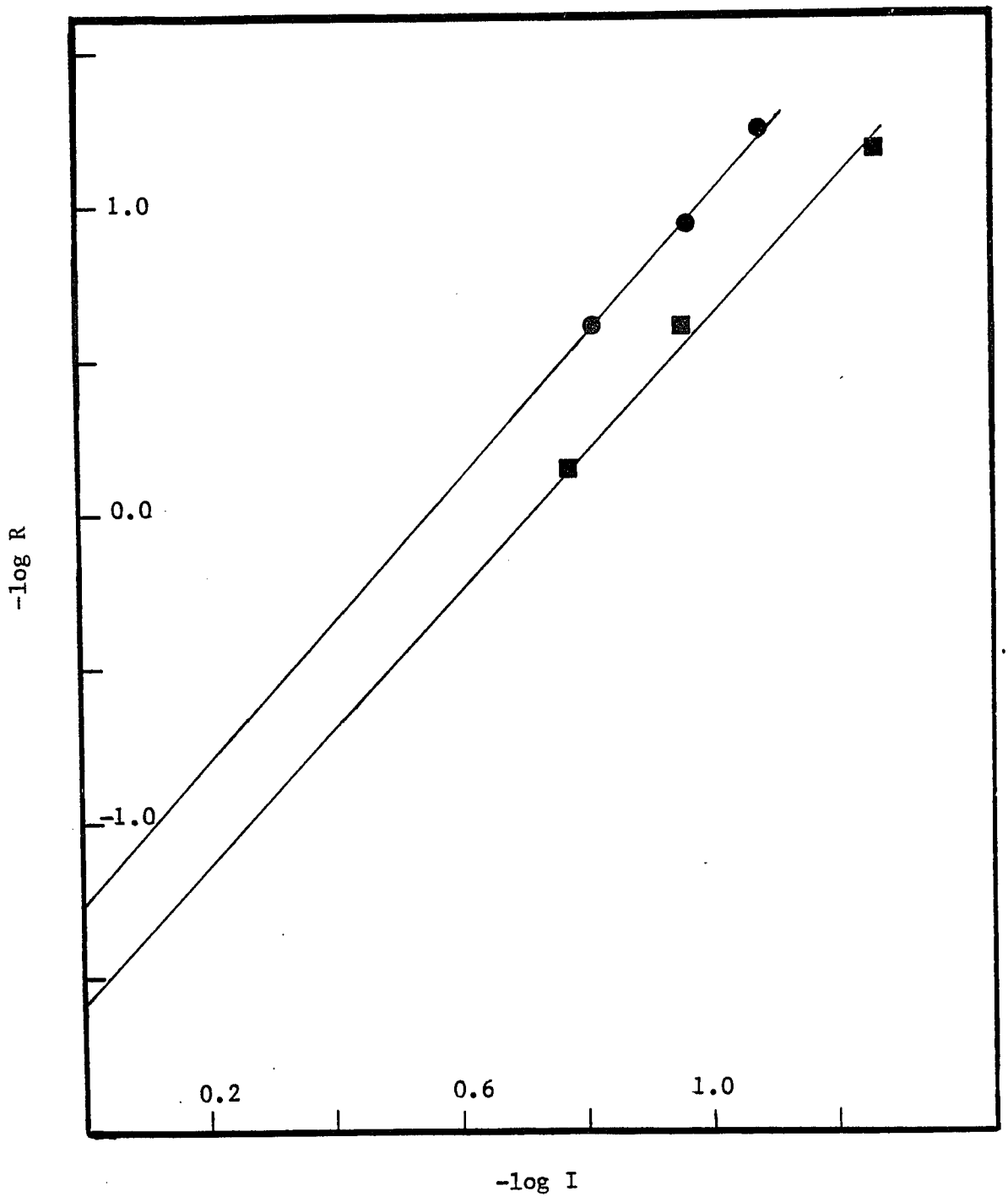

Figure 19

Table 5 - Relative Quantum Yields[a] of $[Ru(bpy)_2(bpy^-)]^+$

moles $Ru(bpy)_3^{2+}$/gm PVG[b]	$\Phi^{rel}_{[Ru(bpy)_2(bpy^-)]^+}$	
	with SnO_2	without SnO_2
5.0×10^{-7}	5.0	5.8
1.1×10^{-6}	11.5	15.4
1.6×10^{-6}	19.1	-
2.0×10^{-6}	25.7	36.3
4.2×10^{-6}	48.9	40.7
9.8×10^{-6}	22.9	9.5

a) from y-intercept of plot of -log R vs. -log I (see text); 457.9-nm Ar laser excitation.

b) 25-mm x 25-mm x 1-mm samples.

Figure 20

Plot of the relative quantum yield of formation of $[Ru(bpy)_2(bpy^-)]^+$ *vs.* moles of $Ru(bpy)_3^{2+}$/gm PVG. 457.9-nm photolysis of PVG samples in presence (●) and absence (■) of a conducting SnO_2/1%Sb film.

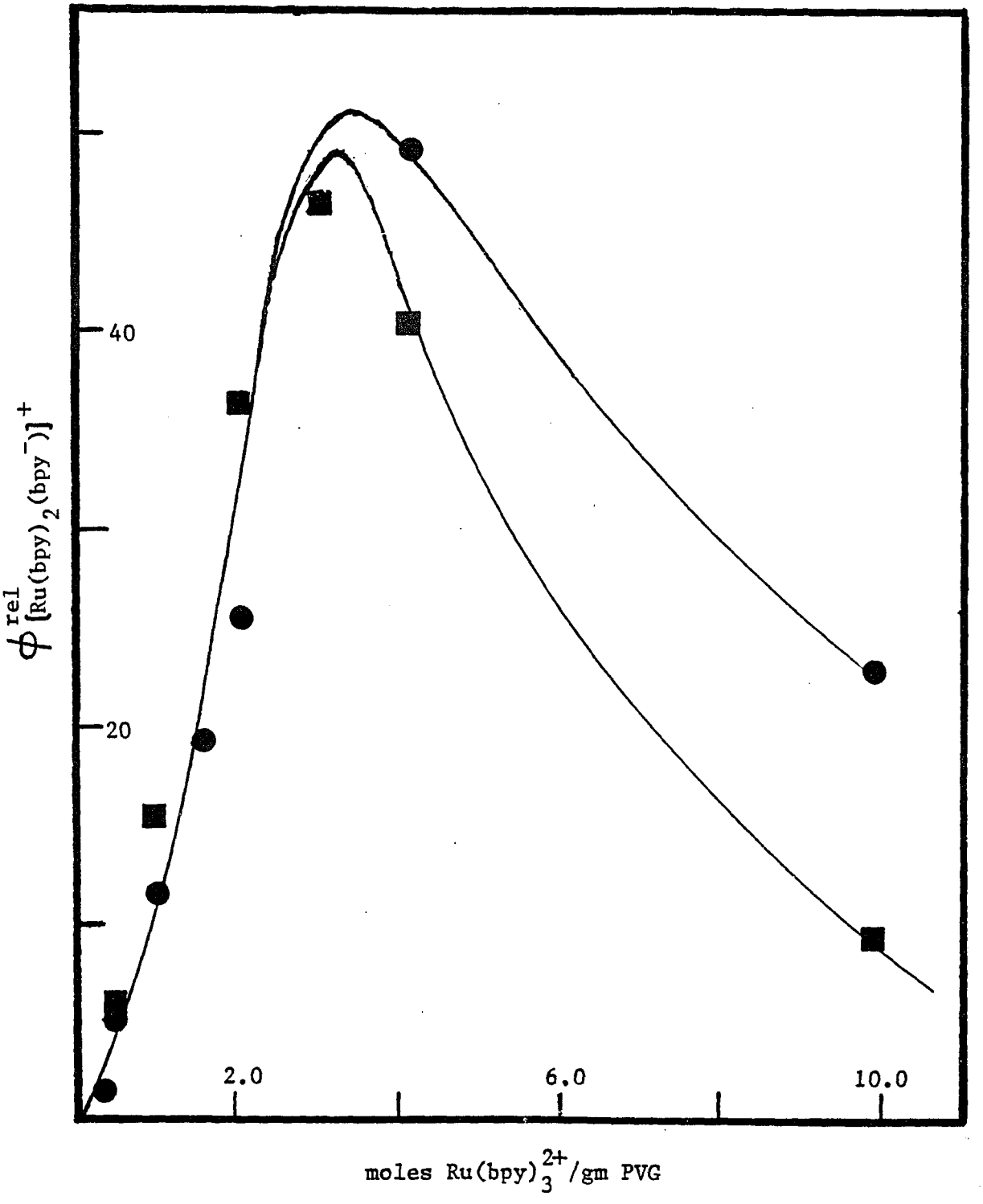
40
20
2.0
6.0
10.0
$\phi^{rel}_{[Ru(bpy)_2(bpy^-)]^+}$
moles $Ru(bpy)_3^{2+}$/gm PVG

gram is increased beyond 2.7×10^{-6}, however, the quantum yield of $[Ru(bpy)_2(bpy^-)]^+$ falls, although the decline is more pronounced in the absence of SnO_2.

These observations suggest that a photoinduced disproportionation of the dication, analogous to that previously reported in PVG, occurs in the presence of an optically transparent, conducting film of SnO_2 doped with Sb.

(vii) Quantum Yield of Emission from $Ru(bpy)_3^{2+}$ads

The luminescence quantum yield of a compound is defined as the fraction of molecules that emit a photon after direct excitation by the source.[183] Since only a fraction of the total number of emitted photons reach the detector in an emission spectrophotometer, the use of a compound with a known emission quantum yield as a standard for photon counting requires that the geometries of absorption of source intensity and emission from the standard match those of the sample. However, in this study, the sample and standard, an impregnated glass and a solution, respectively, are of dissimilar dimensions. In order to meet the above requirement, several approximations are made to prepare glass samples and solutions of similar absorbance that are placed in nearly identical positions in the sample compartment relative to source and detector.

Figure 21 provides a comparison of the relative emission intensities from 1-mm path length cells containing aqueous

Figure 21

Relative emission intensities from room temperature, 22±1°C PVG samples impregnated with $Ru(bpy)_3^{2+}$ ads (■), and H_2O solutions of $Ru(bpy)_3^{2+}$ (●) vs. $Ru(bpy)_3^{2+}$ absorbance at 452 nm. H_2O solutions are in a 1-mm path length cell. PVG samples and solutions are excited at 452 nm, and the emission intensities are monitored at 620 nm, using 11-nm excitation and emission slit widths.

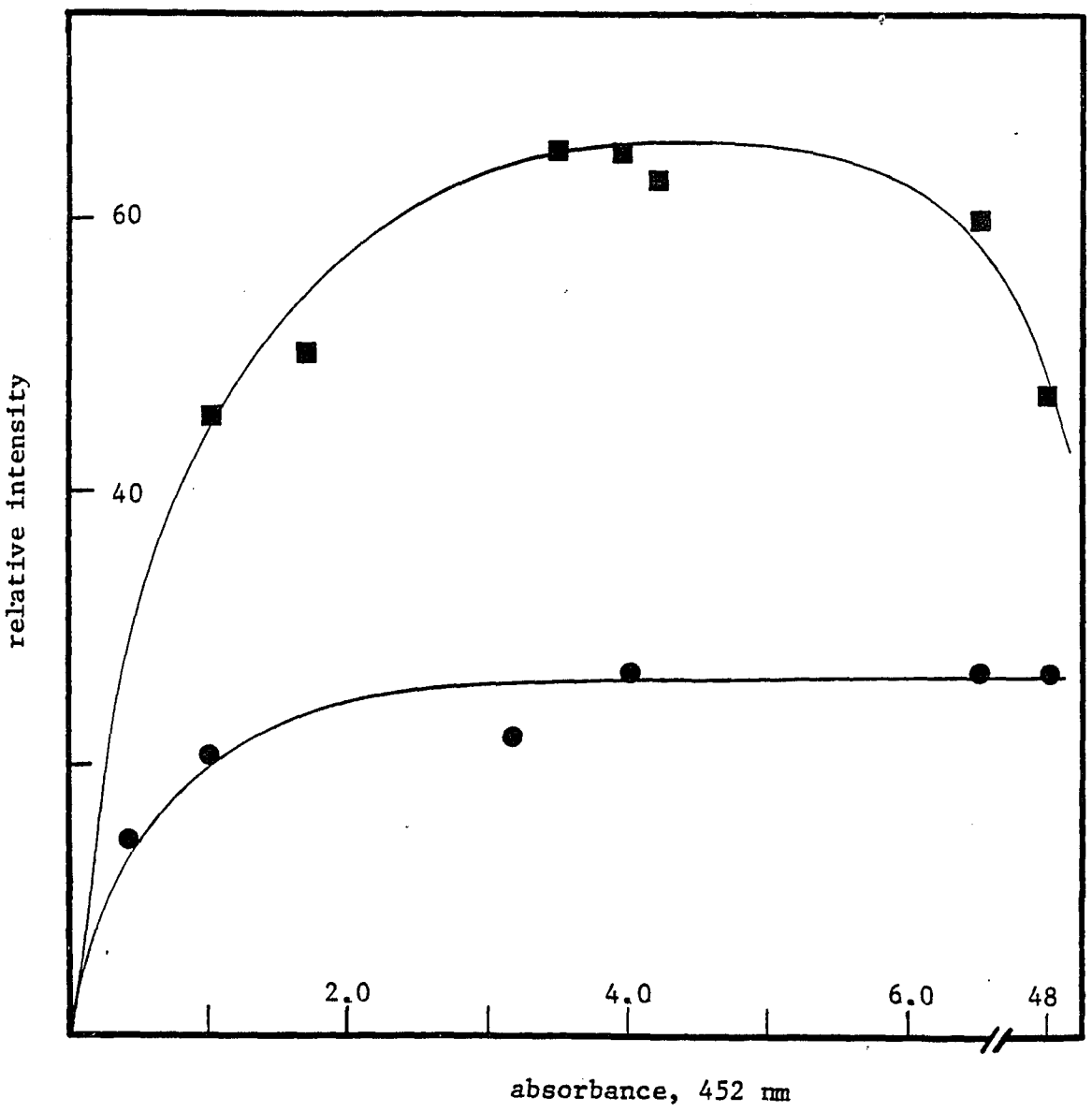

Figure 21

solutions of $Ru(bpy)_3^{2+}$ to those from $Ru(bpy)_3^{2+}$ads at 620 nm. Listed in Table 6 are the relative emission intensities and absorbances of the solution standards and glass samples, and their concentrations and number of moles/gm PVG of $Ru(bpy)_3^{2+}$, respectively. Since the absorbance of $Ru(bpy)_3^{2+}$ in the glass and in solution obeys Beer's Law, to facilitate comparisons in the two media, the emission intensities are plotted as a function of absorbance at 450 nm in Figure 21, rather than concentration (solution) or moles of $Ru(bpy)_3^{2+}$/gm PVG (glass). In solutions of absorbance <4 the emission intensity increases nearly linearly with increasing absorbance, but when the absorbance is $\geq$4, essentially all of the exciting light is aborbed within a very narrow path length, therefore the emission intensities from the latter group of solutions are essentially identical. Similarly, a rise in the emission intensity with increasing absorbance is found for $Ru(bpy)_3^{2+}$ads as the absorbance approaches 4, however at absorbance $\geq$4, the emission intensity declines with increasing absorbance.

Aqueous solutions of $Ru(bpy)_3^{2+}$, when compared to PVG impregnated with $Ru(bpy)_3^{2+}$ having the same absorbance at 450 nm, display significantly less emission intensity. At an absorbance of 4, the ratio of the emission intensity from $Ru(bpy)_3^{2+}$ to that from $Ru(bpy)_3^{2+}$ in aqueous solution is $64\pm3/27\pm1$ or

Table 6

Relative Emission Intensities from $Ru(bpy)_3^{2+}$ in Aqueous Solution and in Porous Vycor Glass at 22±1°C

I. H_2O Solution[a]

Absorbance, 452 nm[b]	$[Ru(bpy)_3^{2+}]$, M	Relative Emission Intensity, 620 nm[c]
0.42	3.5×10^{-4}	14±1
1.0	8.3×10^{-4}	21±1
2.1[d]	1.8×10^{-3}	22±1
3.2[d]	2.7×10^{-3}	27±1
4.0[d]	3.3×10^{-3}	27±1
6.5[d]	5.4×10^{-3}	27±1
12.5[d]	1.0×10^{-2}	27±1
24.5[d]	2.0×10^{-2}	27±1
44.0[d]	3.7×10^{-2}	27±1
>48[d]	4.0×10^{-2}	27±1

II. Porous Vycor Glass[e]

Absorbance, 452 nm	moles $Ru(bpy)_3^{2+}$/gm PVG[f]	Relative Emission Intensity, 620 nm[c]
1.0	1.6×10^{-7}	46
1.7	2.7×10^{-7}	50
3.5[d]	5.5×10^{-7}	65±3
3.9[d]	6.1×10^{-7}	64±3
4.2[d]	6.6×10^{-7}	63±1
6.5[d]	1.0×10^{-6}	60±2
48.8[d]	7.6×10^{-6}	47±2

a) deaerated solutions.

b) 1-mm path length cells.

c) λ_{ex} = 452 nm; excitation and emission slit widths = 11 nm.

Table 6, continued

d) calculated via $\text{absorbance}_{520\ nm} \times \left(\frac{\epsilon_{452\ nm}}{\epsilon_{520\ nm}}\right)$ or,

$$\text{absorbance}_{550\ nm} \times \left(\frac{\epsilon_{452\ nm}}{\epsilon_{550\ nm}}\right).$$

e) degassed samples.

f) 25-mm x 25-mm x 4-mm PVG samples.

2.4 ± 0.2. A basic assumption in this comparison is that similar fractions of the total emitted light are detected when the solution standard and glass sample are placed at the same distance from and angle with the source and detector. Then, the ratio of the relative emission intensities, where most of the exciting light is absorbed in a narrow region nearest the source, multiplied by a factor to correct for the differing indices of refraction of H_2O and PVG, gives the ratio of the luminescence quantum yields in the two media. Therefore, the quantum yield of emission from $Ru(bpy)_3^{2+}$ads is given by,[184]

$$2.4 \times \left(\frac{1.5}{1.33}\right)^2 \times 0.042 \qquad (19)$$

where 1.33 and 1.5 are the refractive indices of H_2O[171b] and PVG[172], respectively, and 0.042 is the luminescence quantum yield of $Ru(bpy)_3^{2+}$ in H_2O.[36] A luminescence quantum yield of 0.12 ± 0.01 is calculated for $Ru(bpy)_3^{2+}$ads via equation 19.

B. Spectral and Photophysical Properties of Ru(II) Complexes with 2-(Phenylazo)pyridine

(i) Resonance Raman Spectra

When excited close to the maximum of the visible absorption band, the resonance Raman spectra of $Ru(azpy)_2L^{n+}$ complexes consist of a series of bands in the 200-1650 cm^{-1} region. The most intense bands, however, appear between 950 and 1400 cm^{-1}. Resonance Raman spectra of several of the $Ru(azpy)_2L^{n+}$

complexes within the latter frequency region appear in Figure 22, along with a spectrum of $Ni(azpy)_2Cl_2$, although the latter is most likely a pre-resonance spectrum.[185] Table 7 lists the frequencies of the four band showing the most significant resonance enhancement for the $Ru(azpy)_2L^{n+}$ series. With the exception of one band, the frequencies vary ≤ 10 cm^{-1} over the entire series of complexes. Because of this invariance and their commonality to the entire series of complexes, regardless of the coligands, these vibrations are assigned to the azpy ligand. No additional bands attributable to any source other than solvent apppear in the resonance Raman spectra.

The assignment of all resonance Raman bands awaits a normal coordinate analysis, however, several qualitative assignments can be made. In contrast to the 3 bands listed in Table 7, whose frequencies vary by ≤ 10 cm^{-1}, there is one band, typically the most intense in the spectrum, which varies in frequency from 1337 cm^{-1} ($L = 2Cl^-$) to 1392 cm^{-1} ($L = 2CN^-$) for the Ru(II) complexes, and appears at 1433 cm^{-1} for the Ni(II) complex. Since the frequencies of this band correspond to those reported for the N=N stretch in the IR spectra,[93,94] this band is assigned to the azo stretching mode in azpy.

Bands near 980, 1205, and 1315 cm^{-1} show significant resonance enhancement, with some variations in relative intensity from spectrum to spectrum. Because of their intensities, these bands must be associated with bonds

Figure 22

Raman spectra of azpy, $Ni(azpy)_2Cl_2$, $Ru(azpy)_2(CN)_2$, and $Ru(azpy)_2(NO_2)_2$. Latter two are resonance enhanced, obtained via laser excitation at 514.5 nm.

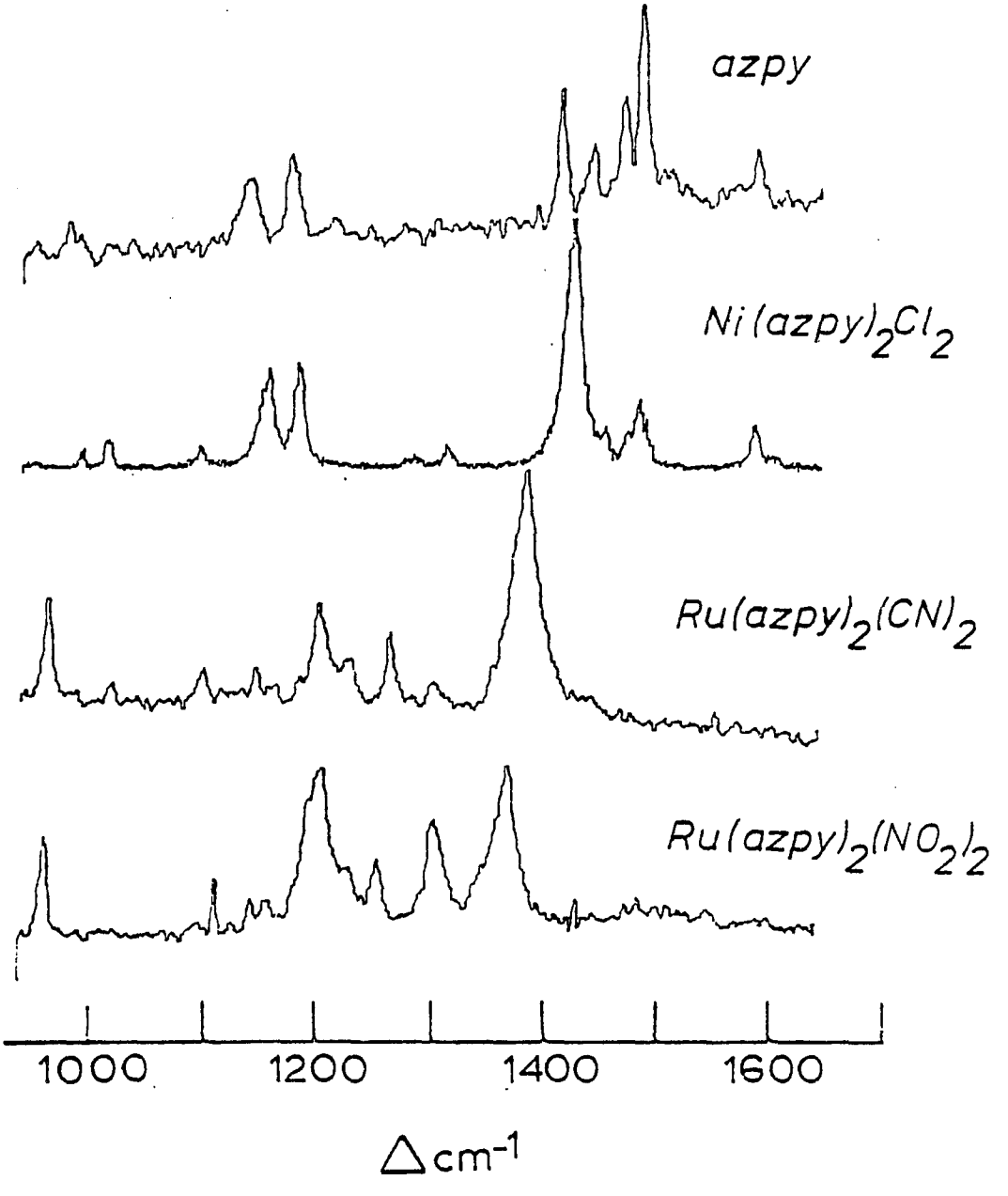
azpy
Ni(azpy)2Cl2
Ru(azpy)2(CN)2
Ru(azpy)2(NO2)2
1000
1200
1400
1600
Δcm-1

Figure 22

Table 7 - Raman Bands[a] for $Ru(azpy)_2L^{n+}$ Complexes Showing Greatest Enhancement

coligand (L)	phenyl	No. 2	No. 3	N=N
2 CN^-	975	1211	1309	1392
2 NO_2^-	974	1215	1313	1378
btz	975,991	1204	1315	1360,1375sh
bpy	976	1201	1317	1364
azpy	966,975	1200	1317	1368,1384sh
en	980	1209	1316	1360
$acac^-$	981	1207	1313	1346
2 Br^-	978	1212	1311	1350
2 N_3^-	977	1216	1309	1338
2 Cl^-, α[b]	977	1209	1311	1345
2 Cl^-, β[c]	976	1209	1310	1337

a. frequency in cm^{-1}.

b. alpha isomer.

c. beta isomer.

contiguous to the N=N bond in the azpy ligand, including the C-N(pyridine) and N-C(phenyl) bonds. Also, the 980 cm^{-1} band is within the region expected for a phenyl ring breathing mode.

Despite direct coordination of the ring nitrogen to Ru(II), vibrations assignable to the pyridyl ring of the azpy ligand are very weak. In particular, pyridyl symmetric breathing modes, generally found in the 1000 to 1050 cm^{-1} region, and typically the most intense in the resonance Raman spectra of pyridine and polypyridine substituted metal complexes[110] are observed, but are of extremely low relative intensity. Low intensity bands above 1450 cm^{-1}, assignable to other pyridyl ring modes, are also present.

(ii) Absorption and Emission Spectra

All of the $Ru(azpy)_2L^{n+}$ complexes display intense visible absorption bands between 498 nm (L = azpy) and 615 nm (L = $2N_3^-$) (see Table 3). Excitation with the 514.5-nm line from a CW Ar ion laser at room temperature, 22±1°C, induces near-IR emission from solid samples of $Ru(azpy)_2L^{n+}$, where L = azpy, bpy, btz, en, $acac^-$, $2NO_2^-$, $2CN^-$, and weaker emissions from room temperature fluid solutions of $Ru(azpy)_3^{2+}$, $Ru(azpy)_2bpy^{2+}$, $Ru(azpy)_2btz^{2+}$, and $Ru(azpy)_2(CN)_2$. The unusual asymmetry of the representative emission spectrum in Figure 23 is the result of a sharp decline in photomultiplier spectral sensitivity

Figure 23

Emission spectrum of $Ru(azpy)_3^{2+}$ in H_2O at room temperature, $22\pm1^{\circ}C$. Excited at 514.5 nm with argon ion laser.

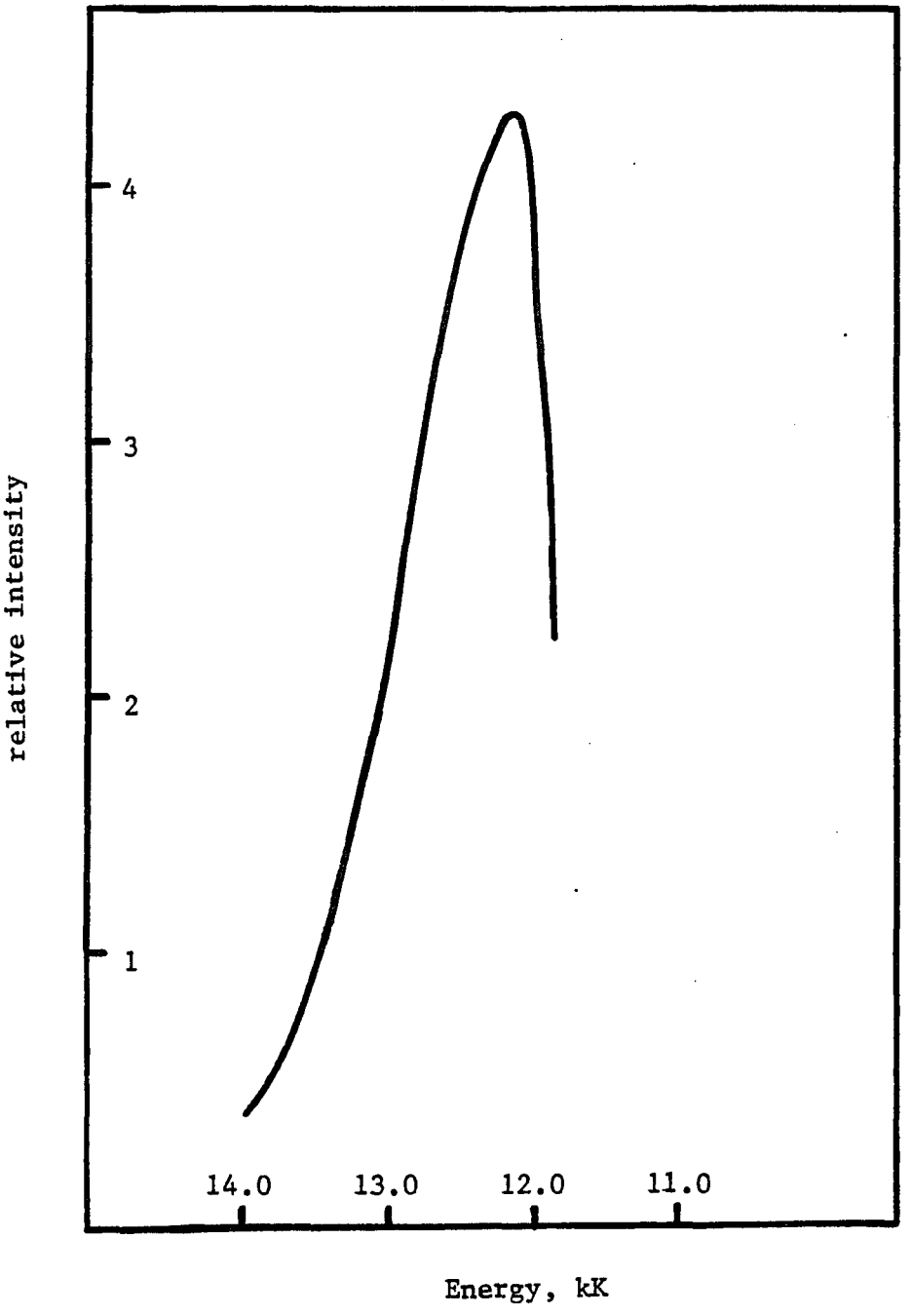

Figure 23

at $\lambda \geq 870$ nm. Consequently, all emission spectra truncate at 870 nm, and for many of the complexes listed in Table 8, only the short-wavelength limits of the actual emission maxima are experimentally accessible. For those complexes which display measureable emission maxima, the difference between the energies of the visible absorption band and the emission band maxima are relatively constant.

As indicated in Table 8, room temperature solid samples of $[Ru(azpy)_3](PF_6)_2$ and $[Ru(azpy)_2btz](ClO_4)_2$ show two emission maxima. Although the emission maxima of the btz complex differ from those found at 77°K,[94] the difference is attributed to the spectral sensitivities of the detectors and the 755 and 822-nm transitions at 77°K correspond, respectively, to the 776 and 833-nm transitions at room temperature. Maxima at 784 and 846 nm are observed in the room temperature emission spectrum of solid samples of $[Ru(azpy)_3](PF_6)_2$, whereas a single maximum at 764 nm was found in the low temperature spectrum. Since the energy difference between the 784 and 764-nm transitions, 334 cm^{-1} is similar to the shift of the higher energy $[Ru(azpy)_2btz](ClO_4)_2$ transition, 358 cm^{-1}, the maxima are assigned to the same transition, and the absence of a second peak in the low temperature spectrum is attributed to the spectral sensitivity of the detector rather than a fundamental molecular change.

Table 8

Emission Maxima and Redox Potentials of the $Ru(azpy)_2L^{n+}$ Complexes.

Coligand	Emission Maxima[a] (nm)	E, V[b] III→II	E, V[b] II→I
Azpy	784, 846 (835)	-	0.30
Btz	776, 833 (≳870)	2.0	-0.19
Bpy	854 (≳870)	-	0.17
$(CN)_2$	≳870	-	-0.24
Acac	≳870	1.78	-0.14
en	≳870	-	-0.07
$(NO_2)_2$	≳870	-	-0.22
$(tu)_2$	-	1.38	-0.08
$(Br)_2$	-	1.43	-0.30
$(N_3)_2$	-	1.2	-0.28
α-$(Cl)_2$[c]	-	1.45	-
β-$(Cl)_2$[c]	-	1.39	-

a. Values in parentheses are emission maxima from room temperature acetone solutions of the complexes.

b. Reduction potentials relative to the standard hydrogen electrode.

c. Refer to the α and β isomers, respectively.

When $[Ru(azpy)_3](PF_6)_2$ is disolved in acetone, the 784 and 846-nm emissions are replaced by a single emission with a maximum at 835 nm. When the btz complex is dissolved in acetone, the 776 and 833-nm emissions disappear and the spectrum consists only of a short-wavelength tail of one or more emissions with maxima at $\geq$870 nm.

(iii) Emission Quenching

To test conclusions arrived at for the photoredox properties of $^*Ru(azpy)_3^{2+}$, namely that the excited state lies, energetically, below the 3+ and above the 1+ ground redox states, quenching of $^*Ru(azpy)_3^{2+}$ emission by a series of reversible, one-electron redox couples was investigated. The quenchers range in oxidation potential from -1.61 V ($Ce^{3+} + e^- \longrightarrow Ce^{4+}$) to +0.44 V ($MV^+ + e^- \longrightarrow MV^{2+}$), where MV^{2+} denotes the N,N'-dimethyl, 4,4'-bipyridinium dication (Table 9). Quenching via energy transfer is discounted since the excited state energies of all quenchers exceed that of $^*Ru(azpy)_3^{2+}$, and, as described below, the observed quenching is in accord with the predicted energetics of photoinduced redox reactions. Comparing the absorption spectra of $Ru(azpy)_3^{2+}$ in the presence and absence of quencher establishes that none of the quenchers undergo a reaction with ground state $Ru(azpy)_3^{2+}$.

The quenching data is summarized in Table 9. Quenching of $^*Ru(azpy)_3^{2+}$ emission in aerated room temperature, 22±1°C, fluid solution was found for Fe^{3+}, $Fe(CN)_6^{4-}$, and Ce^{4+}, while Fe^{2+}, $Fe(CN)_6^{3-}$, Ce^{3+}, and MV^{2+} did not quench the emission. Where quenching occurs, plots of the relative $^*Ru(azpy)_3^{2+}$ emission intensity, I_o/I, measured at 835 nm, vs. [Q] are linear throughout >90% of the quenching. The Stern-Volmer constants, K_{SV}, for the various quenchers are summarized in Table 9. The bimolecular quenching rate constants, k_b, listed in Table 9, are calculated from $K_{SV} = k_b t_o$, where t_o is the luminescent lifetime of $^*Ru(azpy)_3^{2+}$ in aerated, room temperature fluid solution. The lifetime is calculated from a plot of ln I_{em} vs. time, which, as shown in Figure 24, is linear throughout >95% of the emitted light and yields a first-order emission decay rate constant of 2.39±0.12 x 10^6 sec^{-1}, corresponding to an emission lifetime of 419±20 nsec.

There are no net chemical reactions between $^*Ru(azpy)_3^{2+}$ and any of the quenchers. The $^*Ru(azpy)_3^{2+}$ emission intensity in the presence of quenchers exhibits no time dependence and absorption spectra of solutions containing $Ru(azpy)_3^{2+}$ and the quenchers, recorded before and after quenching experiments, are identical.

Table 9

Stern-Volmer Constants and Bimolecular Rate Constants for Quenching of $Ru(azpy)_3^{2+}$ in Aqueous Solution and the Standard Potentials for Oxidation or Reduction of the Quenchers.

Quencher	K_{sv} (M^{-1})	k_b[a] ($M^{-1}sec^{-1}$)	E^o[b] V
MV^{2+}	10	-	-0.44
Fe^{2+}	1.5×10^4	3.6×10^{10}	-0.77
Fe^{3+}	10	-	+0.77
$Fe(CN)_6^{4-}$	7.4×10^3	1.8×10^{10}	-0.36
$Fe(CN)_6^{3-}$	10	-	+0.36
Ce^{3+}	10	-	-1.61
Ce^{4+}	1.5×10^3	3.6×10^9	+1.61

a. Calculated according to $K_{sv} = k_b t_o$ where t_o = 418 nsec.

b. from ref 174, appendix I.

Figure 24

Plot of ln I_{em} vs. time for $Ru(azpy)_3^{2+}$ in aerated, aqueous solution at room temperature, 22±1°C.

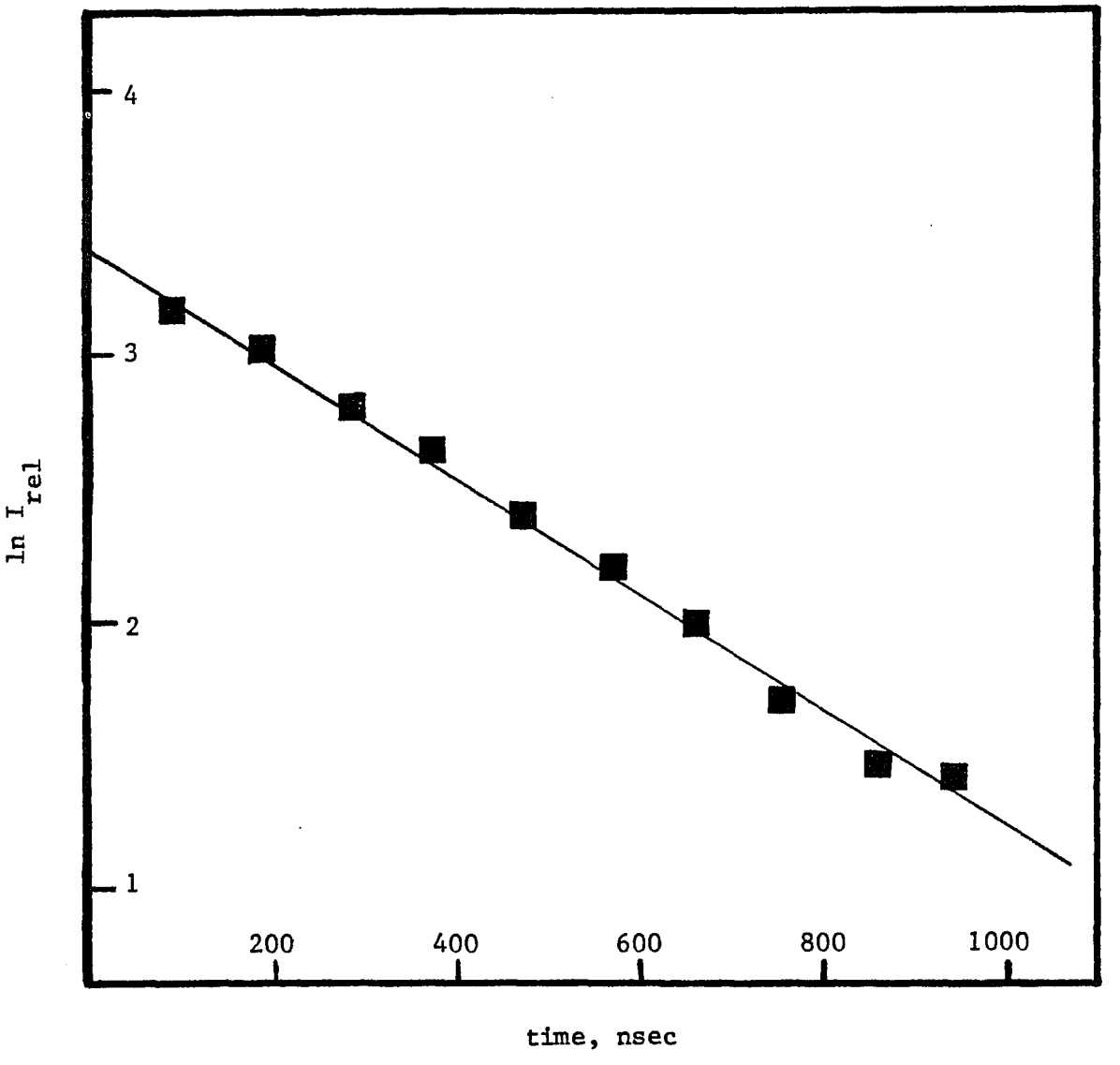

Figure 24

IV. Discussion

A. Photophysical and Photoredox Properties of $Ru(bpy)_3^{2+}$ads

(i) Characterization of $Ru(bpy)_3^{2+}$ads and the Nature of the Binding Interaction with PVG

Silica surfaces are of practical importance as cation exchange materials in a wide number of applications.[186-188] The high surface area of most powdered silicas accounts for their use as highly effective adsorbents. Unfortunately, transmission spectroscopic studies of silica are hindered by the large degree of light scattering by the powder surface.

As an alternative to powdered silica, Corning code 7930 porous Vycor glass has been extensively utilized in studies of physical adsorption and surface activity since, in addition to a having a high surface area (~ 200 m^2g^{-1}), it features transparency to visible and IR radiation.[189] The porous glass used in these studies consists of a matrix of interconnected cavities or pores of diameter 70 ± 21 A^o, and has an average surface area of 130 m^2g^{-1}.[138] Pores are formed by acid leaching of a conventional borosilicate glass and, neglecting H_2O, the finished product is comprised of 96% SiO_2, 3% B_2O_3, and 1% as various metal oxides, e.g. Na_2O, Al_2O_3.[189] Thus, in terms of chemical composition, porous Vycor glass is closely related to silica gel,[190,191] although the former has a higher B/Si ratio

(1:3) on the surface than in the bulk (1:18),[192] leading to the presence of a larger number of Lewis acid-type sites per gram of active surface area in porous glass than in commercial silica gel. In addition to Lewis acid sites on the porous Vycor surface, there are Bronsted sites, present predominately in the form of SiOH and hydrogen-bonded H_2O,[193-195] which are activated by proton dissociation from hydroxyl groups.[187] H_2O.[203-205] As indicated by the decrease in pH of the surrounding aqueous medium, and the development of a negative zeta potential when powdered PVG is dispersed in H_2O,[144] the surface hydroxyl groups are relatively acidic. A number of workers have noted the acidity of porous silicas in the presence of metal ions.[196,197] Ahrland and coworkers, for example, have shown that for each equivalent of metal ion adsorbed, one equivalent of H^+ is evolved from the silica into the aqueous phase.[143] The binding of $Ru(bpy)_3^{2+}$ to the PVG surface is also consistent with a mechanism involving cation exchange with acidic hydroxyl groups. Figure 25 shows that the complex ion is adsorbed without concurrent adsorption of the Cl^- counterion.

The similarity in the absorption, emission, and resonance Raman spectra, (Figures 8 and 9) as well as the luminescence lifetime of the adsorbed complex to that of $Ru(bpy)_3^{2+}$ in aqueous or alcoholic solution establishes that the chemical integrity of the complex is

Figure 25

The mole fraction, f_a, of $Ru(bpy)_3^{2+}$ and Cl^- adsorbed to PVG *vs.* the time a 1.25-gm piece of glass remains in 25 ml of a 1.03×10^{-4} M aqueous solution of $Ru(bpy)_3^{2+}$.

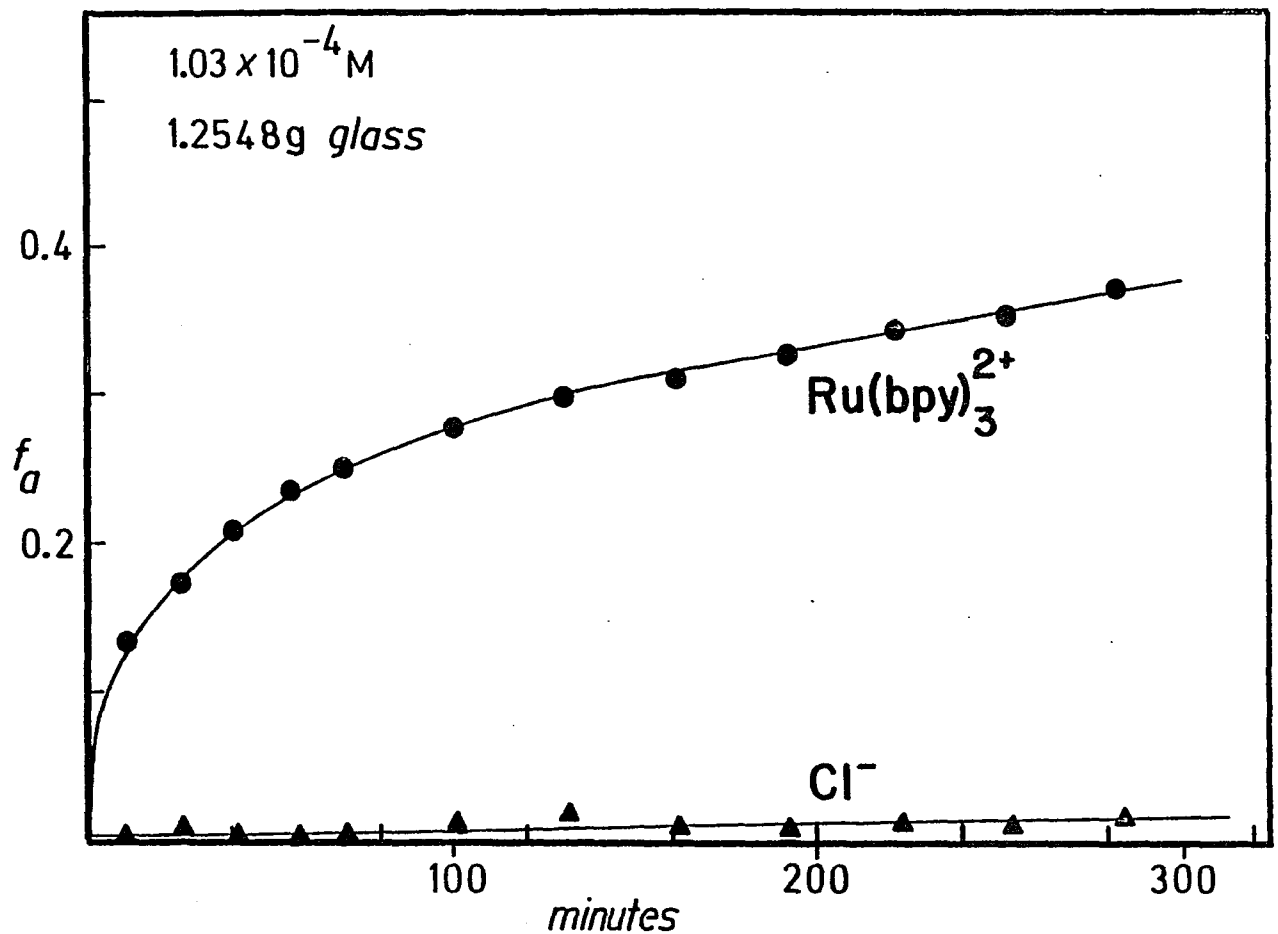
1.03 x 10⁻⁴ M
1.2548g glass
0.4
0.2
f_a
Ru(bpy)$_3^{2+}$
Cl⁻
100
200
300
minutes

Figure 25

retained on adsorption to PVG, and also suggests that the glass is an environment similar to a hydroxylic solvent. The PVG surface is, in fact, extensively hydrated at room temperature, and elevated temperature is required for complete dehydration. Thermal gravimetric analysis of PVG demonstrates that H_2O is continuously being evolved at temperatures ranging from 100° to 600°C.[198] Furthermore, bands assignable to chemisorbed H_2O remain present in the IR spectra of PVG until temperatures nearing the consolidation temperature of the glass (700°C) are attained.[193,199] Thus, even after removal of bulk water by pumping following the adsorption of $Ru(bpy)_3^{2+}$ from aqueous solution, the glass still contains a considerable amount of chemisorbed, i.e., hydrogen-bonded H_2O.

The above comparison is not intended to imply the absence of any interaction between the adsorbed complex and the glass, nor to suggest the equivalence of the glass to a hydroxylic solvent, but rather to draw an analogy between the two environments through spectral and photophysical similarities. The absence of macroscopic diffusion by $Ru(bpy)_3^{2+}$ once bound to the support, and the necessity of an electrolyte in order to displace the complex from the glass[144] suggests that adsorption to a site involves a significant degree of interaction. Although the picture of the binding site is complicated by the presence of acidic hydroxyl groups of several types, the nature of

the binding interaction is apparently electrostatic. Adsorption involving covalent interaction between $Ru(bpy)_3^{2+}$ and Lewis acid sites, which would probably require dissociation of a Ru-N bond, is discounted by the absence of any detectable changes in the UV-VIS and resonance Raman spectra of the complex upon adsorption from aqueous solution. Instead, the exclusive adsorption of the cation and the weak acid character of the glass point to ionic bonding to an anionic silanol site which, to maintain electrical neutrality, must be composed of 2 SiO^- groups.

(ii) Distribution of $Ru(bpy)_3^{2+}$ads on PVG

Essential to any rationalization of the photobehavior of $Ru(bpy)_3^{2+}$ in porous Vycor is some knowledge of its distribution on the glass. The distribution of the adsorbed complex will be governed by the availibility of sites on the support. The gross number of silanol sites on PVG could, in principle, be limited to a number of active sites for adsorption of $Ru(bpy)_3^{2+}$ by the cavity size and geometry. However, under the conditions of these experiments where the amount of complex adsorbed does not exceed 10^{-5} moles of $Ru(bpy)_3^{2+}$/gm PVG, size of the cavities will not limit capacity. Since the number of cavities per gram PVG is $1.2\pm0.3 \times 10^{18}$,[146] even at the maximum level of impregnation of samples used in these experiments, there are an average of 6 molecules/cavity. The molecular radius of $Ru(bpy)_3^{2+}$, taken as 7.4

A^{o}, is ca. 10% of the mean cavity radius, 70 A^{o}, and assuming spherical molecules and cavities, a molecule of $Ru(bpy)_3^{2+}$ occupies ca. 0.1% of the available cavity volume.

Electrostatics are undoubtedly important in determining the distribution of the adsorbed complex. The vast amount of cavity volume available to $Ru(bpy)_3^{2+}$ suggests that the distribution on the glass is not affected by the cavity dimensions nor by electrostatic repulsion between dipositive ions. If that is the case, then electrostatic interaction between $Ru(bpy)_3^{2+}$ and anionic sites on the glass dictates the adsorption process, and the distribution of the adsorbed complex reflects the distribution of binding sites within the glass. Although the latter are randomly distributed throughout the glass,[200,201] the distribution of $Ru(bpy)_3^{2+}$ is uniform on the surface, but not through the 4-mm thickness of the glass (Fig. 10). The complex does not penetrate beyond a depth of ca. 0.2 mm, however this may not be an actual penetration as much as a reflection of the deviation from planarity in the glass surface. The latter is a likely explanation in that the glass has a wavy surface and, when viewed through a microscope, the appearance of a series of concentric irregular circles suggests that the pore openings may have a funnel-like shape. The surface irregularities may be pore openings which, being funnel-like, would have a higher density of sites - and

therefore be more conducive to binding a dication - within, than on the outer surface.

(iii) Luminescence Quantum Yield of $Ru(bpy)_3^{2+}$ads in PVG

Despite a great many similarities between the spectral and photophysical properties of $Ru(bpy)_3^{2+}$ on the glass and in aqueous media, there is a noticeable difference in the luminescence quantum yield in the two media. The quantum yield in water is 0.042[36], while that in PVG is 0.12. Although several assumptions were made in order to obtain the luminescence quantum yield in PVG, the calculated value of 0.12 is reasonable. A very similar value was reported for the luminescence yield in hectorite by Van Damme and coworkers.[135] The latter found that the luminescence intensity of $Ru(bpy)_3^{2+}$ in a dry hectorite clay membrane increases by a factor of 2-3 when the clay is progressively saturated with H_2O. Saturating PVG impregnated with $Ru(bpy)_3^{2+}$ with H_2O results in a >10-fold increase in emission intensity. The increase in emission intensity in water-saturated hectorite is attributed to the formation of a covalently hydrated Ru(II) complex. As noted above, PVG is extensively hydrated at room temperature, even after evacuation, suggesting that adsorbed H_2O may contribute to the higher emission yield in the glass than in aqueous solution, as well as the observed increase in the emission intensity when the glass is saturated with H_2O.

The formation of a covalently hydrated species in hectorite is accompanied by a 7-nm red shift in the $Ru(bpy)_3^{2+}$ MLCT absorption maximum. Likewise, a 5 to 7-nm red shift in the MLCT absorption maximum occurs on saturation with H_2O of a PVG sample impregnated with $Ru(bpy)_3^{2+}$ (Figure 26). Although an unambiguous identification of the covalently hydrated species was not presented, Van Damme and coworkers did propose several possibilites. A Ru(II) complex with a ligand having the following structure is reasonable and would account for the spectral and emission intensity changes when the amount of water is changed on the surface if it undergoes an acid-base equilibrium.

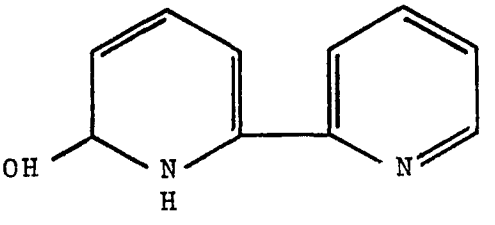

The following alternative structure could account for an increase in emission intensity since the rings are not coplanar.

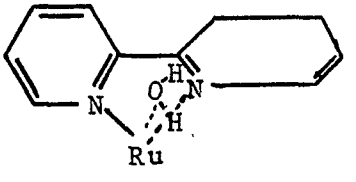

Unfortunately, spectral evidence for the formation of a complex having the above structure, i.e. the $\pi - \pi^*$ absorption band, could not be obtained since the glass is opaque in the UV. However, the spectral changes in the

Figure 26

Absorption spectra of $Ru(bpy)_3^{2+}$ ads (2.0×10^{-7} moles/gm PVG), evacuated overnight (——), and after saturation of the glass with H_2O (---).

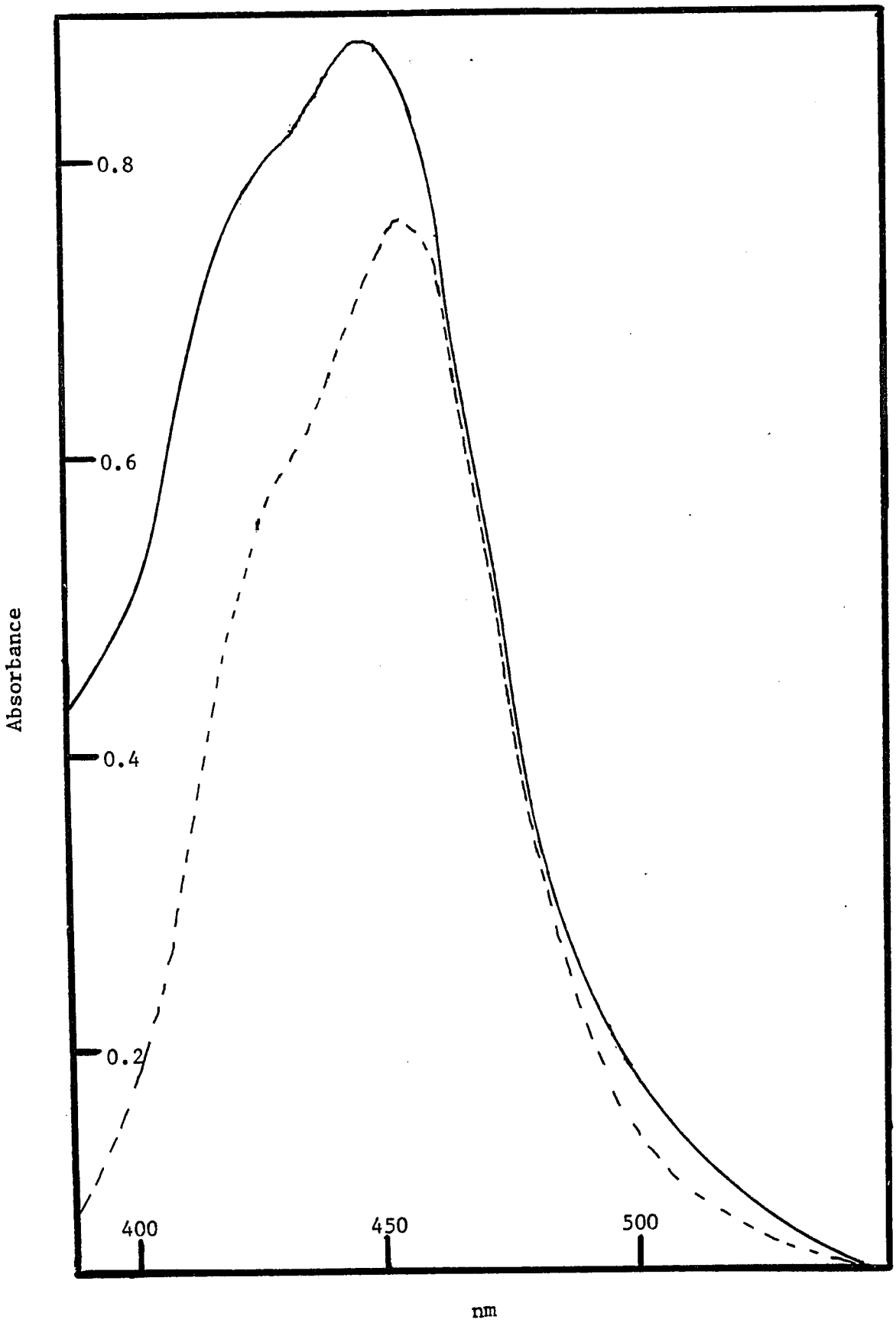

Figure 26

visible region suggest that H_2O in some unspecifiable manner interacts with the adsorbed complex.

Another dissimilarity between the emission behavior of $Ru(bpy)_3^{2+}$ads and that in fluid media, is the decline in emission intensity as the amount of luminescent complex present on the glass is increased beyond ca. 6.5×10^{-7} moles/gm PVG. Figure 21 demonstrates this effect with a comparison to the emission intensity from the complex in aqueous solutions of varying concentration. The x-axis is in absorbance units rather than moles/gm and M, for convenience in comparing the emission intensities in PVG and water, respectively. Although a similar trend is observed in the two media when the absorbance is <4, there is significant difference at higher absorbance values. While the emission intensity from aqueous solutions remains essentially constant in the latter group of solutions, that from glass samples falls as more complex is adsorbed to the glass.

This observation is not the result of a triplet-triplet annihilation. Doubling the excitation slit width resulted in a similar gain in the emitted light in both solutions and glass samples. Concentration quenching, which has been reported for $Ru(bpy)_3^{2+}$ in cellulose under similar conditions of high concentration and low excitation intensity,[147] could account for the decline in emission intensity in PVG at higher impregnation levels.

(iv) Quenching of the $^*Ru(bpy)_3^{2+}$ads Luminescence by Gases

One of the purposes for adsorbing $Ru(bpy)_3^{2+}$ to porous Vycor is to explore luminescence quenching of the adsorbed complex by gases. In these experiments, a major goal was the initiation of a photoinduced redox reaction between $Ru(bpy)_3^{2+}$ and one of the gases, particularly SO_2. Although there was no net photochemistry, the gases SO_2, O_2, and N_2O quench the luminescence of the adsorbed complex. Since the quenching reactions are reversible, a mechanistic distinction between energy transfer and electron transfer can only be based upon the energetic feasibility of each process. Such a distinction is possible with N_2O and SO_2, but not with O_2.

Previous studies of the quenching of $*Ru(bpy)_3^{2+}$ by O_2 and the resulting chemistry in fluid solution have led to different conclusions regarding mechanism. Demas and coworkers[82] propose an energy transfer mechanism while Srinivasan and coworkers[162] propose an electron transfer mechanism. PVG has a surface pH of 4-5.[176] Assuming that adsorption does not radically change the O_2 excited singlet state energies[202] and the reduction potential of adsorbed O_2 is equivalent to that in pH 4-5 aqueous solution, -0.63V,[203,204] a similar ambiguity exists with the adsorbed species and prevents a mechanistic distinction.

Recent calculations indicate that the excited states of N_2O lie at energies $\geq$5.4eV above the ground state,[205] although a very weak absorption in the

spectrum of N_2O has been reported at 4.05eV.[206] Assuming, in view of the low extinction coefficient, that the 4.05eV absorption positions the lowest triplet excited state, energy transfer from $^*Ru(bpy)_3^{2+}$ to N_2O is endergonic by $\geq$2.0eV. Similar arguments lead to the same conclusion regarding quenching by SO_2, where the lowest lying triplet state is 3.20 eV above the ground state.[207] Consequently, quenching of $^*Ru(bpy)_3^{2+}$ads by N_2O and SO_2 must proceed by an electron transfer mechanism.

In aqueous solution SO_2 is a reductant with an oxidation potential which increases with increasing basicity.[208] Extrapolating this behavior to SO_2 adsorbed onto PVG suggests reductive quenching,

$$Ru(bpy)_3^{2+}ads + SO_2ads \underset{k_{th}}{\overset{h\nu}{\rightleftharpoons}} [Ru(bpy)_2(bpy^-)]^+ads + SO_2^+ads. \quad (20)$$

$[Ru(bpy)_2(bpy^-)]^+$ and SO_2^+ represent the reduced complex with an electron in the bipyridine π^* orbital and the oxidized quencher, respectively. Previous experiments in this laboratory show that $[Ru(bpy)_2(bpy^-)]^+$ has an unusually long lifetime when adsorbed onto PVG,[146] but spectra recorded before and after these quenching experiments do not indicate a net formation of the reduced complex. This suggests, as indicated in reaction 20, that a thermal back reaction complements the quenching reaction.

In contrast to SO_2, the use of N_2O as an electron scavenger and its mild oxidizing properties toward

low-valent transition metal complexes[164] suggests oxidative quenching,

$$Ru(bpy)_3^{2+}ads + N_2Oads \underset{k_{th}}{\overset{h\nu}{\rightleftharpoons}} Ru(bpy)_3^{3+} + N_2O^-ads. \quad (21)$$

Similar to the results with SO_2, the absence of a spectral change indicative of $Ru(bpy)_3^{3+}$ suggests a complementary thermal reverse reaction which is competitive with the decomposition of N_2O^-.[209]

Although N_2O and SO_2 quench by electron transfer processes, the formation of the donor-quencher pair proceeds by different pathways. With N_2O, the equivalence of intensity and lifetime quenching suggest a collisional process whereas the dominance of intensity quenching by SO_2 and O_2 implies formation of a donor-quencher pair prior to excitation. The physical arrangement of donor and quencher in these experiments - $*Ru(bpy)_3^{2+}$ is adsorbed onto the support while the quencher is in equilibrium between the vapor and adsorbed phases - suggests that dynamic quenching can be due to either the flux of gaseous molecules onto the surface or adsorbed N_2O molecules which, through long range interactions or migration, quench the adsorbed complex.

A number of observations, although individually not conclusive, collectively support dynamic quenching by N_2O molecules adsorbed onto the surface rather than gaseous N_2O molecules impinging on the surface. The flux of N_2O molecules onto the surface per second per cm^2 is $P/(2\pi mkT)^{1/2}$,[210] where P is the gas

pressure and m, k, and T are, respectively, the molecular mass, Boltzman constant, and temperature which in these experiments is 295°K. Letting P = 0.1 atm and substituting the other appropriate values yields a flux of 5.1×10^{-2} moles N_2O/sec-cm^2. However, this represents the flux onto a principally vacant surface since the fractional surface coverage due to $Ru(bpy)_3^{2+}$ is ≤ 0.01. Therefore, assuming a $^*Ru(bpy)_3^{2+}ads$-N_2Oads collision is necessary for quenching, the rate of quenching by N_2O molecules impinging on the surface is $\leq 5.1 \times 10^{-4}$ moles/sec-cm^2. This rate of quenching by impinging N_2O molecules is also equal to $k_b(m_{N_2O})(m_{^*Ru(bpy)_3^{2+}ads})$ where k_b is the bimolecular quenching rate constant and m_{N_2O} and $m_{^*Ru(bpy)_3^{2+}ads}$ are the moles of gaseous N_2O and $^*Ru(bpy)_3^{2+}ads$, respectively. Since ca. 1 cm^2 of the impregnated sample is exposed to the exciting light, an upper limit of $m_{^*Ru(bpy)_3^{2+}ads}$ is the moles of $Ru(bpy)_3^{2+}ads$ per cm^2 of PVG or 5.71×10^{-8} moles/cm^2. Taking this value, $m_{N_2O} = 6.6 \times 10^{-4}$ moles (P = 0.1-atm), and a rate of 5.1×10^{-4} moles/sec-cm^2, the above equality yields a bimolecular rate constant of 1.4×10^7 moles^{-1}sec^{-1}. Comparing the calculated value with the experimental value, $k_b = 4.7 \times 10^9$moles^{-1}sec^{-1} (Table 4),

suggests the rate at which N_2O molecules impinge upon the surface is not sufficient to account for the observed quenching rate constant. Furthermore, since the number of collisions with the surface, $P/(2\pi mkT)^{1/2}$, increases linearly with increasing pressure, dynamic quenching due to the flux of gaseous N_2O molecules onto the surface would exhibit a linear pressure dependence. Yet, as shown in Figure 12a, quenching is a function of m_{ads} and the latter is not a linear function of pressure. In addition, quenching is not a reproducible function of pressure, but rather a reproducible function of the moles of N_2O adsorbed per gram by the different samples of impregnated PVG. These observations lead to the conclusion that dynamic quenching of $*Ru(bpy)_3^{2+}ads$ involves principally N_2O molecules which are themselves adsorbed to PVG.

Dynamic quenching by coadsorbed molecules, as noted in a recent report by Thornton and Laurence,[130] implies either long range interactions or migration of the adsorbed species on the surface. Since N_2Oads quenches by an electron transfer mechanism, a long range interaction implies long range electron transfer where the driving force for the transfer arises from the photoinduced $*Ru(bpy)_3^{2+}ads$-N_2Oads redox couple. Recent experiments have examined the relationship between driving force and electron transfer distance. In the thermal back reaction between $Ru(bpy)_3^{3+}$ and homologues of methyl viologen, which have driving forces of 0.1 to 0.6eV, Guarr

and McLendon find that the mean separation between the reactants ranges from a contact distance to 10 A^{o} in glycerol at $0^{o}C$.[211] Experiments in this laboratory indicate that in the thermal back reaction between photogenerated $Ru(bpy)_3^{3+}$ads and $[Ru(bpy)_2(bpy^-)]^+$, which has a driving force of 2.5eV, the mean separation between reacting molecules is $\leq$20 A^{o}.[146] Although the one electron reduction potential of N_2O is not known, N_2O is a mild oxidant and the driving force for oxidative quenching by N_2O, reaction 21, must be $\geq$0.84 eV. Since $Ru(bpy)_3^{3+}$ is a significantly stronger oxidant than N_2O and $[Ru(bpy)_2(bpy^-)]^+$ is a stronger reductant than $*Ru(bpy)_3^{2+}$, a conservative upper limit of the $*Ru(bpy)_3^{2+}$ads-N_2Oads driving force is $\leq$2.5 eV. Consequently, the above correlations between driving force and electron transfer distance seem to suggest that that driving force for oxidative quenching by N_2O, 0.84 eV $\leq\Delta E \leq$ 2.5eV, is not sufficient for long range electron transfer.

Since the rates of adsorption and desorption indicate that N_2O is weakly adsorbed, a more likely explanation for dynamic quenching is that N_2Oads migrates amongst many sites some of which are close enough to $*Ru(bpy)_3^{2+}$ for quenching to occur. The measured rate constant (Table 4), which is the product of the surface diffusion rate and the quenching efficiency, indicates that

the rate of diffusion of N_2O_{ads} on PVG is $\geq 4.7 \times 10^9$ $moles^{-1}sec^{-1}$. Surface migration of species physisorbed onto porous supports has been noted by Beeck[212] and others.[213] However, since the maximum fraction quenched by N_2O, Table 4, is always less than unity, not all $Ru(bpy)_3^{2+}$ is accessible to N_2O_{ads}. In the quenching of a silica supported Mo species, Iwasawa and Ogasawara[214] report similar results and suggest that the region of the Stern-Volmer plot with zero slope corresponds to adsorbed species which for some unspecified reason is unable to interact with the adsorbed gas. Regardless of whether 0.2 mm represents the actual penetration of $Ru(bpy)_3^{2+}$ into interior cavities or the degree of deviation from planarity of the PVG surface, the inability of the adsorbed gas to completely quench the emission suggests that not all $Ru(bpy)_3^{2+}{}_{ads}$ is equally accessible as would be the case on a uniform flat surface. The implication is that N_2O_{ads} migration is not throughout the entire pore volume, but is restricted to the outer surfaces of PVG and can only quench $^*Ru(bpy)_3^{2+}$ on the outer surfaces.

SO_2 and O_2 are more strongly adsorbed and the extent of quenching, f_{max} in Table 4, parallels the adsorption coefficients of the gases. The larger fraction quenched indicates that, when adsorbed onto PVG, the distribution of SO_2 and O_2 more closely resemebles that of the complex than in the case of N_2O, and like

$Ru(bpy)_3^{2+}$, both SO_2 and O_2 are capable of binding to sites within the cavities or pore openings of PVG. Despite apparently having much better access to $*Ru(bpy)_3^{2+}$, SO_2 and O_2 exhibit a similar limit for dynamic quenching as N_2O, i.e., the maxima for t_o/t for the 3 gases (Fig. 12a-c) are nearly the same. This suggests that, in agreement with the above conclusion for quenching by N_2Oads, dynamic quenching by SO_2 and O_2 is limited primarily to $*Ru(bpy)_3^{2+}$ located in the outermost pore structure. This could be the situation if the pores are, indeed, funnel-like and thus, becoming narrower towards the interior of the glass, hinder diffusion by the gases into this region of the support.

The greater accessibility of O_2 and SO_2 is reflected primarily in the predominance of static quenching by these gases, illustrated in Figures 12b and 12c. Static quenching, which was absent in quenching by N_2O, can involve the formation of a precursor complex between the donor and quencher,[153b,154] however adsorption of SO_2 and O_2 is independent of whether the PVG contains $Ru(bpy)_3^{2+}$ads. Furthermore, the absorption spectrum of the adsorbed complex is unaffected by the presence of these gases. Rather, adsorption of these gases appears to be a random process in which some of the gas molecules are adsorbed to sites sufficiently close to $Ru(bpy)_3^{2+}$ads for static quenching to occur. Being random, quenching is analogous to static quenching observed

in frozen homogeneous solution and thus, is amenable to a similar analysis, although concentrations are now expressed as moles adsorbed/gm of adsorbent. The general expression for simultaneous static and dynamic quenching[215] is

$$I_o/I = (1 + K_{SV}(Q))EXP(k'(Q)). \qquad (22)$$

I_o and I are the steady state emission intensities in the absence and presence of the gas, respectively, K_{SV} is the Stern-Volmer constant for dynamic quenching, k' is the constant for static quenching, and Q represents the moles of gas adsorbed/gm PVG. Substitution of t_o/t for the dynamic component, $1 + K_{SV}(Q)$, yields

$$\ln(I_o/I)(t_o/t)^{-1} = k'(Q) \qquad (23)$$

and, as shown by Figures 27a and 27b, the data are in accord with the equation. Evaluated from the initial slope, k' is equal to AN, where A is an active quenching area represented by a circle of radius r containing an adsorbed quencher molecule at the center, and N is Avogadro's number. With a molecule of $Ru(bpy)_3^{2+}$ads at a distance less than r away from a coadsorbed quencher molecule (center to center distance), quenching occurs with unit probability.[216] By the same token, if no $Ru(bpy)_3^{2+}$ molecule is within the active quenching area of a particular quencher molecule, quenching will not occur. Sometimes referred to as the quenching radius, r provides an estimate of the donor-quencher interaction distance, and is related to the slope, k', by

$$r = (k'/f\,\pi N)^{1/2} \qquad (24)$$

Figure 27

Static quenching of $Ru(bpy)_3^{2+}$ ads by (a) SO_2 and (b) O_2 (see text).

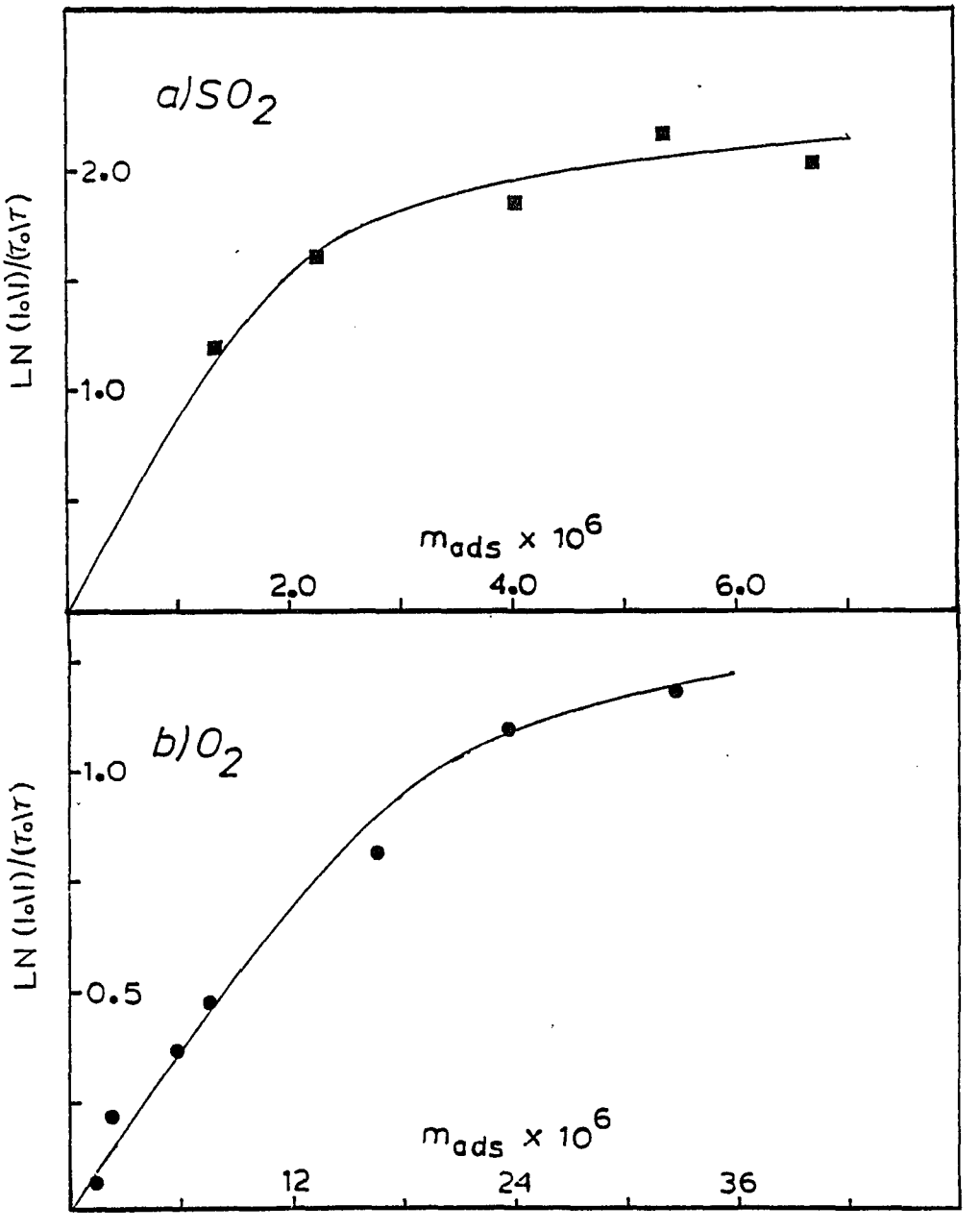
a) SO_2
2.0
1.0
LN $(I_o/I)/(\tau_o/\tau)$
$m_{ads} \times 10^6$
2.0
4.0
6.0
b) O_2
1.0
0.5
LN $(I_o/I)/(\tau_o/\tau)$
$m_{ads} \times 10^6$
12
24
36

Figure 27

where f is the fraction of the total surface area accessible to the quenching gas. Since the extent of penetration of SO_2 and O_2 into PVG is unknown and therefore f is unknown, the specific values of r corresponding to each gas are not accessible. However, limits of r can be calculated by assuming two possible uniform distributions for the adsorbed gas. The upper limit, f = 1, is obtained by assuming that SO_2 and O_2 diffuse throughout the pore volume, and therefore adsorb over the entire surface area of PVG, 130 m^2/gm. Since SO_2 and O_2 quench 89±1% and 70±1% of the adsorbed complex, respectively, the lower limit of surface area to which the gas is adsorbed is taken as the surface area within that volume of PVG impregnated with $Ru(bpy)_3^{2+}$ads. $Ru(bpy)_3^{2+}$ is uniformly distributed on the outer surface of PVG. Assuming that 0.2 mm represents the depth of penetration of the complex into the glass, 28% of the total sample volume contains $Ru(bpy)_3^{2+}$ads, and therefore, the lower limit of f is taken as 0.28. Using these limits for f, the slopes of Figures 27a and 27b yield $11\pm1\ A^o \leq r \leq 17\pm2\ A^o$ and $27\pm2\ A^o \leq r \leq 42\pm4\ A^o$ for quenching distances for O_2 and SO_2, respectively.

Although the data gathered in these experiments do not specify whether quenching by O_2 involves energy or electron transfer, considering the difference in media, the estimated range for r is in good agreement with previous measurements of the energy transfer quenching radius of

O_2. In the quenching of the naphthalene triplet state by O_2 in a 3-methylpentane glass at 77°K, Siegel and Judeikis find a quenching radius of 10.5 A°.[217] Bowen and Metcalf report that in the quenching of anthracene fluorescence by O_2 in paraffin solvents of differing viscosity the O_2 quenching radius is 20 A°.[218] The range of r obtained in these experiments for quenching by O_2 is reasonable in view of these past results and lends some credence to the estimate of the distribution of the adsorbed gas, but the range of r calculated for SO_2 under the same approximations, particularly the upper limit, is exceptionally large. However, the rapid rate of adsorption of SO_2 suggests that the gas does not diffuse into the interior cavities of PVG and this perhaps discounts the upper limit. On the other hand, SO_2 does quench ca. 90% of the adsorbed complex. Assuming a random distribution - no evidence is available to suggest otherwise - 90% quenching implies a distribution of SO_2 similar to that of the adsorbed complex. Since SO_2 quenches $Ru(bpy)_3^{2+}$ads by an electron transfer mechanism, random distribution within the volume of PVG impregnated with the complex implies an electron transfer distance of 27 ± 2A°. Although still quite large, the distance is surprisingly similar to the electron transfer distances of ca. 25 A° reported by Miller, Hartman, and Abrash for the quenching of N,N,N',N'-tetramethyl-p-phenylenediamine by phthalic anhydride in a 2-methyltetrahydrofuran glass at 77°K.[219]

(v) Photoinduced Disproportionation of $Ru(bpy)_3^{2+}$ads in the Presence of SnO_2

The data obtained from these quenching experiments suggest the feasibility of long range electron transfer between molecules bound to porous Vycor. However, despite implications that the reactants may be separated by 25 A^o or more, the photoinduced redox reactions between $Ru(bpy)_3^{2+}$ads and the coadsorbed gases are all reversible. Circumventing thermally activated electron transfer can be accomplished by spatial separation of the reactants and is one of the main objectives in binding $Ru(bpy)_3^{2+}$ to a solid support. Under ideal conditions, the reactants are close enough for photoinitiated electron transfer and at the same time far enough apart so that the thermal back transfer of an electron does not occur. In reality, the optimum distance between reactants will be some compromise between these two limiting distances.

Previous experiments were instrumental in establishing the relationship between the distribution of a particular reagent, $Ru(bpy)_3^{2+}$, on the glass, and its photobehavior.[144-146,168] Furthermore, these studies demonstrated that the photoredox chemistry, per se, is not radically altered in the new environment. However, the properties of the support can be exploited towards the control of various aspects of photoinduced redox reaction dynamics.

The solvated electron, e_{aq}^-, has been observed via flash photolysis and pulse radiolysis of aqueous solutions of $Ru(bpy)_3^{2+}$, and is formed by a biphotonic ionization of the latter.[96] This species has been implicated as the reducing agent in the photoinduced disproportionation of $Ru(bpy)_3^{2+}$ in fluid solution. However, the photoproducts, $[Ru(bpy)_2(bpy^-)]^+$ and $Ru(bpy)_3^{3+}$, are transitory due to a diffusion-controlled thermal electron transfer reaction to regenerate the dicationic complex.

The photoinduced disproportionation of the dication in PVG proceeds via a mechanism analogous to that in fluid solution, although the lifetime of photogenerated $[Ru(bpy)_2(bpy^-)]^+$ in PVG is $\geq$36 hours, in marked contrast to the lifetime of 2.0$\pm$0.6 msec reported for this species in fluid solution.[96] The unusual stability of the photoproducts is apparently the result of electrostatic binding to the glass, thereby eliminating collisions which would necessarily result in a thermally activated back-reaction since the driving force for that process is ca. 2.5 V.

The involvement of e_{ads}^-, the equivalent in the glass of the solvated electron in solution, in the disproportionation mechanism was established via its direct detection in a flash photolysis experiment, and by the addition of e^- scavengers which inhibit the formation of $[Ru(bpy)_2(bpy^-)]^+$.[146] With knowledge of the

distribution of the adsorbed complex, it was determined that the maximum quantum yield of $[Ru(bpy)_2(bpy^-)]^+$ is obtained when the dicationic complexes are separated by a mean distance of 50 A^o. Since the adsorbed complex cannot diffuse within the glass matrix, the implication is that e_{ads}^- must migrate 50 A^o on the glass surface to account for the observed reduction of $Ru(bpy)_3^{2+}$.

In the presence of an optically transparent, conducting, SnO_2 film doped with 1%Sb, the formation of $[Ru(bpy)_2(bpy^-)]^+$ is second order in light intensity. Furthermore, the photoproduct has a lifetime of $\geq$36 hr. The similarity of these observations to those which were made previously, in the absence of SnO_2, suggests that the disproportionation mechanism is not changed by the presence of SnO_2.

More important is the influence exerted by the semiconductor upon electron migration on the glass surface. A bandgap of 3.5 eV, similar to the bandgap of SnO_2 in a pH 1 aqueous electrolyte,[182] is calculated from the absorption spectrum for SnO_2 on PVG. Although the flat band potential of a semiconductor, and hence, the degree of band bending in the conduction band depends upon the pH,[220] which for the glass is 4-5, it does not appear that the SnO_2 band structure is radically different on the glass from what it is in a solution at pH 1. Electron injection from the LMCT excited state of $Ru(bpy)_3^{2+}$

into the conduction band of SnO_2 at pH 1 is favorable by ca. 0.7 V on the NHE scale.[128] Assuming no radical differences in the band structure of the adsorbed semiconductor from that in solution, electron injection where the sensitizer has absorbed two photons, into the conduction band of adsorbed SnO_2 seems thermodynamically feasible.

If the photoionized electron is injected into the SnO_2 conduction band, then its ability to migrate on the glass surface should be enhanced in the presence of a conductive SnO_2 film. A longer migration distance should be reflected by an increase in the quantum yield of $[Ru(bpy)_2(bpy^-)]^+$ when the mean separation between the adsorbed complex ions is >50 A^o. However, there is no evidence of this nature for the ability of e_{ads}^- to migrate further in the presence of SnO_2. As shown in Figure 20, the maximum quantum yield of $[Ru(bpy)_2(bpy^-)]^+$ is not shifted to lower $Ru(bpy)_3^{2+}$ impregnation levels by SnO_2. Furthermore, the quantum yields at loading levels of $<2.7 \times 10^{-6}$ moles/gm PVG are uninfluenced by the semiconductor. On the other hand, the presence of SnO_2 does result in an increase in the quantum yield of $[Ru(bpy)_2(bpy^-)]^+$ if the glass contains 2.7×10^{-6} moles/gm of the dicationic complex.

The absence of any observable evidence for the increased conductivity of the glass due to SnO_2 in the form of a

change in the quantum yield of $[Ru(bpy)_2(bpy^-)]^+$ until the amount of sensitizer reaches a certain level may be rationalized in terms of what has been reported by investigators of charge transport phenomena in derivatized SnO_2 electrodes. For example, Ghosh and Spiro found that ca. 1000 layers of $Ru(bpy)_3^{2+}$, covalently bound to a SnO_2 electrode, are necessary for a 2-fold enhancement of anodic photocurrent over that for SnO_2 in contact with an aqueous solution of $Ru(bpy)_3^{2+}$.[221] This suggests that intimate contact between the sensitizer and electrode may be necessary in order for electron injection to take place. A very recent report by Ghosh and Bard[222] supports this argument. The authors observed electroactivity for $Ru(bpy)_3^{2+}$ suspended in a clay film adhering to a SnO_2 electrode where 50-100 layers of the electroactive species are present. In addition, Gratzel and coworkers verified that the photocatalytic cleavage of H_2O on platinized, colloidal TiO_2 with visible light proceeds only when the sensitizer can adhere strongly to the semiconductor particle.[169]

These observations suggest that in PVG, contact between SnO_2 deposited as a film on the outer surface of the glass and $Ru(bpy)_3^{2+}$, which, to some extent, may be impregnated within cavities could be a requirement for electron injection from an excited state of $Ru(bpy)_3^{2+}$ads into the SnO_2 conduction band.

Quite possibly, this prerequisite is not satisfied until there is a sufficient amount of $Ru(bpy)_3^{2+}$ adsorbed to the glass. As the amount of $Ru(bpy)_3^{2+}$ads is increased, the number of $Ru(bpy)_3^{2+}$ molecules that are, in effect, adhering to the SnO_2 film might be expected to increase. At higher impregnation levels there is also expected to be a change in the distribution of excited states on the glass. Distribution studies suggest that $Ru(bpy)_3^{2+}$ penetrates 0.2 mm into the glass, regardless of the level of impregnation, and is uniformly distributed throughout the outer pore volume. Thus, in a dilute glass, some light is absorbed by $Ru(bpy)_3^{2+}$, that is well below the outermost surface. However, as the glass is made more concentrated, larger fractions of the total amount of light absorbed is by molecules that are situated closer to the outermost surface. In the latter case, a non-homogeneous distribution of excited states, where the maximum density is located primarily on the outermost surface, is produced by optical excitation. When there are 3×10^{-6} moles of $Ru(bpy)_3^{2+}$/gm PVG, the absorbance at 457.9-nm, the laser excitation wavelength, is ca. 10. Since beyond this impregnation level most of the source photons are absorbed within a very narrow path, there is a greater probability for biphotonic absorption near the outermost surface, where the conducting SnO_2 film is situated, than within the cavities of the glass. Thus, at higher impregnation levels charge injection is more

favorable if sensitizer-semiconductor contact is a requirement for the latter.

(vi) Water Photolysis with Platinized TiO_2 Adsorbed to PVG

The success of microheterogeneous systems in catalysis of multielectron transfer processes lies not only in the high surface area of the support but also in the capability for organization of the catalysts into a very limited region of space.[111,169] Platinized colloidal particles of TiO_2, ca. 200 A^o in diameter, are catalytically active in the photoreduction of H_2O to H_2.[122,223,224] The Pt catalyst is adsorbed directly onto the semiconductor particle, behaving as if it were a microelectrode short-circuited to the latter. Therefore, efficient channeling of TiO_2 conduction band electrons to sites on Pt where H_2O reduction can take place occurs, presumably owing to intimate contact between the semiconductor and catalyst.

No evolution of H_2 was found when a PVG sample impregnated with TiO_2 and Pt was irradiated with UV light of energy $\geq$3.5 eV, E_g for TiO_2. Since the adsorbed species are dispersed on the PVG support, there may not have been sufficient contact between TiO_2 and Pt for efficient multielectron channeling from the TiO_2 conduction band to Pt, at least at the loading levels of semiconductor and catalyst employed, 5.4×10^{-6} and 2.3×10^{-6} moles/gm, respectively.

H_2 was not formed even when $Ru(bpy)_3^{2+}$, added as a sensitizer, was irradiated with visible light. It was not possible to measure the anodic photocurrent from TiO_2 on irradiation of coadsorbed $Ru(bpy)_3^{2+}$. Thus, one speculation is that the energetics for electron injection from the latter into the TiO_2 conduction band may not be favorable in the glass. In the spectral sensitization of TiO_2 electrodes by $Ru(bpy)_3^{2+}$ in aqueous media, poorer overlap of the sensitizer excited state energy levels with the unoccupied levels in the TiO_2 conduction band occurs as the pH of the medium increases from 1 towards more basic pH.[128] This effect arises from upward bending of the conduction band induced by changes in the flat-band potential of the semiconductor of 55 mV/pH unit. Since the pH of the glass is 4-5, the conduction band energy of TiO_2 at the semiconductor surface, due to band bending, may be higher on a relative energy scale than $^*Ru(bpy)_3^{2+}$ads, and therefore, electron injection from the latter into the conduction band of the adsorbed semiconductor is thermodynamically unfavorable. In fact, the calculated bandgap of the adsorbed semiconductor, 3.5 eV, is somewhat in excess of that for anatase TiO_2, 3.2 eV,[169] and rutile TiO_2, 3.0 eV,[179] suggesting that the conduction band of the adsorbed semiconductor bends upward on adsorption to PVG and thus, unfavorable thermodynamics for electron injection are, quite possibly, the reason why no H_2 evolution was observed.

However, the failure to detect H_2 even under conditions of direct bandgap irradiation of the semiconductor suggests other possibilities. The need for semiconductor-catalyst contact has already been discussed. It seems unlikely that H_2 is formed and then rapidly scavenged by an oxidant that is present on the glass. Sato and White report that the mechanism of the photoassisted water-gas shift reaction,

$$CO(g) + H_2O(g) \longrightarrow CO_{2(g)} + H_{2(g)} \quad (25)$$

over platinized TiO_2 catalysts involves photodecomposition of H_2O, however in the absence of CO, no H_2 is evolved.[225] The presence of CO, required to scavenge O atoms which combine with H_2 to regenerate H_2O, had no effect in the present study. This suggests that H_2 is never formed in the photolyses of PVG samples containing TiO_2 and Pt.

B. Spectral and Photophysical Properties of Ru(II) Complexes with 2-(Phenylazo)pyridine

(i) Resonance Raman Spectra

The resonance Raman spectra yield a picture of similar excited states throughout the $Ru(azpy)_2L^{n+}$ series. The pronounced enhancement of bands assignable to vibrations of the azpy ligand on excitation at wavelengths near the intense visible absorption maxima of $Ru(azpy)_2L^{n+}$ complexes confirms that the latter is a Ru(II) t_{2g} azpy π^* MLCT transition. Tsuboi's rule states that

the largest enhancement in resonance Raman scattering is observed for the molecular coordinates which undergo the greatest distortion in the excited state.[109] Since the band attributed to the N=N stretch is the most intense, one can infer that charge transferred from the Ru(II) t_{2g} orbitals resides in azpy antibonding π^* orbitals localized principally in the azo linkage and therefore, in the MLCT excited state, the N=N bond is highly distorted. Furthermore, significant resonance enhancement of bands assignable to N-C(phenyl) and (pyridine)C-N suggests that excited state electron density is centered in the pi system which includes the azo linkage and the adjoining C-N bonds. Enhancement of the band attributed to the phenyl ring breathing mode implies that the phenyl ring is an intimate part of the chromophore, and is probably conjugated with the N=N bonding system to some extent. In marked contrast to what is typically found for pyridine and polypyridine substituted Ru(II) complexes, where the pyridine ring system plays an important role in accepting excited state charge,[110] the pyridine ring of the azpy ligand is only weakly involved in charge acceptance in these azpy complexes.

(ii) Absorption and Emission Spectra

Where measurable, the difference between the emission energy and the corresponding MLCT absorption energy remains relatively constant, and in accord with previous assignments,[17] the emissions from $Ru(azpy)_2L^{n+}$

complexes are assigned to LMCT, azpy π^* $\longrightarrow$ Ru(II) t_{2g}, transitions. The observation of 2 emission maxima for the $[Ru(azpy)_3](PF_6)_2$ and $[Ru(azpy)_2btz](ClO_4)_2$ complexes suggest the possibility of multiple emitting levels. Previously, the 2 maxima at 77°K for the btz complex were attributed to transitions originating from azpy π^* and btz π^* orbitals.[94] This assignment is unlikely in view of evidence gathered here. Meyer and coworkers point out the reproducibility of multiple emissions from cis-$Ru(bpy)_2(N\bigcirc\!\!-\!\!\bigcirc N\text{-}CH_3)_2$ under a variety of experimental conditions.[226] Comparing the spectra of different solid samples of either $[Ru(azpy)_3](PF_6)_2$ or $[Ru(azpy)_2btz](ClO_4)_2$ shows that the emission maxima consistently occur at the same wavelength, but the relative intensities of the 2 emission maxima are irreproducible, even with samples taken from the same preparation. Furthermore, multiple emissions originating in π^* orbitals of different ligands can not account for the 2 emissions observed from $[Ru(azpy)_3](PF_6)_2$, yet the emission spectrum of the latter is similar to that of the btz complex. Since the relative emission intensities of the 2 maxima remain constant throughout prolonged exposure to the laser excitation source, the 2 maxima are not the result of a photoinduced redox reaction.

$[Ru(azpy)_3](PF_6)_2$ and $[Ru(azpy)_2btz](ClO_4)_2$ are isolated as a mixture of unresolved

geometric isomers.[94] The most likely explanation for the 2 emissions is that they originate from different isomeric forms of each complex, although the separation between the peak energies, ca. 1000 cm^{-1}, indicates an isomer dependence that is considerably larger than those previously found.[227]

A change in ligation about Ru(II) is not a likely reason for the changes in the emission spectra which occur on dissolution of the solid complexes. Although the entire spectrum is blue-shifted, the relative energies and extinction coefficients of the near UV and visible absorption maxima of $[Ru(azpy)_3](PF_6)_2$ dispersed in nujol oil between two glass slides, are equivalent to those obtained from acetone solutions of the complex. If the hypothesis regarding isomers is correct, the occurence of one emission may be the reuslt of a facile interconversion to one dominant isomeric form or only one isomer being luminescent in fluid solution.

In both the solid state and acetone solution, the Stokes shifts of the luminescence from these $Ru(azpy)_2L^{n+}$ complexes exceed those found for the luminescent $Ru(bpy)_2L^{n+}$ complexes by ca. 2000 cm^{-1}.[17,18,228] Significant enhancement of pyridine ring modes in the resonance Raman spectra of the bpy complexes indicates charge delocalization over a relatively large portion of the bpy ligand in the MLCT excited state.[110] In contrast, the resonance Raman spectra of

the azpy complexes show only weak enhancement of bands assignable to pyridine vibrations with moderate enhancement of phenyl ring modes. By far the largest enhancement in the spectra of the azpy complexes is seen for the bands assigned to the N=N stretch in the azpy ligand, and the vibrations of the bonds contiguous to the azo function. Assuming that the molecular distortions of the emissive CT state parallel those of the MLCT state populated on absorption, i.e., the state resonant with 514.5-nm excitation, then in the luminescent state the transferred charge populates π^* orbitals in close proximity to the metal ion and is localized principally in the azo function. The resultant reduction in the bond strength within the chromophore, along with the greater flexibility of the azpy ligand, suggests that azpy, in contrast to bpy, can accomodate the transferred charge by larger distortions of a more limited region of the ligand.

(iii) Photoredox Properties and Emission Quenching

In fluid solution, the luminescent LMCT state of $Ru(azpy)_3^{2+}$ lies 1.48 eV above the ground state. Although the LMCT states of the remaining $Ru(azpy)_2L^{n+}$ complexes can not be positioned exactly, they must lie at $\leq$1.42 eV since the emission maxima occur at $\geq$870 nm. In past studies, the redox potentials of the LMCT state have been calculated from the difference between the excited state energies and the thermal redox potentials of the ground state.[38] Although the

oxidation and reduction potentials of the $Ru(azpy)_2L^{n+}$ complexes, listed in Table 3, depend upon the coligand, in general, the thermal redox chemistry, as a result of the strong pi acidity of the azpy ligand, is characterized by very unfavorable oxidation potentials, and only mildly unfavorable reduction potentials. Even with the additional redox capability due to the input of excitation energy, these large differences in ground state oxidizability and reducibility result in an LMCT state, as illustrated in Figure 28, which is positioned, energetically, between the ground redox states. The emission spectra of the other $Ru(azpy)_2L^{n+}$ complexes yield only upper limits for their LMCT excited state energies, and therefore, only limits for their excited state redox potentials can be calculated. However, the limits listed in Table 9 suggest that, subject to slight changes in relative energies, Figure 28 is representative of all $Ru(azpy)_2L^{n+}$ complexes.

The energy level ordering for $Ru(azpy)_3$ in Figure 28 is out of the ordinary in the sense that the LMCT state of the dication is an exergonic oxidant and endergonic reductant. This is in contrast to $Ru(bpy)_3^{2+}$ which typifies Ru(II) polypyridyl complexes, where the LMCT state is an essentially equally exergonic oxidant and reductant (Fig. 1). Consequently, $Ru(azpy)_3^{2+}$ offers a convenient test of the reliability of the luminescence-electrochemical cycles used to calculate

excited state redox potentials. Figure 28 suggests that, with a series of related redox couples, the reduced member of the pair, R, will reductively quench the LMCT state of $Ru(azpy)_3^{2+}$, i.e.,

$$^*Ru(azpy)_3^{2+} + R \longrightarrow Ru(azpy)_3^{+} + O \quad (26)$$

provided the oxidation potential of the (R/O) couple is $\geq$-1.18 V. On the other hand, the oxidized partner, O, will quench oxidatively, i.e.,

$$^*Ru(azpy)_3^{2+} + O \longrightarrow Ru(azpy)_3^{3+} + R \quad (27)$$

only if the sum of its reduction potential and the energy of $^*Ru(azpy)_3^{2+}$, 1.48 eV, exceeds the ground state oxidation potential of $Ru(azpy)_3^{2+}$, $\geq$2.0 eV.

The Stern-Volmer constans an corresponding bimolecular rate constants listed in Table 9 corroborate the calculated energetics of photoredox quenching of $^*Ru(azpy)_3^{2+}$. Oxidative quenching of the LMCT state by MV^{2+} is calculated to be endergonic by $\geq$0.9 eV, and consistent with the calculated energetics, no quenching by MV^{2+}, $K_{SV} \leq 10\ M^{-1}$, occurs. The reduction potentials of $Fe(CN)_6^{3-}$ and Fe^{3+} are +0.36 and +0.77 V, respectively. The absence of quenching by either of these species, $K_{SV} \leq 10\ M^{-1}$, suggests that oxidation of the LMCT state,

$$^*Ru(azpy)_3^{2+} \longrightarrow Ru(azpy)_3^{3+} + e^- \quad (28)$$

is endergonic by $\geq$0.8 eV. Combining the latter value with the LMCT state energy, 1.48 eV, yields an oxidation potential for ground state $Ru(azpy)_3^{2+}$ of $\geq$2.3 eV,

Figure 28

Ground and excited state redox potentials of $Ru(azpy)_3^{2+}$ in aqueous solution at 25°C (see text).

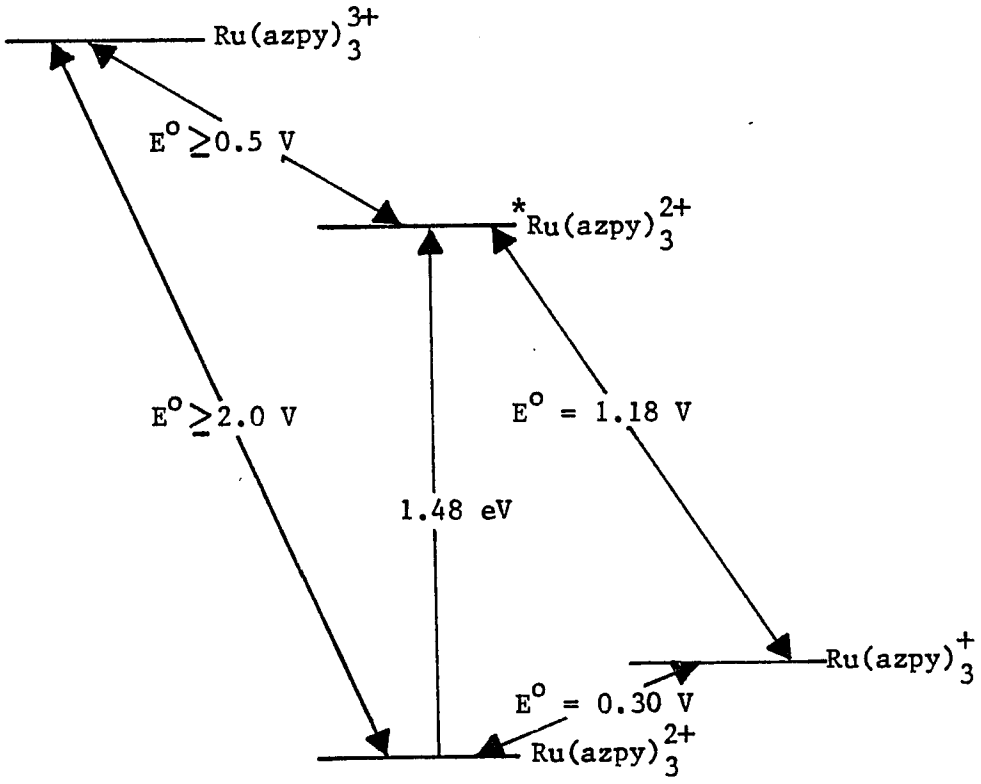
Ru(azpy)$_3^{3+}$
$E^o \geq 0.5$ V
*Ru(azpy)$_3^{2+}$
$E^o \geq 2.0$ V
$E^o = 1.18$ V
1.48 eV
Ru(azpy)$_3^{+}$
$E^o = 0.30$ V
Ru(azpy)$_3^{2+}$

which is in reasonable agreement with the value of +2.2 V obtained via differential pulse polarimetry.[229] In view of the energetics of reaction 28, it is not surprising that the only species found to quench $^{*}Ru(azpy)_3^{2+}$ oxidatively is the strong oxidant Ce^{4+}. The driving force for the reaction

$$^{*}Ru(azpy)_3^{2+} + Ce^{4+} \longrightarrow Ru(azpy)_3^{3+} + Ce^{3+} \quad (29)$$

is $\leq$+0.8 V, and quenching by Ce^{4+} occurs at essentially a diffusion controlled rate, $k_b = 3.6 \times 10^9$ $M^{-1}sec^{-1}$. Since a driving force of $\geq$+0.3 V leads to a diffusion controlled rate for a thermal electron transfer reaction,[111] assuming a similar driving force is required for a diffusion controlled rate for a photoinduced electron transfer reaction, a conservative estimate of the upper limit for the excited state oxidation potential of $Ru(azpy)_3^{2+}$ is $\leq$+1.3 eV. Thus, the limits for the driving force of reaction 28 are +0.8 V$\leq \Delta E \leq$+1.3 V. Although reaction 29 has a favorable driving force, the $^{*}Ru(bpy)_3^{2+}$ emission intensity in the presence of Ce^{4+} is not time dependent and absorption spectra recorded before and after the quenching experiments indicate no net chemical change. This suggests that concurrent with reaction 29 is an exergonic thermal back reaction, $\Delta E \geq$+0.7 V, which regenerates $Ru(azpy)_3^{2+}$ and Ce^{4+},

$$Ru(azpy)_3^{3+} + Ce^{3+} \longrightarrow Ru(azpy)_3^{2+} + Ce^{4+} \quad (30)$$

In contrast to the endergonicity of reaction 28, reduction of $^*Ru(azpy)_3^{2+}$ has a favorable driving force, and reductive quenching by species with oxidation potentials of $\geq$-1.18 V is energetically feasible. Since the oxidation potential of Ce^{3+}, -1.61 V, is too unfavorable, reductive quenching by Ce^{3+} is not predicted and, as indicated in Table 9, no quenching, $K_{SV} \leq 10\ M^{-1}$, is detected. On the other hand, the reductive quenching reactions

$$^*Ru(azpy)_3^{2+} + Fe^{2+} \longrightarrow Ru(azpy)_3^{+} + Fe^{3+} \quad (31)$$

and

$$^*Ru(azpy)_3^{2+} + Fe(CN)_6^{4-} \longrightarrow Ru(azpy)_3^{+} + Fe(CN)_6^{3-} \quad (32)$$

have driving forces of +0.47 V and +0.82 V, respectively, and the data listed in Table 9 show that both Fe^{2+} and $Fe(CN)_6^{4-}$ are capable quenchers. Neither quenching reaction leads to spectrally detectable net chemical change since both are complemented by exergonic thermal back reactions,

$$Ru(azpy)_3^{+} + Fe^{3+} \longrightarrow Ru(azpy)_3^{2+} + Fe^{2+} \quad (33)$$

and

$$Ru(azpy)_3^{3+} + Fe(CN)_6^{3-} \rightarrow Ru(azpy)_3^{2+} + Fe(CN)_6^{4-}. \quad (34)$$

The large bimolecular rate constant for quenching by $Fe(CN)_6^{4-}$, $k_b = 1.8 \times 10^9\ M^{-1}sec^{-1}$, seems reasonable in view of the electrostatic attraction between the reactant species, but the value for Fe^{2+}, $k_b = 3.6 \times 10^{10}\ M^{-1}sec^{-1}$ appears unusually large for a diffusion controlled reaction between two

dipositive ions,[230] in spite of the additional 0.35 V of driving force. However, the ionic strength of the medium, μ = 1.5, is relatively high, and Silverman and Dodson point out that the self exchange rate of the (Fe^{2+}/Fe^{3+}) couple increases with increasing ionic strength of the medium.[231]

In view of the favorable energetics for the reduction of $Ru(azpy)_3^{3+}$ to the LMCT state, attempts were made to observe reductive chemiluminescence. Unfortunately, although the addition of strong oxidants, e.g. $S_2O_8^{2-}$, to solutions of $Ru(azpy)_3^{2+}$ resulted in the formation of a transient blue color, thought to be $Ru(azpy)_3^{3+}$, a brown precipitate ultimately forms, the apparent result of decomposition of the complex.

References

1) Kalyanasunduram, K., Coord. Chem. Rev. (1982), 46, 161, and the references therein.

2) Lytle, F.E. and Hercules, D.M., J. Am. Chem. Soc. (1969), 91, 253.

3) Allsopp, S.R., Cox, A., Jenkins, S.A., Kemp, T.J., and Tunstall, S.M., Chem. Phys. Lett. (1976), 43, 135.

4) Allsopp, S.R., Cox, A., Kemp, T.J., and Reed, W.J., J. Chem. Soc. Faraday Trans. 1 (1978), 74, 1275.

5) Demas, J.N. and Adamson, A.W., J. Am. Chem. Soc. (1971), 93, 1800.

6) Sabbatini, N. and Balzani, V., J. Am. Chem. Soc. (1972), 94, 7587.

7) Wrighton, M. and Markham, J., J. Phys. Chem. (1973), 77, 3042.

8) Gafney, H.D. and Adamson, A.W., J. Am. Chem. Soc. (1972), 94, 8238.

9) Demas, J.N. and Adamson, A.W., J. Am. Chem. Soc. (1973), 95, 5159.

10) Veening, H. and Brandt, W.W., Anal. Chem. (1960), 32, 1426.

11) Lytle, F.E. and Hercules, D.M., J. Am. Chem. Soc. (1966), 88, 4745.

12) Klassen, D.M. and Crosby, G.A., Chem. Phys. Lett. (1967), 1, 127.

13) Paris, J.P. and Brandt, W.W., J. Am. Chem. Soc. (1959), 81, 5001.

14) Porter, G.B. and Schlafer, Ber. Bunsenges. Phys. Chem. (1964), 68, 316.

15) Crosby, G.A., Perkins, W.G., and Klassen, D.M., J. Chem. Phys. (1965), 43, 1498.

16) Palmer, R.A. and Piper, T.S., Inorg. Chem. (1966), 5, 861.

17) Klassen, D.M. and Crosby, G.A., J. Chem. Phys. (1968) 48, 1853.

18) Demas, J.N. and Crosby, G.A., J. Am. Chem. Soc. (1971), 93, 2841.

19) Crosby, G.A., Hipps, K.W., and Elfring, W.H., J. Am. Chem. Soc. (1974), 96, 629.

20) Crosby, G.A., Acc. Chem. Res. (1975), 8, 231.

21) Balzani, V., Boletta, F., Gandolfi, M.T., and Maestri, M., Topics Curr. Chem. (1978), 75, 1.

22) Balzani, V. and Carrasiti, V., "Photochemistry of Coordination Compounds", Academic Press, New York, 1970, pp.57-59.

23) Harrigan, R.W. and Crosby, G.A., J. Chem. Phys. (1973), 59, 3468.

24) Harrigan, R.W., Hager, G.D., and Crosby, G.A., Chem. Phys. Lett. (1973), 21, 487.

25) Forster, M. and Hester, R.E., Chem. Phys. Lett. (1981), 81, 42.

26) Dallinger, R.F. and Woodroff, J. Am. Chem. Soc. (1979), 101, 4391.

27) Motten, A.G., Hanck, K., and DeArmond, M.K., Chem. Phys. Lett. (1981), 79, 541.

28) Lachish, U., Infelta, P.P., and Gratzel, M., Chem. Phys. Lett. (1979), 62, 317.

29) Bensasson, R.V., Salet, C., and Balzani, V., R. Acad. Sci. Ser. B. (1979), 289, 41.

30) Creutz, C., Chou, C., Netzel, T.L., Okumura, M., and Sutin, N., J. Am. Chem. Soc. (1980), 102, 1309.

31) Durham, B., Walsh, J.L., Carter, C.L., and Meyer, T.J., Inorg. Chem. (1980), 19, 860.

32) Gleria, M., Minto, F., Beggiato, G., and Bortolus, P., J. Chem. Soc. Chem. Commun. (1978), 285.

33) Van Houten J. and Watts, R.J., Inorg. Chem. (1978), 17, 3387.

34) Hoggard, P.E. and Porter, G.B., J. Am. Chem. Soc. (1978), 100, 1457.

35) Wallace, W.M. and Hoggard, P.E., Inorg. Chem. (1980), 19, 2141.

36) Van Houten, J. and Watts, R.J., J. Am. Chem. Soc. (1976), 98, 4853.

37) Watts, R.J. and Crosby, G.A., J. Am. Chem. Soc. (1971), 93, 3184.

38) Bock, C.R., Meyer, T.J., and Whitten, D.G., J. Am. Chem. Soc. (1975), 97, 2909.

39) Lin, C.-T. and Sutin, N., J. Am. Chem. Soc. (1975), 97, 3543.

40) Young, R.C., Keene, F.R., and Meyer, T.J., J. Am. Chem. Soc. (1977), 99, 2468.

41) Laurence, G.S. and Balzani, V., Inorg. Chem. (1974), 13, 2976.

42) Bock, C.R., Meyer, T.J., and Whitten, D.G., J. Am. Chem. Soc. (1974), 96, 4710.

43) Creutz, C. and Sutin, N., Inorg. Chem. (1976), 15, 496.

44) Ferreira, M.I.C., and Harriman, A., J. Chem. Soc. Faraday Trans. 2 (1979), 75, 874.

45) Taylor, D.G. and Demas, J.N., J. Chem. Phys. (1979), 71, 1032.

46) Hazelton,, M.A., Lin, C.-T., Schwartz, H.A., and Sutin, N., J. Am. Chem. Soc. (1978), 100, 2383.

47) Baggott, J.E. and Pilling, M.J., J. Phys. Chem. (1980), 84, 3012.

48) Demas, J.N. and Addington, J.W., J. Am. Chem. Soc. (1976), 98, 5800.

49) Creutz, C. and Sutin, N., J. Am. Chem. Soc. (1976), 98, 6384.

50) Creutz, C., Inorg. Chem. (1979), 17, 1046.

51) Sutcliffe, E., Neumann-Spallart, M., and Kalyanasunduram, K., unpublished results.

52) Foreman, T.K., Gianotti, C., and Whitten, D.G., J. Am. Chem. Soc. (1980), 102, 1170.

53) Chandrasekaran, K., Foreman, T.K., and Whitten, D.G., Nouv. J. Chim., (1981), 5, 275.

54) DeGraff, B.A. and Demas, J.N., J. Am. Chem. Soc. (1980), 102, 6169.

55) Boletta, F., Juris, A., Maestri, M., and Sandini, D., Inorg. Chim. Acta (1980), 44, L175.

56) Neumann-Spallart, M., Kalyanasunduram, K., Gratzel, C., and Gratzel, M., Helv. Chim. Acta (1980), 62, 1111.

57) Creutz, C., Sutin, N., and Brunschwig, B.S., J. Am. Chem. Soc. (1979), 101, 1297.

58) Pelizetti, E., Mentasti, E., and Pramauro, E., Inorg. Chem. (1976), 15, 2898.

59) Juris, A., Gandolfi, M.T., Manfrin, M.F., and Balzani, V., J. Am. Chem. Soc. (1976), 98, 7432.

60) Juris, A., Manfrin, M.T., Maestri, M., and Serpone, N., Inorg. Chem. (1978), 17, 2258.

61) Toma, H.E. and Creutz, C., Inorg. Chem. (1977), 16, 545.

62) Gafney, H.D. and Adamson, A.W., J. Am. Chem. Soc. (1972), 94, 8238.

63) Navon, G. and Sutin, N., Inorg. Chem. (1974), 13, 2159.

64) Demas, J.N., Harris, E.W., and McBride, R.P.M., J. Am. Chem. Soc. (1977), 99, 3547.

65) Boletta, F., Maestri, M., Moggi, L., and Balzani, V., J. Phys. Chem. (1974), 78, 1374.

66) Darwent, J.R. and Kalyanasunduram, K., J. Chem. Soc. Faraday Trans. 2 (1981), 77, 373.

67) Bock, C.R., Connor, J.A., Gutierrez, A.R., Meyer, T.J., Whitten, D.G., Sullivan, B.P., and Nagle, J.K., J. Am. Chem. Soc. (1979), 101, 4815.

68) Young, R.C., Meyer, T.J., and Whitten, D.G., J. Am. Chem. Soc. (1975), 97, 4781.

69) Kalyanasunduram, K., Kiwi, J., and Gratzel, Helv. Chim. Acta (1978), 61, 2720.

70) Gaines, G.L., J. Phys. Chem. (1979), 83, 3088.

71) Takuma, K., Kajiwara, M., and Matsuo, T., Chem. Lett. (1977), 1199.

72) Amouyal, E., Zidler, B. Keller, P., and Moradpour, A.,

Chem. Phys. Lett. (1980), 74, 314.

73) Nagle, J.K., Bernstein, J.S., Young, R.C., and Meyer, T.J., Inorg. Chem. (1981), 20, 1760.

74) Nagle, J.K., Young, R.C., and Meyer, T.J., Inorg. Chem. (1977), 16, 3366.

75) Maestri, M. and Gratzel, M., Ber. Bunsenges. Phys. Chem. (1977), 81, 504.

76) Deronzier, A. and Meyer, T.J., Inorg. Chem. (1980), 19, 2912.

77) Favaro, G. and Masetti, F., J. Phys. Chem. (1979), 83, 2129.

78) Ballardini, R., Varani, G., Scandola, M.A., and Balzani, V., J. Am. Chem. Soc. (1976), 98, 7432.

79) Sabbatini, N., Scandola, M.A., and Carassiti, J. Phys. Chem. (1973), 77, 1307.

80) Sabbatini, N., Scandola, M.A., and Balzani, V., J. Phys. Chem. (1974), 78, 541.

81) Boletta, F., Maestri, M., and Balzani, V., J. Phys. Chem. (1976), 80, 2499.

82) Demas, J.N., Dimiente, D., and Harris, E.W., J. Am. Chem. Soc. (1973), 95, 6865.

83) Sutin, N. and Creutz, C., Pure Appl. Chem. (1980), 52, 2717.

84) Kurimura, Y. and Onimura, R., Inorg. Chem. (1980), 19, 3516.

85) Lin, C.-T., Bottcher, W., Chou, C., Creutz, C., and Sutin, N., J. Am. Chem. Soc. (1976), 98, 6536.

86) Belser, P. and von Zelewsky, A., Helv. Chim. Acta (1980), 63, 1675.

87) Fabian, R.H., Klassen, D.M., and Sonntag, R.W., Inorg. Chem. (1980), 19, 1977.

88) Crutchley, R.J., and Lever, A.B.P., J. Am. Chem. Soc. (1980), 102, 7128.

89) Sullivan, B.P., Salmon, D.J., Meyer, T.J., and Peedin, J., Inorg. Chem. (1979), 18, 3369.

90) Matsubara, T. and Ford, P.C., Inorg. Chem. (1976), 15,

1107.

91) Dose, F.V. and Wilson, L.J., Inorg. Chem. (1978), 17, 2660.

92) Cloninger, K.K. and Callahan, R.W., Inorg. Chem. (1981), 20, 1611.

93) Krause, K. and Krause, K., Inorg. Chem. (1980), 19, 2600.

94) Krause, K. and Krause, K., Inorg. Chem. (1982), 21, 1714.

95) Tokel-Takvoryan, N.E., Hemingway, R.E., and Bard, A.J., J. Am. Chem. Soc. (1973), 95, 6582.

96) Meisel, D., Matheson, M.S., Mulac, W.A., and Rabani, J., J. Phys. Chem. (1977), 81, 1449.

97) Hercules, D.M. and Lytle, F.E., J. Am. Chem. Soc. (1966), 88, 4795.

98) Lytle, F.E. and Hercules, D.M., Photochem. Photobiol. (1971), 13, 123.

99) Tokel, N.E. and Bard, A.J., J. Am. Chem. Soc. (1972), 94, 2862.

100) Jonah, C.D., Matheson, M.S., and Meisel, D., J. Am. Chem. Soc. (1978), 100, 1449.

101) Martin, J.E., Hart, E.J., Adamson, A.W., Gafney, H.D., and Alpern, J., J. Am. Chem. Soc. (1972), 94, 9238.

102) Gafney, H.D. and Adamson, A.W., J. Chem. Educ. (1975), 52, 480.

103) Wallace, W. and Bard, A.J., J. Phys. Chem. (1979), 83, 1350.

104) Itoh, K. and Honda, K., Chem. Lett. (1979), 99.

105) Luttmer, J.R. and Bard, A.J., J. Phys. Chem. (1981), 85, 1155.

106) Glass, R.S. and Faulkner, J. Phys. Chem. (1981), 85, 1160.

107) Rubenstein, I. and Bard, A.J., J. Am. Chem. Soc. (1981), 103, 512.

108) Rubenstein, I. and Bard, A.J., J. Am. Chem. Soc. (1980), 102, 6641.

109) Nishimura, Y., Hirakawa, A.Y., and Tsuboi, M., Adv. IR Ram. Spect. (1979), 5.

110) Basu, A., Gafney, H.D., and Strekas, T.C., Inorg. Chem. (1982), 21, 2231.

111) Gratzel, M., Acc. Chem. Res. (1981), 14, 376.

112) Moradpour, A., Amouyal, E., Keller, P., and Kagan, H., Nouv. J. Chim. (1978), 2, 547.

113) Kiwi, J. and Gratzel, M., J. Am. Chem. Soc. (1979), 101, 7214.

114) Kalyanasunduram, K., Kiwi, J., and Gratzel, M., Helv. Chim. Acta (1978), 61, 2720.

115) Koryakin, B.V., Dzhabler, T.S., and Shilov, A.E., Dokl. Akad. Nauk. SSSR (1977), 298, 620.

116) Lehn, J.M. and Sauvage, J.-P., Nouv. J. Chim. (1977), 1, 449.

117) Chan, S.F., Chou, M., Creutz, C., Matsubara, T., and Sutin, N., J. Am. Chem. Soc. (1981), 103, 369.

118) Brown, G.M., Brunschwig, B.S., Creutz, C., Endicott, J., and Sutin, N., J. Am. Chem. Soc. (1979), 101, 1298.

119) Turkevich, J., Aika, K., Ban, L.L., Okura, I., and Naimba, S., J. Res. Inst. Hokkaido Univ. (1976), 24, 54.

120) Harriman, A., Porter, G., and Richoux, M.C., J. Chem. Soc. Faraday Trans. 2 (1981), 77, 1939.

121) Kawai, T. and Sakata, T., Chem. Phys. Lett. (1980), 72, 87.

122) Sato, S. and White, J., Chem. Phys. Lett. (1980), 72, 83.

123) Borgarello, E., Kiwi, J., Pelizetti, E., Visca, M., and Gratzel, M., J. Am. Chem. Soc. (1981), 103, 6324.

124) Kiwi, J., Borgarello, E., Pelizzetti, E., Visca, M., and Gratzel, M., Angew. Chem. Int. Ed. Engl. (1980), 19, 646.

125) Borgarello, E., Kiwi, J., Pelizzetti, E., Visca, M., and Gratzel. M.. Nature (London) (1981), 289, 158.

126) Gleria, M. and Memming, R., Z. Phys. Chem. (Frankfurt am Main) (1975), 98, 303.

127) Gleria, M. and Memming, R., Z. Phys. Chem. (Frankfurt am Main) (1976), 101, 171.

128) Clark, W.D.K. and Sutin, N., J. Am. Chem. Soc. (1977), 99, 4676.

129) Mackor, A. and Schoonman, J., Rec. Trav. Chim. Pays-Bas, (1980), 99, 71.

130) Thornton, A. and Laurence, G.S., J. Chem. Soc. Chem. Commun. (1978), 408.

131) DeWildes, W., Peeters, G., and Lunsford, J.H., J. Phys. Chem. (1980), 84, 2306.

132) Quayle, W.H. and Lunsford, J.H., Inorg. Chem. (1982), 21, 97.

133) Calvin, M., Acc. Chem. Res. (1978), 11, 369.

134) Rodgers, M.A.J. and Becker, J.C., J. Phys. Chem. (1980), 84, 2762.

135) Krenske, D., Abdo, S., Van Damme, H., Cruz, M., and Fripiat, J.J., J. Phys. Chem. (1980), 84, 2447.

136) Abdo, S., Canesson, P., Cruz, M., Fripiat, J.J., and Van Damme, J. Phys. Chem. (1981), 85, 797.

137) Lee, P.C. and Meisel, D., J. Am. Chem. Soc. (1980), 102, 5477.

138) Elmer, T.H., et al, J. Amer. Ceram. Soc. (1970), 53, 171, and the references therein.

139) Janowski, V.F. and Heyer, W., Z. fur Chemie (1979), 19, 1. An extensive listing of references on the properties of PVG.

140) DeBoer, J.H. and Vleeskens, J.M., Proc. Koninkl. Ned. Akad. Wertenschap. Ser. B (1958), 61, 2.

141) Strazhesko, D.N., Strelko, V.B., Belyakov, V.N., and Rubank, S.C., J. Chromatog. (1974), 102, 191.

142) Vydra, F. and Markova, M., J. Inorg. Nucl. Chem. (1964), 26, 1319.

143) Ahrland, S., Grenthe, I., and Noren, B., Acta Chem. Scand. (1960), 14, 1059.

144) Kennelly, T., Gellis, P., and Gafney, H.D., unpublished results.

145) Gafney, H.D. and Wei, S., submitted for publication.

146) Kennelly, T. and Gafney, H.D., J. Inorg. Nucl. Chem. (1981), 43, 2988.

147) Milosavijevic, B.H. and Thomas. J.K., J. Phys. Chem. (1983), 87, 616.

148) Lachish, U., Ottolenghi, M., and Rabani, J., J. Am. Chem. Soc. (1977), 99, 8062.

149) Baxendale, J.H. and Rodgers, M.A.J., Chem. Phys. Lett. (1980), 72, 424.

150) Berkoff, R., Krist, K., and Gafney, H.D., Inorg. Chem. (1980), 19, 1.

151) Smay, G.L., J. Non-Cryst. Solids (1980), 38-39, 359.

152) Pink, H., Treitinger, L., Vite, L., Jpn. J. Appl. Phys. (1980), 19, 513.

153) Birks, J.B., "Photophysics of Aromatic Molecules", Wiley-Interscience, London, 1970, a) pp. 434-435; b) p. 442.

154) Balzani, V., Moggi, L., Manfrin, F., Bolletta, F., and Laurence, G.S., Coord. Chem. Rev. (1975), 15, 321.

155) Ross, S. and Olivier, J.P., "On Physical Adsorption", Wiley-Interscience, New York, 1964, a) p. 2; b) pp. 31-33.

156) Slama-Schwok, A., Feitelson, Y., and Rabani, J., J. Phys. Chem. (1981), 85, 2222.

157) DellaGuardia, R.A. and Thomas, J.K., J. Phys. Chem. (1983), 87, 990.

158) Infelta, P.P., Gratzel, M., and Thomas, J.K., J. Phys. Chem. (1974), 78, 190.

159) Maestri, M., Infelta, P.P., and Gratzel, M., J. Chem. Phys. (1978), 69, 1522.

160) Rodgers, M.A.J., DaSilva, E., and Wheeler, M.F., Chem. Phys. Lett. (1978), 53, 165.

161) Winterle, J.S., Kliger, D.S., and Hammond, G.S., J. Am. Chem. Soc. (1976), 98, 3719.

162) Srinivasan, V.S., Podolski, D., Westrick, N.J., and Neckers, D.C., J. Am. Chem. Soc. (1978), 100, 6513.

163) Demas, J.N., McBride, R.P.M., and Harris, E.W., J. Phys. Chem. (1976), 80, 2248.

164) Banks, R.G.S., Henderson, R.J., and Pratt, J.M., J. Chem. Soc. A (1968), 2286.

165) Gordon, S., Hart, E.J., Matheson, M.S., Rabani, J., and Thomas, J.K., Disc. Faraday Soc. (1963) 36, 193.

166) Keene, J.P., Radiation Res. (1964), 22, 1.

167) Hill, J.W., "Chemistry for Changing Times", Third ed., Burgess, 1980, p. 280.

168) Kennelly, T., Ph.D. Thesis, City University of New York, June, 1980.

169) Duonghong, D., Borgarello, E., and Gratzel, M., J. Am. Chem. Soc. (1981), 103, 4685.

170) The signal-to-noise improvement ratio is $(2TC/AD)^{1/2}$, where TC is the observed (electronic) time constant and AD is the aperture width.

171) Handbook of Chemistry and Physics, 61st ed., Chemical Rubber Co., Cleveland, Ohio, 1980; a)p. C-138; b) p. E-392.

172) Elmer, T.H., Corning Glass Co., private communication, 1979.

173) Skoog, D.A. and West, D.M., "Fundamentals of Analytical Chemistry", Holt, Rinehart, and Winston, 1963, p. 452.

174) Latimer, W.M., "The Oxidation States of the Elements and their Potentials in Aqueous Solutions", Prentice-Hall, New York, 1938, pp. 210, 211, and 268.

175) Gafney, H.D., Kennelly, T., and Gellis, P., unpublished results.

176) Goonatillake, H.V. and Gafney, H.D., unpublished results.

177) Langmuir, I., J. Am. Chem. Soc. (1917), 39, 1848.

178) Baxendale, J.H. and Fiti, M., J. Chem. Soc. Dalton Trans. (1972), 1995.

179) Cronemeyer, D.C., Phys. Rev. (1952), 87, 876.

180) Butler, M.A., J. Appl. Phys. (1977), 48, 1914.

181) Koffyberg, F.P., Dwight, K., and Wold, A., Solid State Commun. (1979), 80, 433.

182) Nozik, A.J., Ann. Rev. Phys. Chem. (1978), 29, 189.

183) Demas, J.N. and Crosby, G.A., J. Phys. Chem. (1971), 75, 991.

184) Caspar, J.V. and Meyer, T.J., J. Am. Chem. Soc. (1983), 105, 5583.

185) Clark, R.J.H. and Stewart, B., Struct. Bonding (1979), 36, 1.

186) Stumm, W., Hohl, H., and Dalang, F., Croat. Chim. Acta (1976), 48, 491.

187) Haller, W., Nature (1965), 693.

188) Mizutani, T. and Mizutani, H., Anal. Biochem. (1977), 83, 216.

189) Nordberg, M.E., J. Amer. Ceram. Soc. (1944), 27, 299.

190) Cant, N.W. and Little, L.H., Can J. Chem. (1965), 43, 1252.

191) Chapman, I.D. and Hair, M.L., Trans. Farad. Soc. (1965), 61, 1507.

192) Hair, M.L. and Chapman, I.D., J. Amer. Ceram. Soc. (1966), 49, 651.

193) Sidorov, A.N., Opt. Spectry. USSR English Transl. (1960), 8, 424.

194) Hockey, J.A., Chem. Ind. (London) (1965), 57.

195) Davydov, V.Y., Kiselev, A.V., and Zhuravlev, L.T., a) Trans. Faraday Soc. (1964), 60, 2254; b) J. Phys. Chem. (1964), 38, 1108.

196) Stanton, J.H. and Maatman, R.W., a) J. Colloid Sci. (1963), 18, 132; b) J. Phys. Chem. (1964), 68, 757.

197) Wolf, F. and Heyer, W., Z. Anorg. allg. Chem. (1974), 408, 237.

198) Elmer, T.H. and Nordberg, M.E., "Materials and Design Engineering; Thirsty Glass", Reinhold, 1962.

199) Elmer, T.H., Chapman, I.D., and Nordberg, M.E., J.

Phys. Chem. (1966), 70, 2740.

200) Iler, R.K., "The Chemistry of Silica", Wiley-Interscience, New York, 1979, pps. 673-676, and the references therein.

201) Boehm, H.P., Adv. Catal. (1966), 16, 226.

202) Near UV and visible spectra of various molecules adsorbed to PVG resemble spectra of the molecules in aqueous or alcoholic solutions.

203) Eriksen, J., Foote, C.S., and Parker, T.L., J. Am. Chem. Soc. (1977), 99, 6455.

204) Divisek, J. and Kastening, B., J. Electroanal. Chem. (1975), 65, 603. The value of E = -0.634 V for $H^+ + e^- + O_2 \rightleftharpoons HO_2$ is calculated assuming $E^{o_2} = -0.33$ V, $pK_a = 4.9$, and a surface pH = 4.9.

205) Winter, N., Chem. Phys. Lett. (1975), 33, 300.

206) Sponer, H. and Bonner, L.G., J. Chem. Phys. (1940), 8, 33.

207) Brand, J.C.D., Jones, V.T., and DiLauro, C., J. Mol. Spectrosc. (1973), 45, 404.

208) Cotton, F.A. and Wilkinson, G., "Advanced Inorganic Chemistry", 3rd ed., Wiley-Interscience, New York, 1972, p. 443.

209) Anbar, M., Adv. Chem. Ser. (1965), 50, 67.

210) Atkins, P.W., "Physical Chemistry", W.H. Freeman and Co., San Francisco, 1978, p. 804.

211) Guarr, T. and McLendon, G., Abstr. 182nd Amer. Chem. Soc. Nat. Meeting, Inorganic Paper 20, New York, Aug. 1981.

212) Beeck, O., Advan. Catal. (1950), 2, 151.

213) Bikerman, J.J., "Physical Surfaces", Academic Press, New York, 1970, pp. 335-336.

214) Iwasawa, Y. and Ogasawara, S., J. Chem. Soc. Faraday Trans. 1 (1979), 75, 1465.

215) Frank, J.M. and Vavilov, S.I., Z. Physik. (1931), 69, 100.

216) Turro, N.J, "Modern Molecular Photochemistry",

Benjamin Cummings, Menlo Park, California, 1978, p. 317-319.

217) Siegel, S. and Judeikis, H.S., J. Chem. Phys. (1968), 48, 613.

218) Bowen, E.J. and Metcalf, W.S., Proc. Roy. Soc. A (1951), 206, 937.

219) Miller, J.R., Hartman, K.W., and Abrash, S., J. Am. Chem. Soc. (1982), 104, 4286.

220) Gerischer, H., "Physical Chemistry; An Advanced Treatise", Vol 9A, H. Eyring, D. Henderson, and W. Jost, ed., Academic Press, New York, 1970, p. 463.

221) Ghosh, P.K. and Spiro, T.G., J. Am. Chem. Soc. (1980), 102, 5543.

222) Ghosh, P.K. and Bard, A.J., J. Am. Chem. Soc. (1983), 105, 5691.

223) Mills, A. and Porter, G., J. Chem. Soc. Faraday Trans. 1 (1982), 78, 3659.

224) Bulatov, A.V. and Khidekel, Izv. Akad. Nauk. SSSR, Ser. Khim. (1976), 1902.

225) Sato, S. and White, J.M., J. Am. Chem. Soc. (1980), 102, 7206.

226) Sullivan, B.P., Abrana, H., Finklea, H.O., Salmon, D.J., Nagle, J.K., Meyer, T.J., and Sprintschnik, H., Chem. Phys. Lett. (1978), 58, 389.

227) Krause, R.A. and Ballhausen, C.J., Acta. Chem. Scand., Sect. A (1977), A31, 535.

228) Klassen, D.M., Inorg. Chem. (1976), 15, 3166.

229) Krause, R.A. and Krause, K., unpublished results.

230) Based on Debye-Bronsted equation: $\log k(\mu) = \log k(\mu = 0) + 1.02 z_D z_A \sqrt{\mu}$.

231) Silverman, J. and Dodson, R.W., J. Phys. Chem. (1952), 56, 846.